Studies on Synthesis, Structural Properties and Applications of Fluorescent Chemosensors Based on Thiacalix[4]arenes

September 2016

Department of Advanced Technology Fusion,
Graduate School of Science and Engineering,
Saga University, Japan

Zhao Jianglin

Studies on Synthesis, Structural Properties and Applications of Fluorescent Chemosensors Based on Thiacalix[4]arenes

A dissertation presented to the Graduate School of Science and Engineering of Saga University in partial fulfillment of the requirements for the degree of Doctor of Philosophy

September 2016

By

Zhao Jianglin

Supervisor:

Professor Dr. Takehiko Yamato

CERTIFICATE OF APPROVAL
Ph.D Dissertation

This is to certify that the Ph.D Dissertation of

Zhao Jianglin

has been approved by the Examining Committee for the dissertation requirement for the Doctor of Philosophy degree in Chemistry at the September, 2016 graduation.

Dissertation committee: _____

Supervisor: Prof. Takehiko Yamato

_____

Member, Prof. Tsugio Kitamura

_____

Member, Prof. Takeshi Hanamoto

_____

Member, Prof. Mishinori Takeshita

ACKNOWLEDGEMENTS

Firstly, and most importantly, I would like to express my deepest gratitude to my supervisor, Professor *Takehiko Yamato*, for his invaluable guidance, limitless helping and understanding. His profound knowledge, constructive advices inspired me during the whole doctor course.

I would like to express great appreciate to professor *Tsugio Kitamura*, professor *Mishinori Takeshita*, and professor *Takeshi Hanamoto* and the rest of my thesis committee for their kind cooperation and suggestions. I also wish to convey my sincere thanks to professor *Xi Zeng*, professor *Lan Mu*, professor *Zhu Tao* and others professor at Guizhou University, China, due to their inspiriting discussions and constant encouragement. Furthermore, I must acknowledge to Dr. *Sulfur Rahman* and Prof. *Paris E. Georghiou* (Canada) for DFT computational study and valuable suggestion during my research; thanks to Prof. *David L. Hughes*, Prof. *Carl Redshaw* and Dr. *Mark R. J. Elsegood* (United Kingdom) for single-crystal X-ray analysis in my research works.

I also would like to express my deep gratitude to all of the members in Yamato Lab., especially to Dr. *Xing Feng*, Dr. *Ummey Rayhan*, Dr. *Hang Cong*, Dr. *Cheng-Cheng Jin*, Dr. *Md. Monarul Islam*, Dr. *Hirotsugu Tomiyasu*, Dr. *Zannatul Kowser*, *Xue-Kai Jiang*, *Nobuyuki Seto*, *Tahmina Akter*, *Chong Wu*, *Chuan-Zeng Wang*, *Yusuke Ikejiri*, *Ichiyanagi*, *Noda*, *Kihara*, and *Sakaguti*, who made my research work more enjoyable. Special thanks are given to the staffs and faculty in the International Division of Saga University for their acting concerns.

Finally, I would like to express my deeply appreciation to my parents *Xi-Ping Zhao* and *Bin-Xiang Yu*, my wife *Yu-Lian He*, my son *Ke-Ming Zhao*, my brother *Jiang-Qiu Zhao*, my sister *Jiang-Hong Zhao* and *Jiang-Ying Zhao* for their endless encouragement, understanding and sacrifice. Without their careful assistance, it would not have been possible to complete my doctoral study. I would like to delicate this thesis to my family.

Zhao Jianglin

September, 2016, Saga University, Japan

ABSTRACT

p-tert-butyl-thiacalix[*n*]arene is the second subclass of calix[*n*]arene family, which possessing almost unlimited possibilities for functionalization on the low rim, up rim, bridging sulfur atoms and benzene scaffold. It has been attracted great attention to construct different types of host molecules in many ways. In this dissertation, we further explored the synthesis and application of thiacalix[4]arene derivatives in the fields of chemosensor, allosteric effect and photochemical reaction.

Firstly, a new type fluorescent probe bearing two pyrenyl groups in a 1,3-*alternate* conformation based on thiacalix[4]arene has been introduced. The designed chemosensor exhibited high selectivity toward Cu^{2+} ions versus other metal ions with a low detection limit of 1.44×10^{-7} M. This probe is capable of acting as an efficient ratiometric fluorescent probe at low ion concentration or as a fluorescence quenching type probe due to the heavy atom effect operating in high ionic strength solution.

Secondly, two novel receptors possessing imidazole moieties based on thiacalix[4]arene have been discussed with the allosteric effect. According to the ^{1}H NMR titration experiments, the exclusive formation of mononuclear complexes of di-topic receptor with metal cations is of particular interest revealing a negative allosteric effect in the thiacalix[4]arene family. In the other hand, liquid-liquid extraction experiments suggest that synthesized mono-topic receptor can be utilized as an efficient reusable extractant for dichromate anion by controlling the pH of the aqueous solution.

Finally, a rare and exclusive photochemical reaction was firstly observed. The rare endoperoxide photoproduct which was quantitatively obtained from a thiacalix[4]arene crown-shaped derivative upon irradiation at 365 nm. The prerequisites for the formation of endoperoxide photoproduct have also been investigated.

In summary, it is believed that the design strategy and the remarkable photophysical properties of these receptors in this present thesis would help to further extend applications in the realm of thiacalix[*n*]arene chemistry.

TABLE OF CONTENTS

Chapter 1

Recent Developments

of The Applications about Thiacalix[4]arene Derivatives

in Various Fields

In this chapter a shortly review focus on the applications of thiacalix[4]arene derivatives in various fields.

1.1 General Introduction

Supramolecular chemistry is focusing on the chemical systems which are assembled by a discrete number of molecular components through weak and reversible noncovalent interactions. Since the Nobel Prize in chemistry 1987 was awarded jointly to Donald J. Cram,[1] Jean-Marie Lehn[2] and Charles J. Pedersen[3] "for their development and use of molecules with structure-specific interactions of high selectivity". Much attention has been paid to this field, as it has urged and accelerated the development of numerous new concepts, such as molecular host−guest chemistry, self-assembly, molecular recognition, dynamic covalent chemistry and so on.[4]

Calixarenes[5] are termed 'The third generation' supramolecular molecules[6] in addition to crown ethers[7] and cyclodextrins.[8] which have emerged as the most widely investigated scaffolds among various reported molecular platforms. Calixarene possess the recognizable ability not only for cation and anion, but also for neutral molecule. "Calix" means "beaker" in Latin and Greek, is introduced herein due to the shape of this tetramer which look like the Greek calix. The conventional calix[*n*]arenes $\mathbf{1}_n$ are cyclic oligomers which are composed of phenolic units linked through methylene groups. Compound $\mathbf{1}_n$ possessing well defined conformational properties and controllable cavities (calix[4]arenes to calix[20]arenes) that are able to encapsulate various guest species (Figure 1).

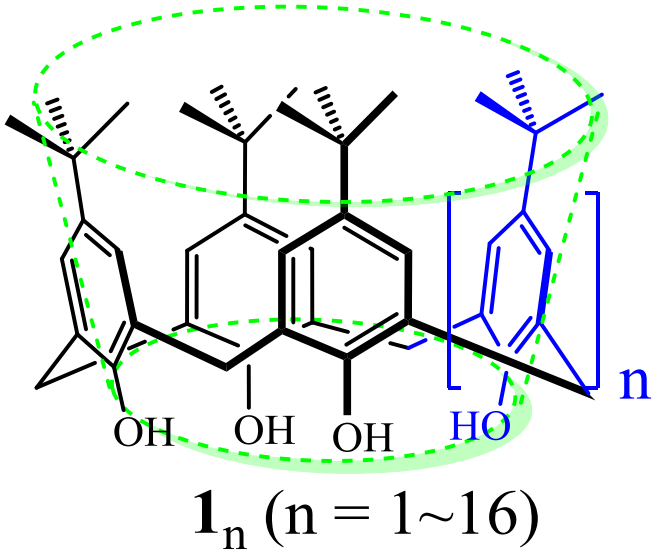

Figure 1. The molecular structure of calix[*n*]arenes.

p-tert-butyl-thiacalix[*n*]arene **2**$_n$ is the second subclass of calix[*n*]arene family, in which the four methylene bridges of *p-tert*-butylcalix[4]arene are replaced by sulfide atom bridges. The first case of synthesis *p-tert*-butylthiacalix[4]arene (**2**$_1$) was obtained in a poor yield (4.1%) by cyclization of a linear tetramer with sulfur dichloride in 1993 by Sone *et al.*[9]. However, the development of thiacalix[4]arene chemistry was limited due to the low yield until 1997. Fortunately, inspired of the treatment of phenols with sulfur at elevated temperatures under basic conditions afforded a complex mixture of phenol oligomers which were joined by sulfide bonds at the *o*-, *o'*-, and/or *p*-positions of the phenol moieties,[10] Miyano *et al.* successfully developed a convenient synthesis method to synthesize *p-tert*-butylthiacalix[4]arene **2**$_1$ in a single step with a highly yield (54%) by heating a mixture of *p-tert*-butylphenol, elemental sulfur S_8, and NaOH in tetraethylene glycol dimethyl ether with concomitant removal of the resulting hydrogen sulfide in 1997[11] (Scheme 1). Additionally, trace amounts of thiacalix[5]arene **2**$_2$ thiacalix[6]arene **2**$_3$ were also observed by Iki N. *et al.*[12] for the first time. The successful of this synthetic strategy for thiacalix[4]arene is the landmark event in the thiacalixarene chemistry, since that, studies on modification and development of the functions based on thiacalixarene are now vividly progressing.

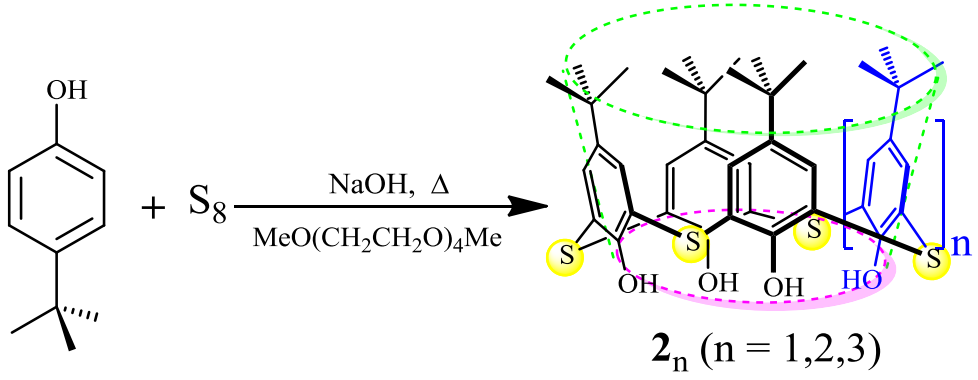

Scheme 1. One-step synthesis of thiacalix[n]arenes.

Soon afterwards, Miyano S. *et al.* further optimized this one-step method which was advantageously replaced by a two-steps procedure (Scheme 2): firstly, a sulfur-bridged linear dimer of 2,2-thiobis(4-tertbutylphenol) **3** was prepared in a good yield (75%) by treating 4-tertbutylphenol with SCl_2 in dry $CHCl_3$ according to the literature procedure; [9a] secondary, the starting dimer **3** was used for the cyclo-condensation with sulfur and NaOH-catalyzed in

Ph_2O to greatly improve the yields of thiacalix[4]arene $\mathbf{2}_1$ to 83% and thiacalix[6]arene $\mathbf{2}_3$ to 5.3%. Furthermore, the present dimer method allowed the isolation of thiacalix[8]arene $\mathbf{2}_5$ in an appreciable amount (4.3%)[13].

In comparison to the similar structural characteristics of the conventional calixarene platform, thiacalixarene is more attractive for the following reasons: (1) the ring linkages containing hetero atom sulfur atoms which may act as extra binding sites upon complexing guest; (2) the bridging sulfur atom could be facilely oxidized to sulfoxide and sulfone which could change the properties of the cavity formed by the calix benzene rings; (3) the ring size of thiacalix[4]arene is 15% larger[14] than that of calix[4]arene which is attribute to the longer bond length of C–S as compared to C–C.

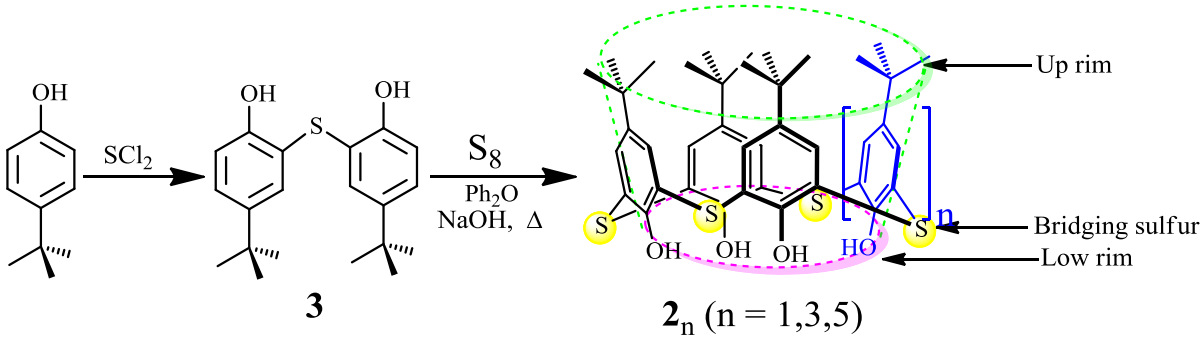

Scheme 2. Two-step synthesis of thiacalix[*n*]arenes.

The thiacalix[*n*]arene scaffold is same as conventional calix[*n*]arene which have two rims: the narrow rim comprised of the phenolic groups is known as the 'low rim', whereas the wider rim comprised of the *para*-tertbutyl-groups is known as the 'up rim' (scheme 2). Recently, significant contributions have been made regarding chemical modifications of their up rim, low rim, bridging sulfide groups, and even in the benzene scaffold. In general, the modification of the low rim of thiacalix[4]arene $\mathbf{2}_1$ is following four types of reactions: alkylation,[15] acylation[16], phosphorylation[17] and silylation[18] which are same with the functionalization of the lower rim of classic calix[4]arene. The modifications of the up rim of thiacalix[4]arene have been carried out primarily via another two methods: (1) *ipso*-substitution of the *tert*-butyl groups by electrophilic agents and (2) electrophilic aromatic substitution at the *para*-position of the phenol residue,[19] such as bromination[20], nitration[21], formylation[22] and sulfonation[23]. Furthermore, the hetero bridging sulfur atoms which can be

further oxidized to sulfone derivatives and sulfoxide derivatives in the presence of an oxidant, such as hydrogen peroxide/trifluoroacetic acid or sodium perborate.[24]

As the conventional calix[4]arene, the conformer distribution of these alkylated thiacalix[4]arenes is generally governed by the different metal template reagents of Na_2CO_3, K_2CO_3 and Cs_2CO_3. For example, the alkylation of thiacalix[4]arenes **2**$_1$ with simple haloalkanes in the presence of different base [M_2CO_3 (M = Na^+, K^+, Cs^+)] leads to different alkylated products in various conformations which are depending on the orientation of the phenolic units with respect to each other,[25] *i.e.* '*cone*', '*partial cone*', '*1,2-alternate*' and '*1,3-alternate*' as shown in Figure 2.[26] The *1,3-alternate* stereoisomer, offers divergently oriented binding sites, which is an excellent candidate structure for studying allosteric effect in metal cation binding, is special interest.[27] During our whole research, we are focusing on synthesizing various thiacalix[4]arene derivatives in *1,3-alternate* conformation and exploring their application in various fields. We should also point out that the conformational preference of the alkylated products not only depends on the metal template effect, but also depends on the up rim substitution of thiacalix[4]arene **2**$_1$. Additionally, the alkylation of thiacalix[4]arenes **2**$_1$ with different amount of haloalkanes yields different substitutions, *i.e.* mono-alkylated, bis-alkylated, tri-alkylated and tetra-alkylated products.

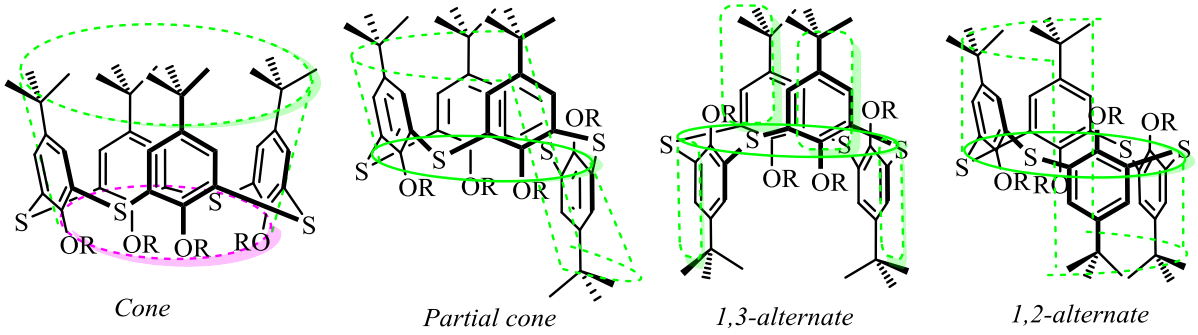

Figure 2. Four conformers of thiacalix[4]arene.

Due to thiacalix[4]arene scaffold possessing almost unlimited functionalization possibilities on the low rim, up rim, bridging sulfur atoms and benzene scaffold, it has been attracted great attention to construct different types of host molecules in many ways. During the past two decades, there are numerous thiacalix[4]arene host molecules have been developed as ion recognition reagents (non-fluorescent receptors), florescent chemosensors (florescent receptors), allosteric effect reagents, molecular switches, logic gates and devices,

self-assembled coordination networks, magnetic materials, luminescent materials and so on. In this chapter, we have summarized all of the application of thiacalix[4]arene derivatives in various fields.

1.2 The application of thiacalix[4]arene derivatives

1.2.1 Encapsulation of neutral smaller molecular

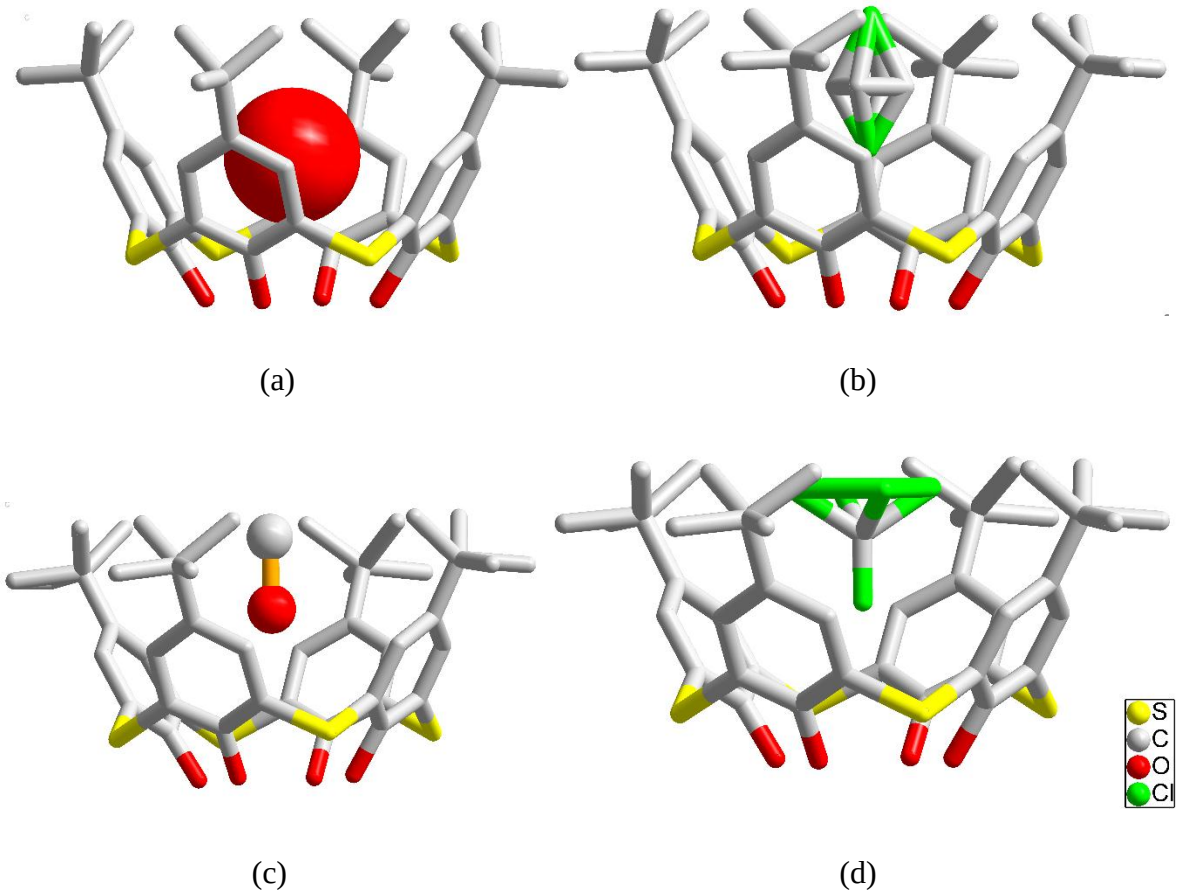

Figure 3. Some examples for the inclusion complexes formed by compound $\mathbf{2}_1$ with neutral molecular: (a) $\mathbf{2}_1 \supset H_2O$, (b) $\mathbf{2}_1 \supset CH_2C1_2$, (c) $\mathbf{2}_1 \supset$ MeOH and (d) $\mathbf{2}_1 \supset CHCl_3$. Hydrogen atoms, has been omitted for clarity.

As we know, there is a bowl-shaped cavity in thicalix[4]arene $\mathbf{2}_1$ which possess the capability of capture the guest molecular. Based on this unique properties, water (a), CH_2C1_2 (b), MeOH (c) and $CHCl_3$ (d) have been captured in the presence of thiacalix[4]arene (Figure 3).[28] Besides, due to the unlimited possibilities for functionalization, we can easily obtain

their corresponding derivatives which would possess unlimited application possibilities. The following are the summarized of various applications for the thiacalix[4]arene derivatives.

1.2.2 Adsorption

1.2.2.1 Adsorption for organic dyes

Yang *et al.* firstly prepared a cyclodextrin-grafted thiacalix [4]arene netty polymer **4** by click chemistry (Figure 4). Polymer **4** exhibited excellent adsorption capacities toward victoria blue B (VB), crystal violet (CV), neutral red (NR), methylene blue (MB), orange G sodium salt (OG) and brilliant ponceau 5R (BP), six kinds of anionic and cationic dyes. Especially for VB, CV, NR and MB were as high as 5.821, 6.825, 6.135 and 5.381 mmol/g, respectively. The adsorption processes were spontaneous and exothermic. The adsorption capacities for anionic dyes (OG and BP) were decreased upon the increasing of pH values. In contrast, the adsorption capacities for cationic dyes (VB, CV, NR and MB) were increased with the increasing of pH values. Additionally, polymer **4** exhibited good cyclic adsorption property after adsorption and desorption in five times' cycles.[29]

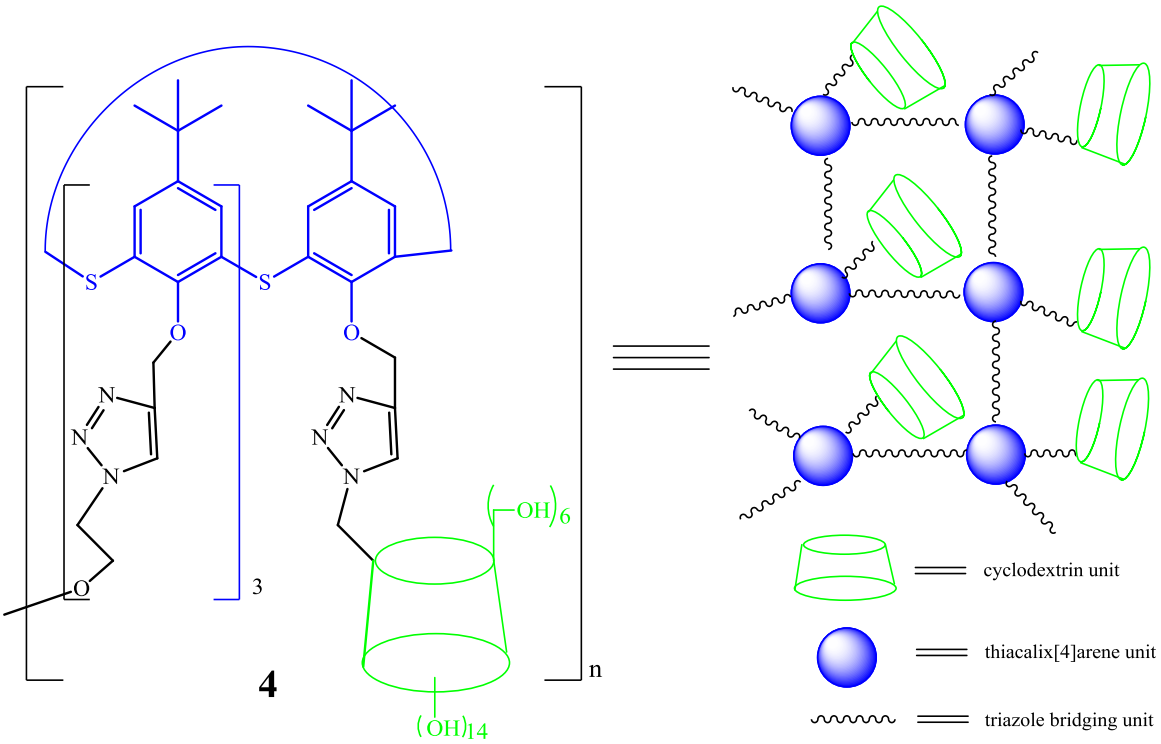

Figure 4. The molecular structure of polymer **4**.

1.2.2.2 Adsorption for biofuels

Notestein *et al.* designed two absorption materials by directly grafted hydrophobic, cavity-containing (thia)calixarenes to porous, hydrophilic SiO_2 surface (Figure 5). These materials have been successfully used for the recovery of *n*-butanol from dilute aqueous

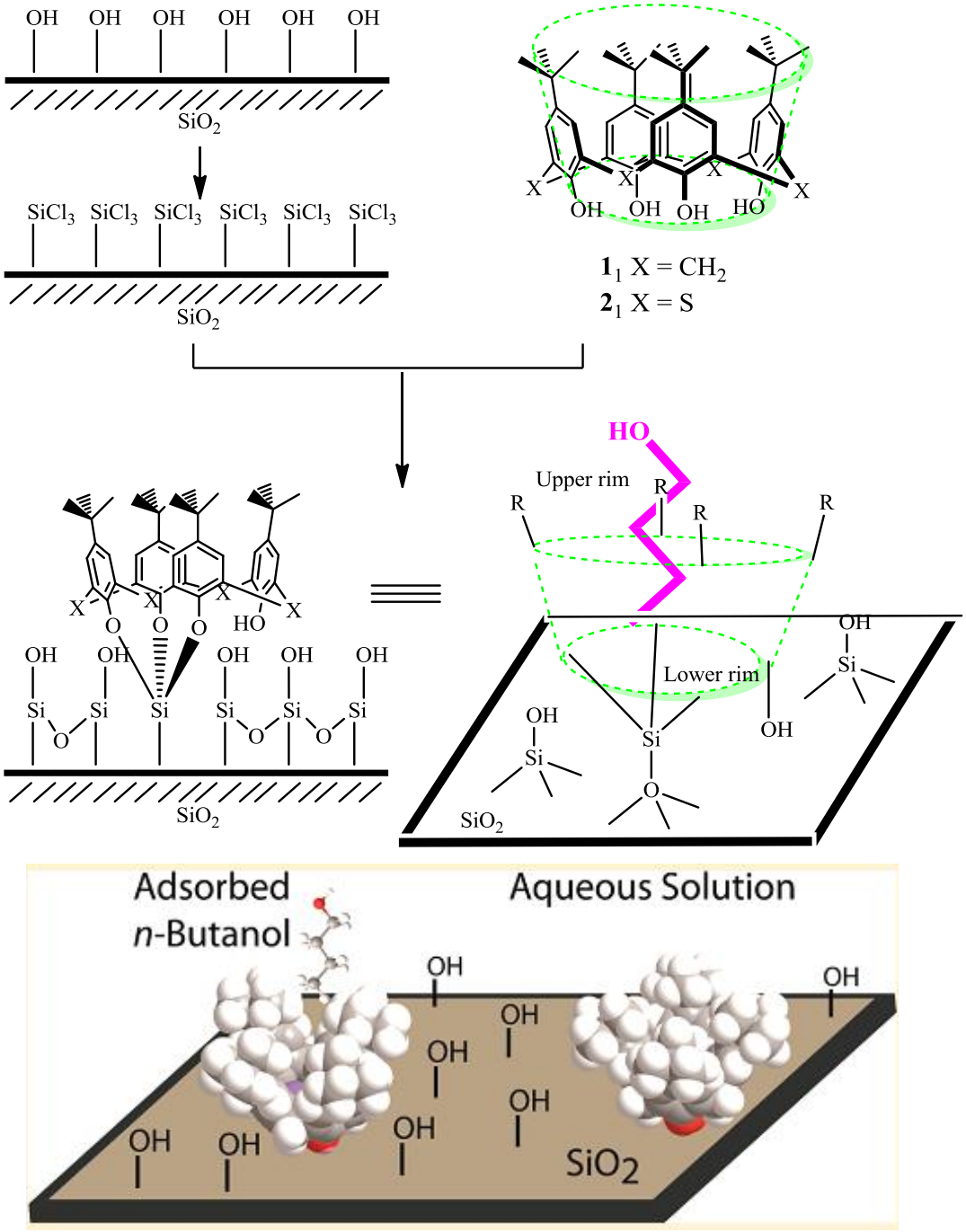

Figure 5. Prepare of adsorption materials from thiacalix[4]arene $\mathbf{2}_1$ and calix[4]arene $\mathbf{1}_1$

solutions. Adsorption energies and uptakes generally become more favorable with the number of hydrophobic contacts present on the upper rim of the (thia)calixarene. The materials which prepared by calix[4]arene exhibited fully reversible adsorption into solution. Further study showed that materials from calixarenes were stable up to about 300 ℃ and butanol was desorbed from the cavity of $\mathbf{1}_1$ at about 150 ℃. In other word, these materials are capable as regenerable adsorbents for *n*-butanol. In the other hands, the materials which prepared by calix[4]arene exhibited irreversible behavior and a stronger uptake than its analogue calix[4]arene $\mathbf{1}_1$ due to the flexibility and the polarizable groups in thiacalix[4]arene $\mathbf{2}_1$.[30]

1.2.3 Application in drug

1.2.3.1 Anti-cancer agent

Koizumi *et al.* designed an coordination complex (**6**) by using an equimolar mixture of water-soluble *p*-tetrasulfonated thiacalix[4]arene (**5**) and cadmium acetate in water. The cadmium-coordinated thiacalix[4]arene tetrasulfate complex (**6**) exhibited anti-tumor activity in mouse xenograft models of human T-cell leukemia Jurkat cell lines. Treatment with **6** showed anti-proliferative effects against any kind of leukemia cell lines, accompanied by induction of apoptosis. Furthermore, the mice which were treated with **6** exhibited significantly less cadmium accumulation in liver and kidney compared to equimolar $CdCl_2$-treated mice. These results strongly suggested that complex **6** can be used as a potential anti-cancer agent in the treatment of T-cell leukemia.[31]

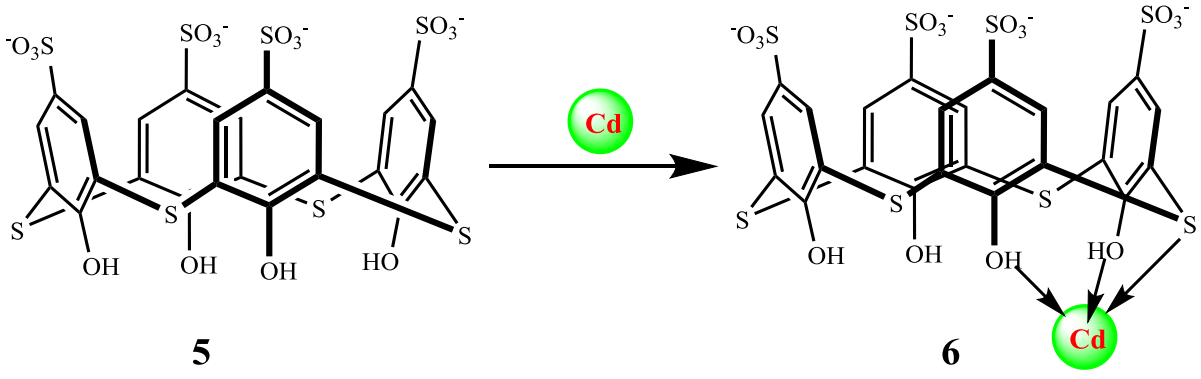

Figure 6. The molecular structure of complex **6**.

1.2.3.2 alkaline phosphatase inhibitors

A. I. Vovk *et al.* employed (thia)calix[4]arene as molecular scaffold to design new effective inhibitors **7** and **8** for alkaline phosphatase. Inhibition kinetics study revealed that phosphonate inhibitor **8** on thiacalix[4]arene platform had exhibited stronger inhibition properties than its analogue structural based on calix[4]arene **7** towards alkaline phosphatases from bovine intestine mucosa, shrimp and human placenta. In order to investigate the molecular mechanism of the inhibition, inhibitors **7** and **8** were docked computationally to the active site of alkaline phosphatase from shrimp. Molecular docking study revealed that there were more hydrogen bonds in thiacalix[4]arene inhibitor **8** than calix[4]arene inhibitor **7**. This maybe attributed that the cavity size of thiacalix[4]arene inhibitor **8** was larger than calix[4]arene inhibitor **7**,[32] which exhibited longer hydrogen bonding between phenolic

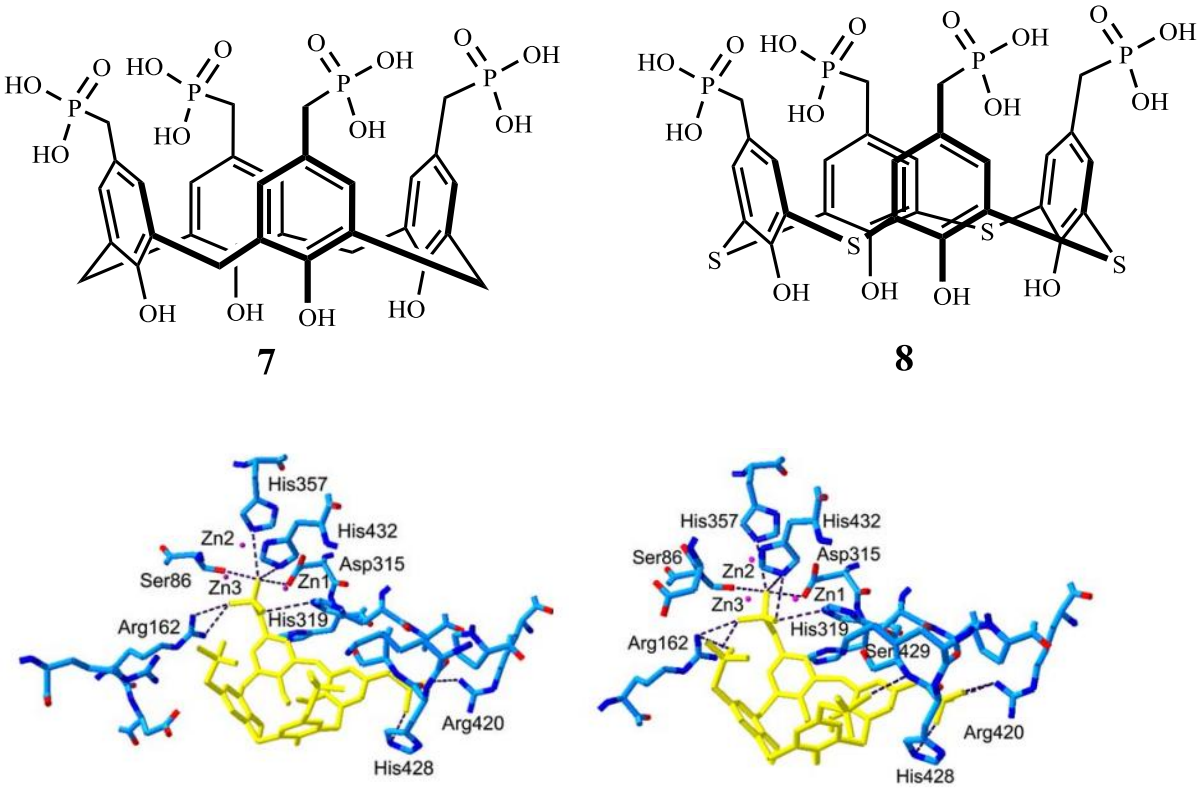

Figure 7. Up: the molecular structure of **7** and **8**. Bottom: the interaction modes of calix[4]arene **7** (left) and thiacalix[4]arene **8** (right) with the adjacent amino acid residues in the active site of shrimp alkaline phosphatase obtained after AutoDock 3.05 calculations. Dotted lines show the hydrogen bonds in which the inhibitor is involved.

groups and greater flexibility of thiacalix[4]arene than calix[4]arene. These inherent nature of thiacalix[4]arene derivative **8** can provide the more effective zinc ion chelation in the enzyme active site and the more extensive network of hydrogen bonds between the amino acid residues and the oxygens of phosphonate groups of alkaline phosphatase. Consequently, the thiacalix[4]arenes scaffold possessed the better potential application for the construction of potent phosphonate inhibitors of the enzymes.[33]

1.2.4 The application in extraction

1.2.4.1 Solvent extraction

Two phase solvent extraction is one of the most commonly used treatment method which employ a selective extractant especially for ions in organic and aqueous solution. Extractants **9** and **10** exhibited selectively extraction for Pd(II) ions from the single-metal, simulated mixed-metal, and automotive catalyst leached solutions in Cl^- media. Further study indicated that the Pd(II) extraction efficiency not only depended on the number of dimethylthiocarbamoyl moieties but also depended on the Cl^- concentration. In contrast, the Pd(II) extraction efficiency independent of the H^+ concentration. The acid durability test

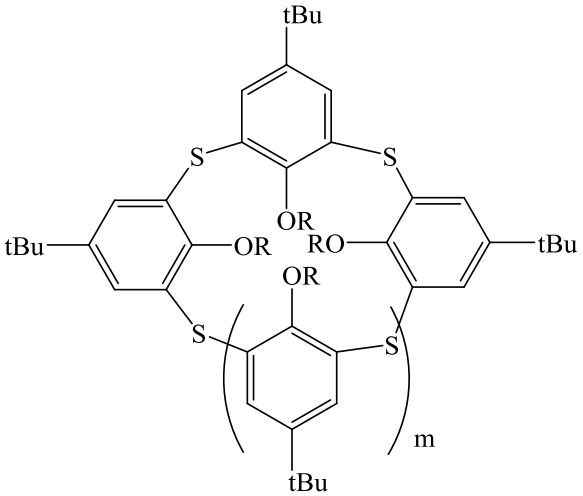

9 (m = 3)
10 (m = 1)
R=$CSN(CH_3)_2$

Figure 8. The molecular structure of **8** and **9**.

revealed that the extractants **9** and **10** were suitable for metal extraction in highly acidic media. In addition, for the practical application, extractants **9** and **10** selectively extracted 99% of Pd(II) ions from an automotive catalyst residue leached solution which was composed of Rh, Pd, Pt, Zr, Ce, Ba, Al, La, and Y in 1.0 M Cl^- media. Hence, extractants **9** and **10** have been considered as effective potential extractants for Pd(II) separation from secondary resources.[34]

1.2.4.2 Membrane Extraction.

Stoikov *et al.* successfully introduced α-aminophosphonate fragments into the thiacalix[4]arene platform for the first time, obtained *cone* mono-substituted thiacalix[4]arene derivative **11** and *1,3-alternate* tetra-substitute thiacalix[4]arene derivative **12**. HPLC analysis results shown that the liquid-impregnated membrane with compound **12** was capable to selectively extract aspartic acid from a mixture of dicarboxylic, α-hydroxy and α-amino acids. However, the treated liquid-impregnated membrane with compound **11** was non-selective. Further study indicated that high selectivity of acid extraction was depending on the spatial complementarity between the binding site of host and the structure of the guest. Thus, the synthesized compound **12** has the potential application in the development of sensors, purification and separation of organic acids.[35]

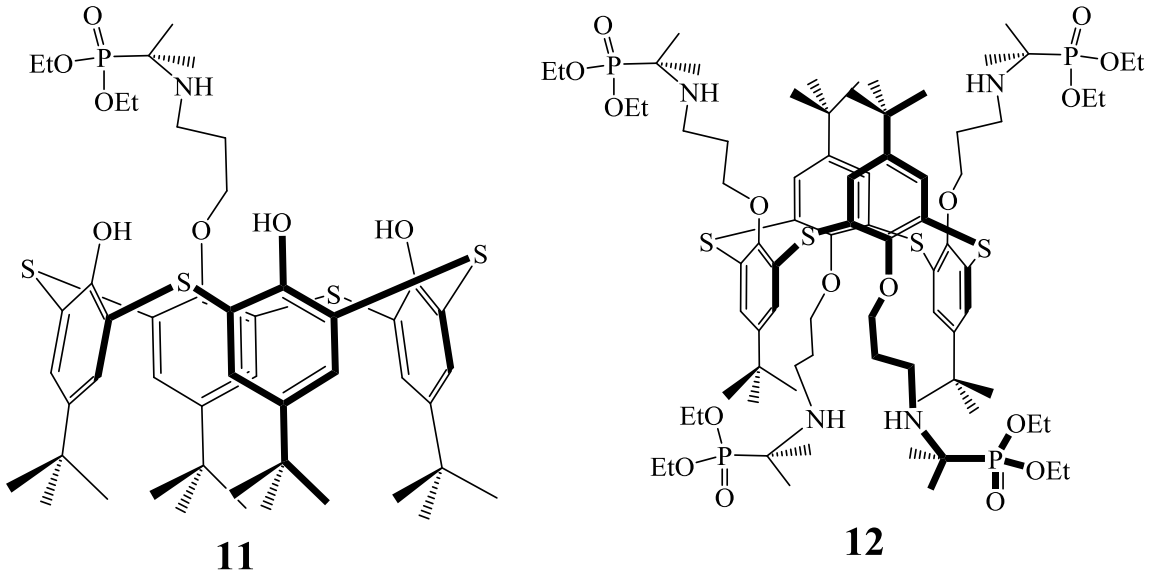

Figure 9. The molecular structure of **11** and **12**.

1.2.5 Chiral recognition

1.2.5.1 Chiral anion recognition

Lhoták *et al.* successfully introduced chiral alkyl substituents into the lower rim of thiacalixarene, obtained a well-preorganized ureido cavities on both sites of chiral compound **13**. ^{1}H NMR titration experiments revealed that compound **13** was capable of chiral anion recognition *via* their NH bonds even in a highly competitive solvent DMSO-d_6 (which competes highly for hydrogen bonding interactions.). A 1 : 1 stoichiometry complexs were observed between host compound **13** and chiral anion guests. Further study shown that compound **13** exhibited a high chiral discrimination for free Ser-OH with a selectivity factor of 3.13 for the $_{D}$-isomer.[36]

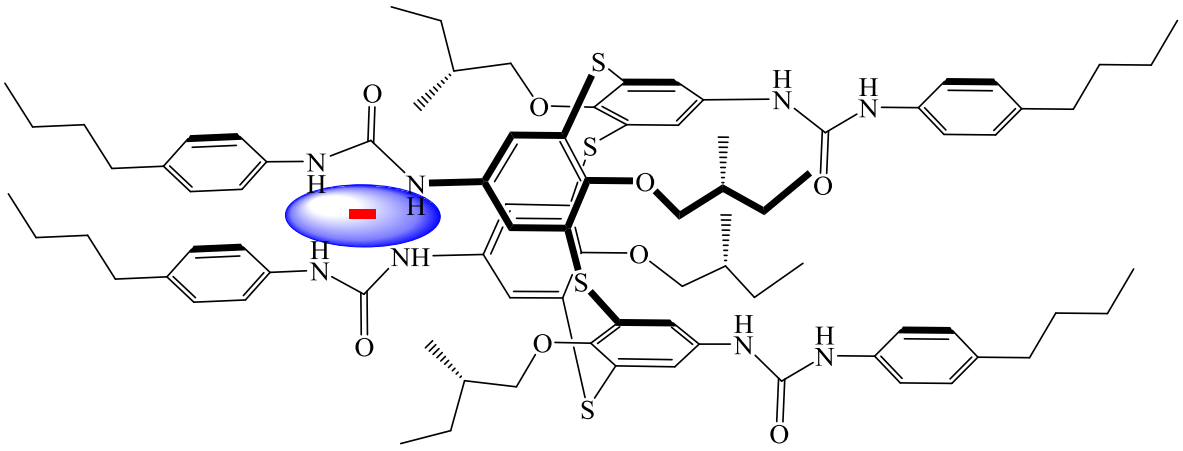

13

Figure 10. The molecular structure of **13**.

1.2.5.2 Chiral molecular recognition

Iki *et al.* designed an (*S*)-1-phenylethylamine modified chiral thiacalix[4]arene derivative **14** which can be used as a chiral stationary phase for capillary gas chromatography. They observed that (*S*)-**14**-coated column shown good separations of enantiomeric amino acid, amine and alcohol derivatives. However, the corresponding calix[4]arene derivative **15** cannot distinguish these enantiomers. This may be attributed to the stereoselective hydrogen bonding between the amide group of the enantiomers and compound **14**.[37]

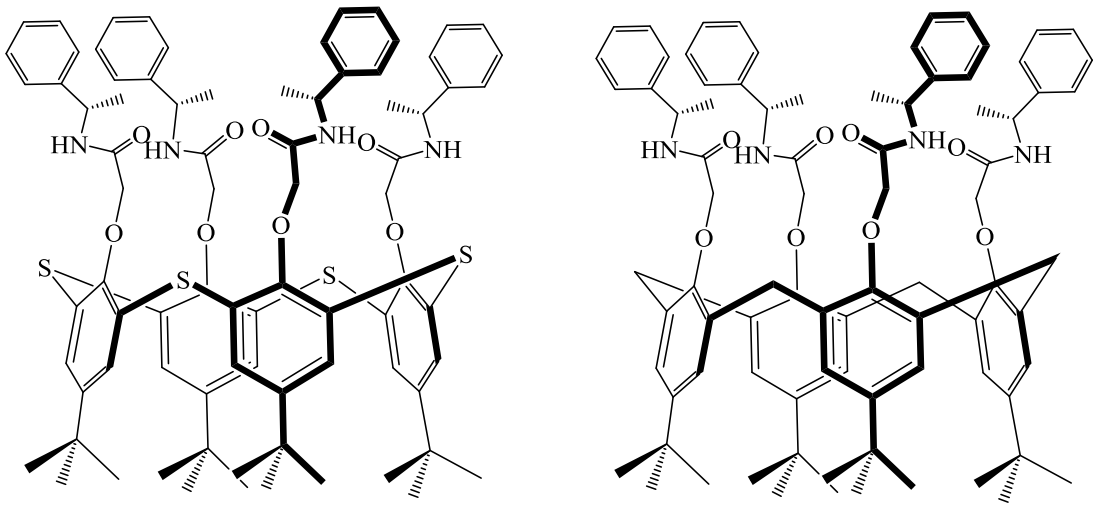

14 **15**

Figure 11. The molecular structure of **14** and **15**.

1.2.6 Allosteric effect.

Yamato *et al.* reported a thiacalix[4]arene receptor **16** which possessing two *p*-nitrophenyl ureido moieties in one site and a crown-ether moiety at the opposite side. The ^{1}H NMR titration experiments revealed that the crown-ether ring moiety can bind with K^{+} ion and the ureido moiety can complex with all of the anions. Furthermore, an interesting positive and negative allosteric effect in receptor **16** was also observed by ^{1}H NMR and UV-vis titration experiments. A positive allosteric effect could be observed by the formation of a heteroditopic dinuclear complex of receptor **16** with Br^{-} and K^{+} ions. On the other hand, a negative allosteric effect was observed by the addition of Cl^{-} ion into the complex of **16** $\cdot K^{+}$ induced the decomplexation of the K^{+} ion from the crown-5 ring.[38]

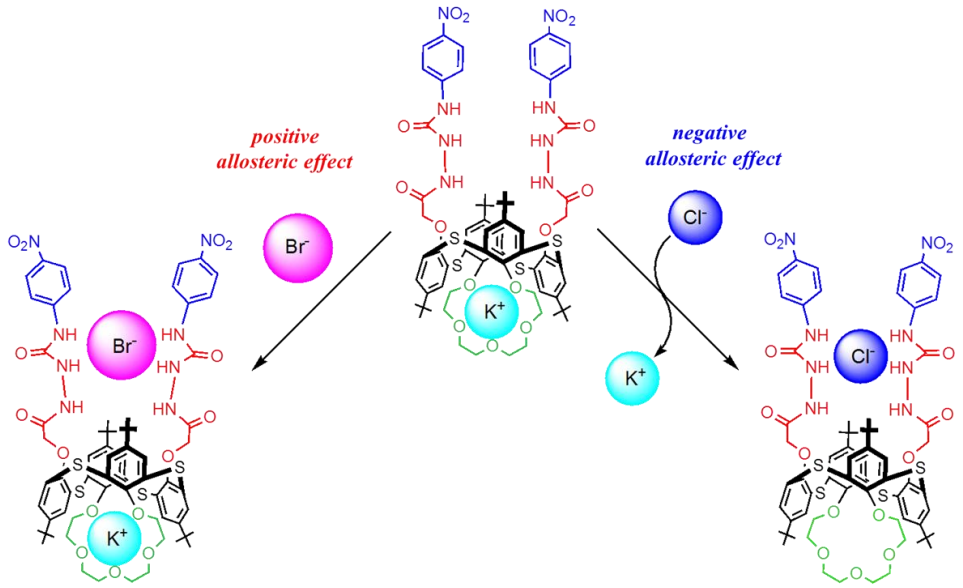

Figure 12. Proposed allosteric effect of compound **16**.

1.2.7 Fluorescent probe.

Fluorescent probe appear to be particularly attractive due to their specificity, high sensitivity, high selectivity, and real-time monitoring with fast response times.[39] The first fluorescent probe based on thiacalix[4]arene was synthesized by Hamada *et al.* in 1998.[40] After that, various florescent probes have been developed.

1.2.7.1 Recognize cation

Zeng *et al.* designed a 1,3-*alternate* thiacalix[4]crown-shaped fluorescent probe **17** which employed phenothiazine moieties as fluorophore. Probe **17** exhibited strong fluorescence emission in THF-water due to multiple noncovalent interactions within the molecule inhibit the intramolecular rotation. When Fe^{3+} or Cr^{3+} were gradually added to the solution of probe **17**, the fluorescence intensity of this solution was gradually decreased until completely quenched. However, there were no obvously change by the addition of any other tested metal ions. It suggested that probe **17** was capable selectively recognized towards Fe^{3+} or Cr^{3+} ions. Further study revealed the quenching mechanism was that the presence of Fe^{3+} or Cr^{3+} ions were capable of catalyzing the cleavage of the Schiff base group of probe **17**. In other word, probe **17** was hydrolyzed in the presence of Fe^{3+} or Cr^{3+} ions *via* loss of the phenothiazine

groups. To the best of our knowledge, this is the first case which quenching mechanism is based on hydrolysis in fluorescent probe.[41]

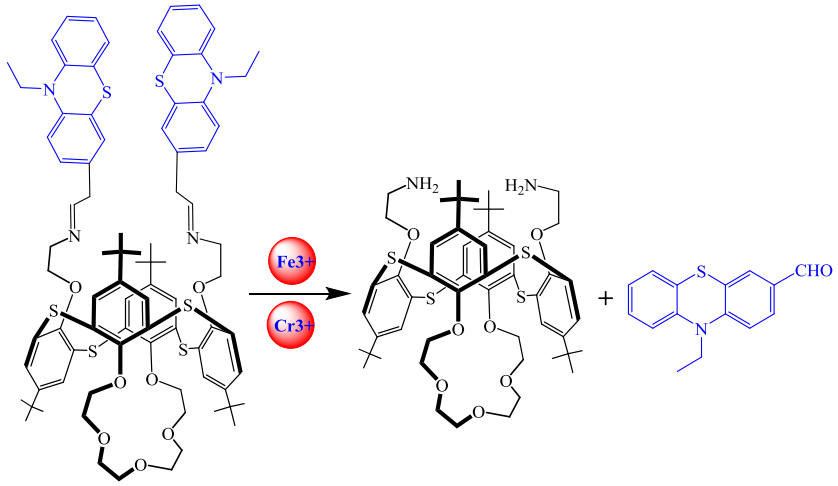

Figure 13. Proposed recognition mechanism of **17.**

1.2.7.2 Recognize anions

Jain *et al.* have synthesized a novel thiacalix[4]arene fluorescent probe **18** which employed quinoline as fluorophore. According to the UV-absorption and fluorescent emission spectra titration results, probe **18** exhibited highly selective recognize for F^- anion among other anions (Cl^-, Br^-, I^-, OH^-, CH_3COO^-, $H_2PO_4^-$ and PO_4^{-3}). Quenching and red shift in emission spectra constituting the signature detection for fluoride. This may be attributed to the photo-induced charge transfer (PCT) mechanism which can be induced by deprotonation of acidic NH proton in the presence of fluoride ion.[42]

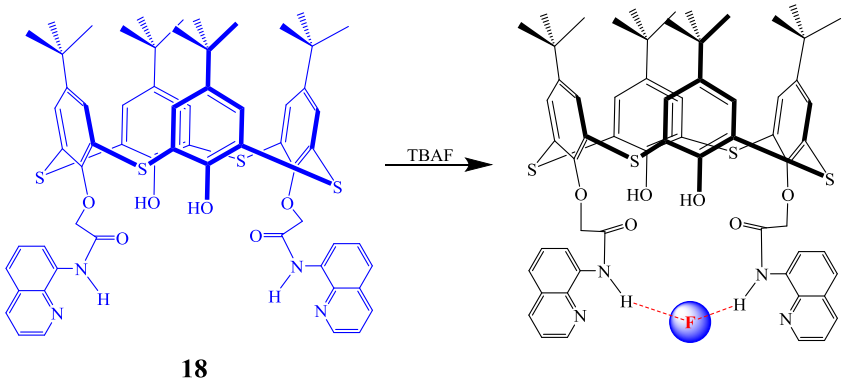

Figure 14. Proposed recognition mechanism of **18** towards $\mathbf{F^-}$.

1.2.8 Chromogenic Detection of Volatile Gases for Rapid Analysis

Jung *et al.* have demonstrated a rare example of a selective chemosensor for the detection of chloride-containing volatile gases (HCl, $SOCl_2$, $(COCl)_2$, and $COCl_2$) with interconversion between structures in the gel state. Two different color gels which were depended on the coordination geometry were formed by simple mixing thiacalix[4]arene-based ligand **19** and Co^{2+} ion. And the color can be interconverted by changing the coordination geometry. The filter paper coated with red color octahedral structure gel could be selectively changed to a blue color by exposure to the toxic VGCl HCl, $SOCl_2$, $(COCl)_2$, and $COCl_2$) gases. The color change was attributed to the change of the coordination geometry from octahedral to tetrahedral. Based on this unique phenomenon, they further developed a concept that using the camera in particular smartphones to fast detect VGCl gas with the help of the histogram of RGB in the Android and iOS application of smartphones.[43]

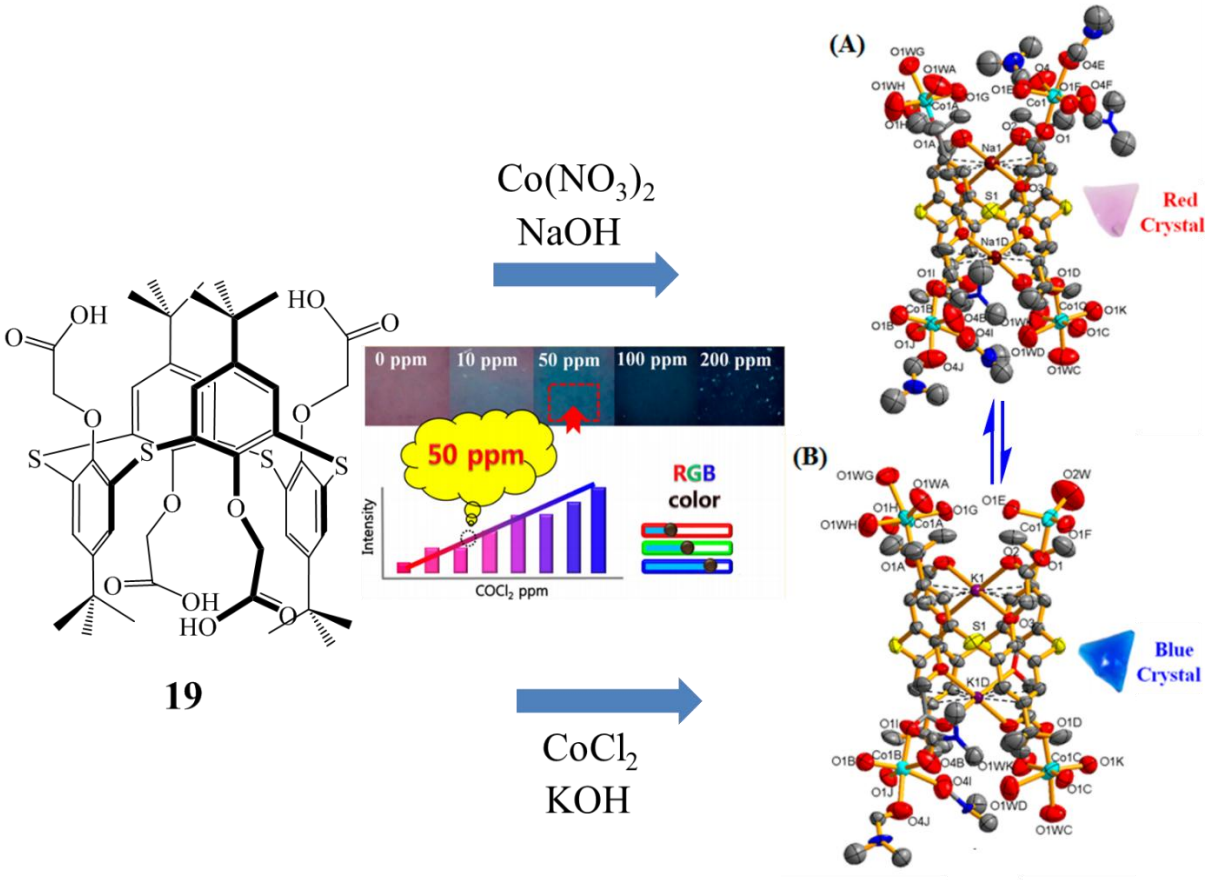

Figure 15. The proposed mechanism for detection of volatile gases by compound **19**.

1.2.9 In Living cell

Chemosensor **20** exhibited high selectivity towards Fe^{3+} ions by fluorescence quenching which was attributed to reverse photo-induced electron transfer (reverse PET) from pyrene units to the carbonyl oxygen atoms. Due to the Fe^{3+} played an important role in human body, and given that the better cell permeability and intracellular fluorescence Imaging of sensor **20**, the author further attempted to apply sensor **20** to monitor Fe^{3+} in living cell. When the living prostate cancer (PC3) cell lines were treated with sensor **20**, it showed strong blue fluorescence emission indicating its high permeability into living cells (Fig. 16). And then, if the treated cells further treated with increasing concentrations of Fe^{3+} (5.0 mM, 10 mM, 20 mM, 30 mM, 40 mM and 50 mM; Fig. 16D–I, respectively), a continuous quenching of intracellular fluorescence emission was observed (Fig. 16E–I). These results indicated that sensor **20** can be used as a Fe^{3+} selective biological sensor to monitor intracellular iron concentration and study its bioactivity in living cells.[44]

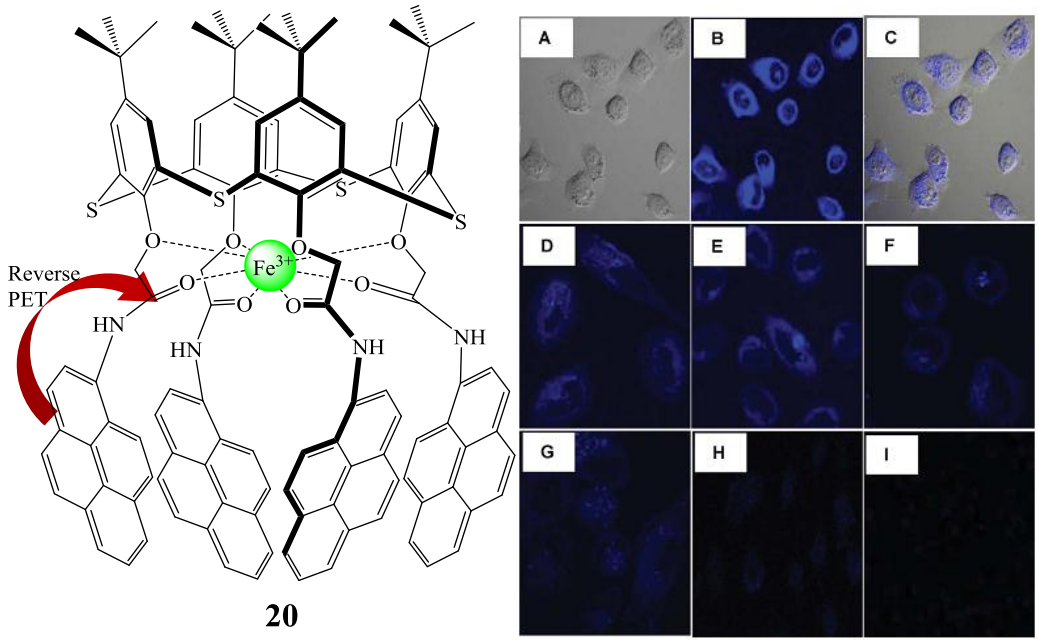

20

Figure 16. Fluorescence and bright field images of prostate cancer (PC3) cells in the presence of compound **20** and Fe^{3+} ions. (A) Bright field image and (B) Fluorescence image of PC3 cells stained with 20 mM of **20** for 2.5 h incubation at 37 ℃, λ_{ex} = 405; (C) Overlay image of (A) and (B); (D)–(I) Fluorescence images of PC3 cells stained with 20 mM of **20** for 2.5 h incubation followed by 5.0 mM (D), 10 mM (E), 20 mM (F), 30 mM (G), 40 mM (H), 50 mM(I) addition of Fe^{3+} ions for 30 min incubation.

1.2.10 Molecular logic gate

Molecular computing, a subarea of unconventional computing has attracted great attention,[45] involving various Boolean logic operations, such as XOR, OR, INH, AND, XNOR, and NOR gates at the molecular level.[46] However, due to the conventional silicon-based devices have been limited at the nanoscale. Thus, the development of materials for information storage and retrieval at the molecular level is urgent. Fluorescence spectroscopy is a useful tool for monitoring molecular events for the high sensitivity and their integration into molecular logic gates and devices. Herein, fluorescent probes based on thiacalix[4]arene were employed in an effort to mimic molecular logic devices such as crossword puzzles, molecular keypad locks, and information storage devices (memory units) involving the sequential integration of various logic gates into combinatorial circuits.[47]

Kumar *et al.* synthesized a florescent probe **21** which shown a selective turn-on fluorescence response *via* CN^- ions induced spirolactone ring opening of fluorescein (Fig. 17a). Furthermore, the resulting cyanide complex **21**·CN^- can further selectively applied to detect copper (Cu^{2+}) ions through fluorescence turn-off. Depending on the different chemical inputs (CN^- and Cu^{2+}) and fluorescence signals as outputs (on and off), they constructed a sequential logic circuit. Two inputs Cu^{2+} and CN^- were designated as In A and In B, respectively. "1" and"0" were designated as the "On" and "Off" states for the readout signals. The table (Table 1) reveals various combinations of inputs for "output" and the sequential logic circuit of "output" emission representing the set/reset element that corresponds to the memory device (Fig. 17b).[48]

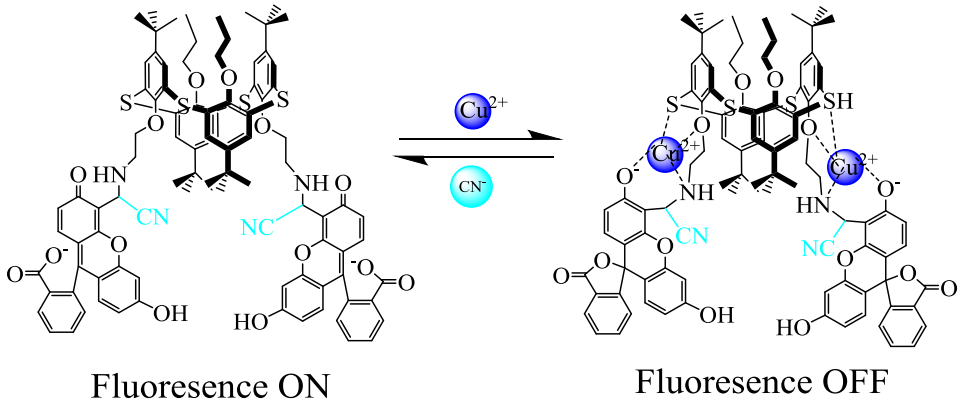

Figure 17a. Possible mechanism for interaction of compound **21** with CN^- and Cu^{2+} ions.

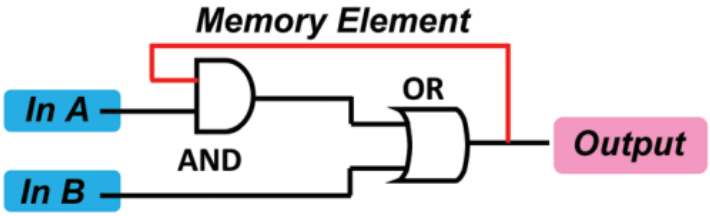

Table 1

Sr. No.	In A	In B	Output (528 nm)
1	0	0	0
2	1	0	0
3	0	1	1
4	1 (1st)	1 (2nd)	1
5	1 (2nd)	1 (1st)	0

Figure 17b. Sequential logic circuit displaying the memory unit with two inputs (In A and In B) and one output. Table 1 is the truth table for the sequential logic circuit.

1.2.11 Phase transfer catalyst

Yang *et al.* have designed two calixarene derivatives (**22** and **23**) and one reference compound (**24**) as phase transfer catalysts. The cavity size of thiacalix[4]arene derivative **22** is larger than the corresponding calix[4]arene derivative **23** due to the S-C bond is longer C-C bond. Compound **22** is comparative unstable and in a mixed conformation, however, compound **23** is stable in cone conformation. The experiments of phase transfer catalysis in water showed that both compounds **22** and **23** showed efficient catalytic properties for aromatic nucleophilic substitution reaction and benzyl nucleophilic substitution. However, the reference compound **24** did not show any catalytic ability. Additionally, it could be pointed out that the catalytic abilities of compound **23** were higher than compound **22**. It strongly suggested that the excellent catalytic abilities were attributed to the presence cavities of calixarene skeleton and the stable confirmation skeleton is more efficient for the catalysis than the unstable conformation.[49]

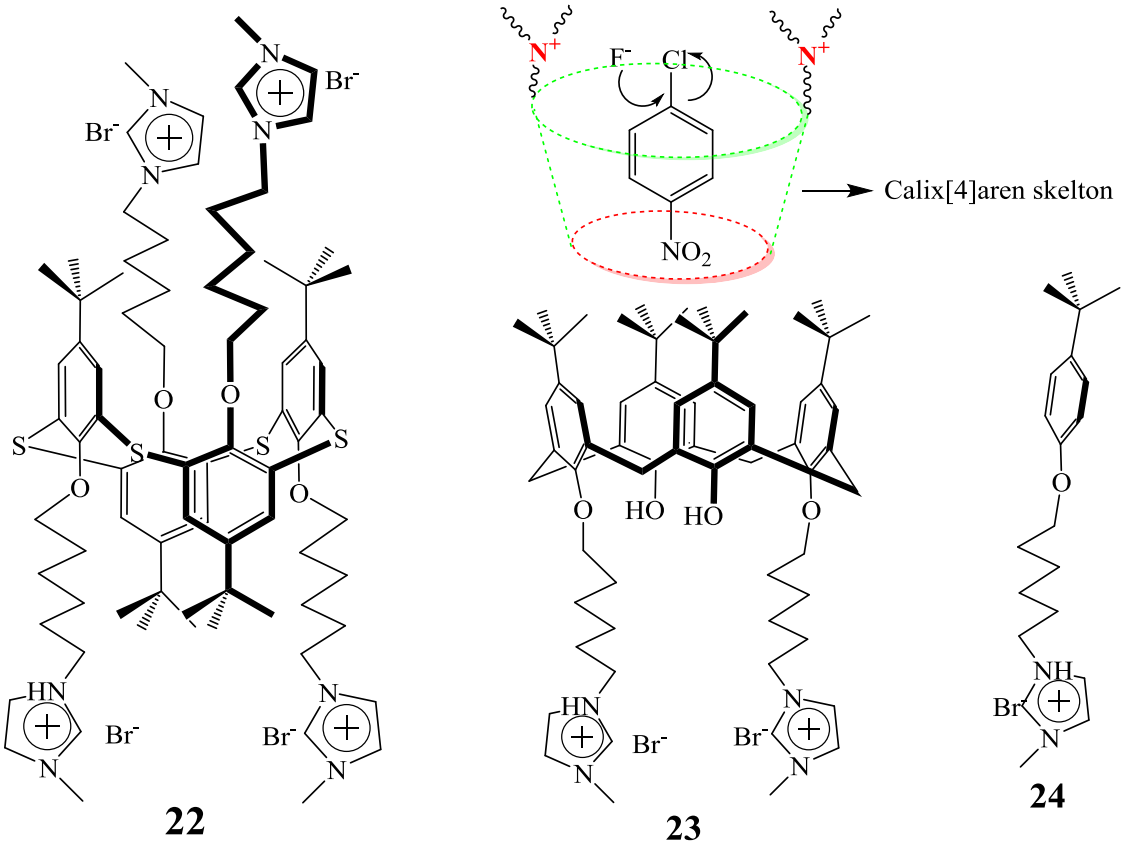

Figure 18. The molecular structure of **22**, **23** and **24**. And the proposal catalytic mechanismfor calixarene ionic liquid.

1.2.12 Modified electrode

1.2.12.1 Electrochemical aptasensor

Hianik *et al.* have developed a novel electrochemical aptasensor for ochratoxin A (OTA) detection base on an Au electrode consecutively coated with electropolymerized layers of neutral red and Ag nanoparticles. The Ag nanoparticles was modified with thiacalix[4]arene ligand **25** bearing catechol fragments. OTA against thiolated aptamers were covalently attached to Ag·**25** nanoparticles *via* S-Ag bonding. The conformational switch of the aptamer by the interaction with OTA, which caused increase of the charge transfer resistance measured by EIS in the presence of ferricyanide ions. The achieved *LOD* was lower to 0.05 nM which was lower than similar aptasensor with the aptamer chemisorbed on bare gold electrode.[50] Furthermore, the aptasensor was confirmed in spiked beer samples.[51]

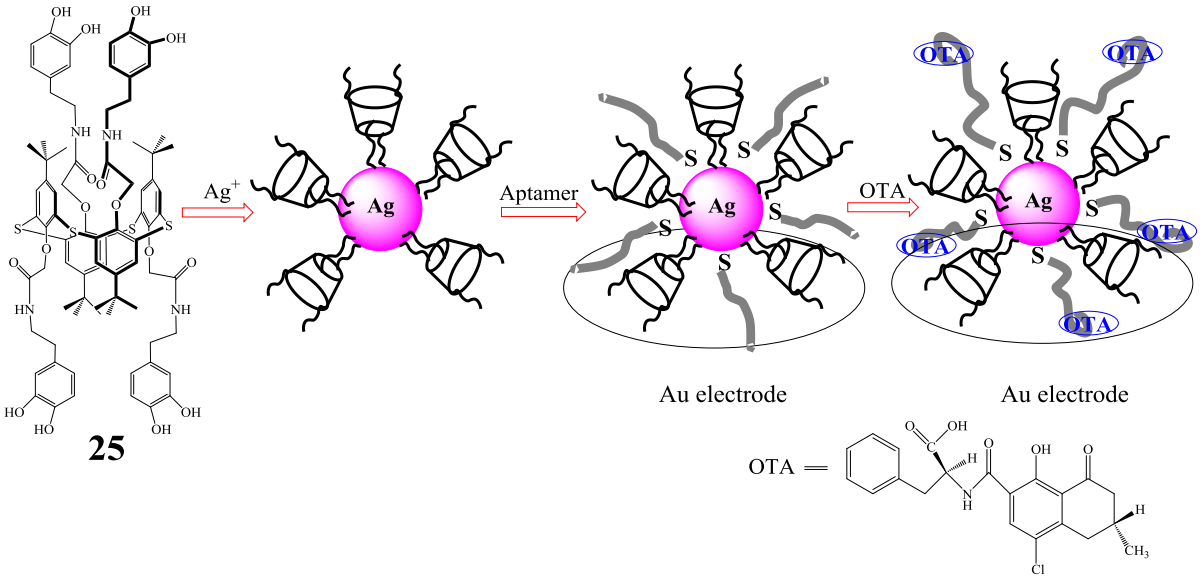

Figure 19. Schematic presentation of Ag nanoparticle synthesis and OTA measurement.

1.2.12.2 Discrimination of apple juice and herbal liqueur brands

Evtugyn *et al.* have designed solid-contact ion-selective electrodes which were based on glassy carbon electrode modified with electropolymerized polyaniline and tetrasubstituted thiacalix[4]arene ionophores with hexyl (**26**) and o-pyridylamido (**27**) functional groups at the lower rim. These solid-contact ion-selective electrodes have the capability to discriminate apple juices and herbal liqueurs brands. The discrimination procedure as follow: firstly, the tested liquids were diluted and spiked with a constant amount of Fe^{3+} ions; and then achieved the variation of the signal for Fe^{3+} ions attribute to their involvement in the reactions with the organic ligands and the antioxidants present. Finally, combination of the three electrodes with various receptors made it possible to discriminate the brands of apple juices and herbal liqueurs by linear discriminant analysis in 95–100% cases. The discrimination procedure was in a short time (20min). Furthermore, we can employ these modified electrodes to detect individual antioxidants in a wide range (5.0×10^{-6} to 1.0×10^{-2} M) by direct potentiometric measurements and redox titration.[52]

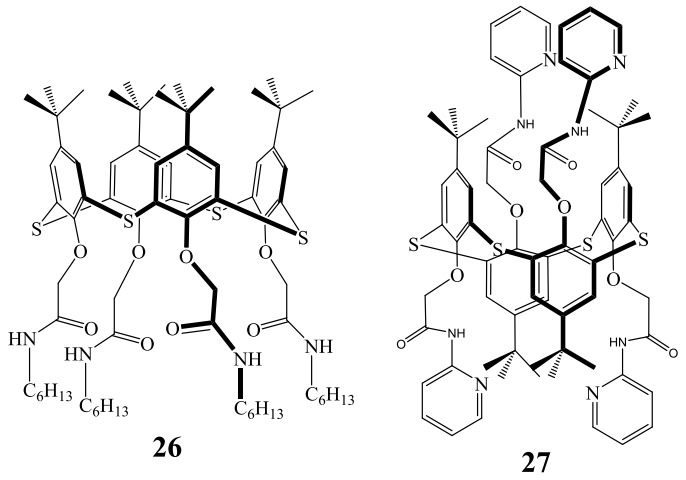

26 **27**

Figure 20. The molecular structure of **26** and **27**.

1.2.13 Supramolecular polymeric materials

Li *et al.* synthesized a novel 1,3-*alternate* thiacalixarene derivatives **28** containing triazole groups by click chemistry. ^{1}H NMR titration experiments revealed that compound **28** was a good Ag^{+} receptors. Further AFM studies revealed that compound **28** formed nanorod-shaped self-aggregates which was induced by silver ions in $CHCl_3$ solutions. The author pointed out that these kind of compounds were potentially applicable to design sophisticated polymeric materials with excellent responsive properties for Ag^{+}.[53]

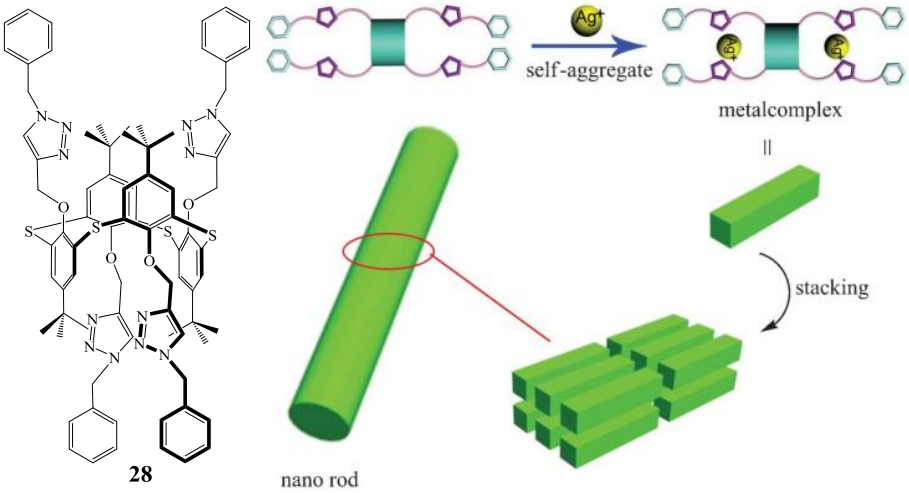

Figure 21. Left: The molecular structure of **28**. Right: Schematic representation of the spherical aggregates assisted by Ag^{+}.

1.2.14 Preparation of nanoparticles

Zhu *et al.* have successfully developed a facile synthesis method for preparation of gold nanoparticles (AuNPs) by using a novel amphiphilic *p-tert*-butyl thiacalix[4]arene grafted with poly(ethylene glycol) monomethyl ether (**29**) under mild conditions. They observed that the presence of poly(ethylene glycol) monomethyl ether (**29**) moiety acted as stabilizer and reductant, the phenolic groups of **29** without poly(ethylene glycol) chain would be oxidized to benzoquinone of **30**. Furthermore, the nanoparticle sizes of AuNPs can be readily controlled by simply adjusting the feeding ratio of $HAuCl_4$/**29**.[54]

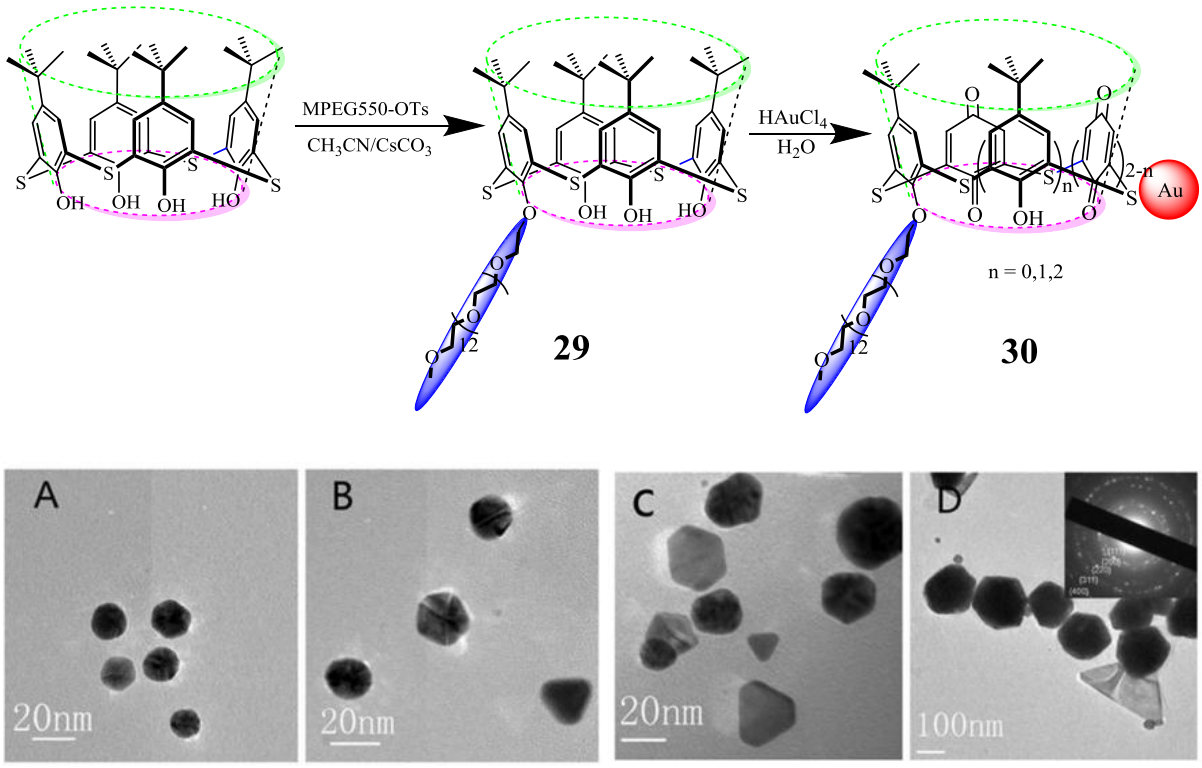

Figure 22. Up: Synthesis of **29** and preparation of **30**. The number of quinone groups depends on the addition of chloroaurate acid. Bottom: HRTEM images of samples A, B, C, D and electron diffraction pattern of sample D. Nanoparticle sizes of AuNPs can be readily controlled by simply adjusting the feeding ratio of Au/S

1.2.15 Non-linear optical material

Parola *et al.* selectively modified thiacalixarenes with phenylazo, ethynylic groups, imino or platinum derived acetylides, which have the potential application in non-linear optical material. These were confirmed by the nonlinear absorption and optical limiting measurements. For instance, the *1,3-alternate* bifunctionalised macrocycle derivative **31** was modified with two different functional groups, one is used for its optical properties and another one is as a precursor for the sol-gel process. Thus, the preparation of nanoscaled homogeneous hybrid materials can be realized by controlling the sol-gel process from the functionalized alkoxide at the molecular level. Besides, these macrocycles are highly soluble in organic solvents and can easily be embedded in inorganic matrix by using the sol-gel routes.[55]

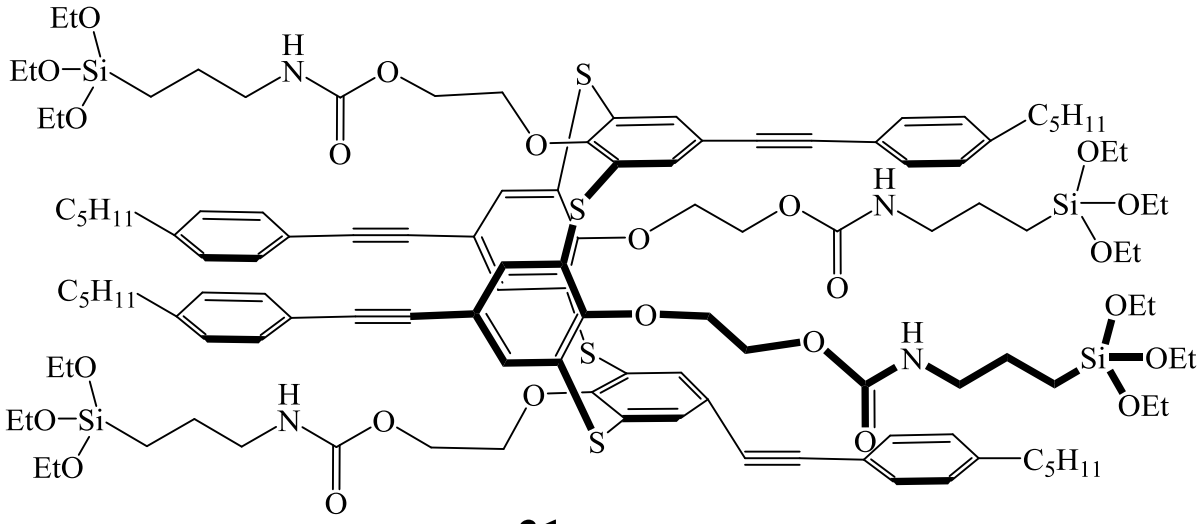

31

Figure 23. Example of designed sol-gel precursor for nanohybrid optical materials.

1.3 Conclusion

In summary, thiacalix[4]arene derivitives not only exhibited higher affinity toward cations (Figure 24, red color marked cations which have been reported) and anions (F^-, Cl^-, Br^-, CN^-, $PhCOO^-$, $H_2PO_4^-$, OAc^-,), but also showed good affinity toward neutral moleculars

(CH_3CN, CH_3NO_2, CH_3COCH_3, EtOAc, DMSO, CH_2Cl_2, $CHCl_3$, *n*-butanol, Cysteine, EtOH, EtCOOH).

^{1}H																^{2}He
^{3}Li	^{4}Be											^{5}B	^{6}C	^{7}N	^{8}O	^{9}F	^{10}Ne
^{11}Na	^{12}Mg											^{13}Al	^{14}Si	^{15}P	^{16}S	^{17}Cl	^{18}Ar
^{19}K	^{20}Ca	^{21}Sc	^{22}Ti	^{23}V	^{24}Cr	^{25}Mn	^{26}Fe	^{27}Co	^{28}Ni	^{29}Cu	^{30}Zn	^{31}Ga	^{32}Ge	^{33}As	^{34}Se	^{35}Br	^{36}Kr
^{37}Rb	^{38}Sr	^{39}Y	^{40}Zr	^{41}Nb	^{42}Mo	^{43}Tc	^{44}Ru	^{45}Rh	^{46}Pd	^{47}Ag	^{48}Cd	^{49}In	^{50}Sn	^{51}Sb	^{52}Te	^{53}I	^{54}Xe
^{55}Cs	^{56}Ba	L	^{72}Hf	^{73}Ta	^{74}W	^{75}Re	^{76}Os	^{77}Ir	^{78}Pt	^{79}Au	^{80}Hg	^{81}Tl	^{82}Pb	^{83}Bi	^{84}Po	^{85}At	^{86}Rn
^{87}Fr	^{88}Ra	A	^{104}Rf	^{105}Db	^{106}Sg	^{107}Bh	^{108}Hs	^{109}Mt	^{110}Ds	^{111}Rg	^{112}Cn	^{113}Uut	^{114}Uuq	^{115}Uup	^{116}Uuh	^{117}Uus	^{118}Uuo

L	^{57}La	^{58}Ce	^{59}Pr	^{60}Nd	^{61}Pm	^{62}Sm	^{63}Eu	^{64}Gd	^{65}Tb	^{66}Dy	^{67}Ho	^{68}Er	^{69}Tm	^{70}Yb	^{71}Lu
A	^{89}Ac	^{90}Th	^{91}Pa	^{92}U	^{93}Np	^{94}Pu	^{95}Am	^{96}Cm	^{97}Bk	^{98}Cf	^{99}Es	^{100}Fm	^{101}Md	^{102}No	^{103}Lr

Figure 24. The red color marked ions which have been reported higher affinity toward thiacliax[4]arene derivatives (until 2016. Feb.).

Since the discovery of a practical method by Miyano *et al.* for the synthesis of sulfur-bridged thiacalixarenes, studies on their modification and development of the functions are now vividly progressing. During the past 20 years, although many efforts have been devoted in thiacalixarene chemistry. However, compare to the conventional calixarene chemistry, there is still a lot of space worthy of us to explore in the future (Fig. 25). Thus, we further explored the synthesis and application of thiacalix[4]arenes in this thesis.

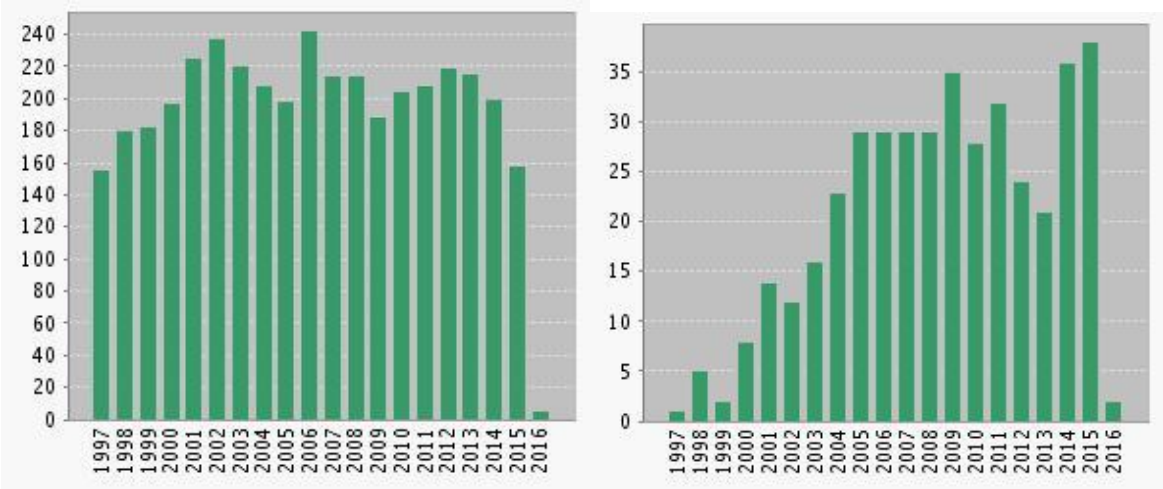

Figure 25. Left: The published papers about calixarene chemistry; Right: The published papers about thiacalixarene chemistry. The data which is obtained from Web of Knowledge, the Thomson corporation by searching the research topic of calixarene or thiacliaxrene.

1.4 References

1. D. J. Cram, *Angew. Chem., Int. Ed.*, 1998, **27**, 1009–1020.
2. J.-M. Lehn, *Angew. Chem., Int. Ed.*, 1998, **27**, 89–112.
3. C. J. Pedersen, *Angew. Chem., Int. Ed.*, 1998, **27**, 1021–1027.
4. (*a*) J. L. Atwood and J. W. Steed, *Encyclopedia of Supramolecular Chemistry*, Taylor & Francis Group: New York, 2005; (*b*) V. Balzani, and L. D. Cola, *Supramolecular Chemistry*, Kluwer Academic: Dordrecht, Netherlands, 1992; (*c*) J.-M. Lehn, *Supramolecular Chemistry. Concepts and Perspectives*, Wiley-VCH: Weinheim, Germany, 1995. (*d*) J. W. Steed, D. R. Turner and K. J. Wallace, *Core Concepts in Supramolecular Chemistry and Nanochemistry*, John Wiley and Sons: West Sussex, U.K., 2007.
5. C. D. Gutsche, *in Calixarenes Revisited, Monographs in Supramolecular Chemistry*, ed. J. F. Stoddart, The Royal Society of Chemistry, Cambridge, 1998.
6. S. Shinkai, *Calixarenes as Third Supramolecular Host, in Advances in Supramolecular Chemistry*, JAI Press Inc., 1993.
7. *Cation Binding by Macrocycles*, ed. Y. Inoue and G. W. Gokel, Marcel Dekker, New York, 1990.
8. J. Szejtli, *Cyclodextrins and their Inclusion Complexes*, Akademjai Kiado, Budapest, 1982.
9. (*a*) Y. Ohba, K. Moriya and T. Sone, *Bull. Chem. Soc. Jpn.*, 1991, **64**, 576–582; (*b*) T. Sone, Y. Ohba, K. Moriya and H. Kumada, *Workshop on Calixarenes and Related Compounds*, Abstr.No. B-36, 2-4 June 1993, Kurume, Japan; (*c*) T. Sone, Y. Ohba, K. Moriya, H. Kumada and K. Ito, *Tetrahedron*, 1997, **53**, 10689–10698;
10. (*a*) A. J. Neale, P. J. S. Bain, T. J. Rawlings, *Tetrahedron*, 1969, **25**, 4593–4597; (*b*) T. Hori, S. Ueda, T. Kojima and H. Kumagai, *Sekiyu Gakkaishi*, 1991, **34**, 446–451.
11. H. Kumagai, M. Hasegawa, S. Miyanari, Y. Sugawa, Y. Sato, T. Hori, S. Ueda, H. Kamiyama and S. Miyano, *Tetrahedron Lett.*, 1997, **38**, 3971–3972.
12. N. Iki, C. Kabuto, T. Fukushima, H. Kumagai, H. Takeya, S. Miyanari, T. Miyashi and S. Miyano, *Tetrahedron*, 2000, **56**, 1437–1443.
13. N. Kon, N. Iki and S. Miyano, *Tetrahedron Lett.*, 2002, **43**, 2231–2234.
14. H. Akdas, L. Bringel, E. Graf, M. W. Hosseini, G. Mislin, J. Pansanel, A. D. Cian and J. Fischer, *Tetrahedron Lett.*, 1998, **39**, 2311–2314.

15. (*a*) P. Lhotak, V. Stanstny, P. Zlatuskova, I. Stibor, V. Michlova, M. Tkadlecova, J. Havelicek and J. Sykora, *Collect. Czech.Chem. Commun.*, 2000, **65**, 757–771; (*b*) K. Iwamoto and S. Shinkai, *J. Org. Chem.*, 1992, **57**, 7066–7073; (*c*) A. A. Tyuftin, S. E. Solovieva, A. A. Muravev, F. M. Polyantsev, S. K. Latypov and I. S. Antipin, *Russ. Chem. Bull., Int. Ed.*, 2009, **58**, 145–151; (*d*) S. N. Podyachev, S. N. Sudakova, B. M. Gabidullin, V. V. Syakaev, A. T. Gubaidullin, W. Dehaen and A. I. Konovalov, *Tetrahedron Lett.*, 2012, **53**, 3135–3139.
16. (*a*) X. Hu, H. Shi, X. Shi, Z. Zhu, Q. Sun, Y. Li and H. Yang, *Bull. Chem. Soc. Jpn.*, 2005, **78**, 138–141; (*b*) H. Akdas, E. Graf, M. W. Hosseini, A. D. Cian and N. K. Gruber, *C. R. Chim.*, 2003, **6**, 565–572; (*c*) M. Simanova, H. Dvorakova, I. Stibor, M. Pojarova and P. Lhotak, *Tetrahedron Lett.*, 2008, **49**, 1026–1029; (*d*) S. Akabori, H. Sannohe, Y. Habata, Y. Mukoyama and T. Ishii, *Chem. Commun.*, 1996, 1467–1468.
17. I. I. Stoikov, O. A. Mostovaya, A. A. Yantemirova, I. S. Antipin and A. I. Konovalov, *Mendeleev Commun.*, 2012, **22**, 21–22.
18. I. I. Stoikov, O. A. Mostovaya, I. S. Antipin, A. I. Konovalov, M. Gruner and W. D. Habicher, *Russ. Chem. Bull., Int. Ed.*, 2007, **56**, 307–312.
19. (*a*) N. Morohashi, F. Narumi, N. Iki, T. Hattori and S. Miyano, *Chem. Rev.*, 2006, **106**, 5291–5316; (*b*) R. Kumar, Y. O. Lee, V. Bhalla, M. Kumar and J. S. Kim, *Chem. Soc. Rev.*, 2014, **43**, 4824–4870.
20. (*a*) P. Lhotak, M. Himl, I. Stibor, J. Sykora and I. Cisarova, *Tetrahedron Lett.*, 2001, **42**, 7107–7110; (*b*) P. Lhotak, J. Svoboda, I. Stibor and J. Sykora, *Tetrahedron Lett.*, 2002, **43**, 7413–7417; (*c*) P. Lhotak, M. Himl, I. Stibor, J. Sykora and I. Cisarova, *Tetrahedron Lett.*, 2001, **42**, 7107–7110; (*d*) O. Kasyan, D. Swierczynski, A. Drapailo, K. Suwinska, J. Lipkowski and V. Kalchenko, *Tetrahedron Lett.*, 2003, **44**, 7167–7170.
21. (*a*) X. Hu, H. Shi, X. Shi, Z. Zhu, Q. Sun, Y. Li and H. Yang, *Bull. Chem. Soc. Jpn.*, 2005, **78**, 138–141; (*b*) X. Hu, N. Xia, F. Ye, J. Ren and X. Shi, *Spectrochim. Acta, part A*, 2004, **60**, 1427–1430; (*c*) O. Kasyan, V. Kalchenko, M. Bolte and V. Boehmer, *Chem. Commun.*, 2006, 1932–1934; (*d*) Y. K. Agrawal and J. P. Pancholi, *Synth. Commun.*, 2008, **38**, 2446–2458; (*e*) O. Kundrat, J. Kroupa, S. Bohm, J. Budka, V. Eigner and P. Lhotak, *J. Org. Chem.*, 2010, **75**, 8372–8375.

22. (*a*) O. Kundrat, I. Cisarova, S. Bohm, M. Pojarova and P. Lhotak, *J. Org. Chem.*, 2009, **74**, 4592–4596; (*b*) O. Kundrat, H. Dvorakova, I. Cisarova, M. Pojarova and P. Lhotak, *Org. Lett.*, 2009, **11**, 4188–4191; (*c*) O. Kundrat, H. Dvorakova, V. Eigner and P. Lhotak, *J. Org. Chem.*, 2010, **75**, 407–411.
23. N. Iki, T. Fujimoto and S. Miyano, *Chem. Lett.*, 1998, 625–626.
24. (*a*) N. Iki, H. Kumagai, N. Morohashi, K. Ejima, M. Hasegawa, S. Miyanari and S. Miyano, *Tetrahedron Lett.*, 1998, **39**, 7559–7562; (*b*) N. Morohashi, N. Iki, A. Sugawara and S. Miyano, *Tetrahedron*, 2001, **57**, 5557–5563; (*c*) G. Mislin, E. Graf, M. W. Hosseini, A. De Cian and J. Fischer, *Chem. Commun.*, 1998, 1345–1346; (*d*) G. Mislin, E. Graf, M. W. Hosseini, A. De Cian and J. Fischer, *Tetrahedron Lett.*, 1999, **40**, 1129–1132
25. P. Lhotak, M. Himl, I. Stibor, J. Sykora, H. Dvorakova, J. Lang and H. Petrickova, *Tetrahedron*, 2003, **59**, 7581–7585.
26. N. Morohashi, F. Narumi, N. Iki, T. Hattori and S. Miyano, *Chem. Rev.*, 2006, **106**, 5291–5316.
27. (*a*) F. Botha, J. Budka, V. Eigner, O. Hudeček, L. Vrzal, I. Císařová and P. Lhoták, *Tetrahedron*, 2014, **70**, 477–483; (*b*) H. Zhao, J. Zhan, Z. Zou, F. Miao, H. Chen, L. Zhang, X. Cao, D. Tian and H. Li, *RSC Adv.*, 2013, **3**, 1029–1032; (*c*) F. Miao, J. Zhan, Z. Zou, D. Tian and H. Li, *Tetrahedron*, 2012, **68**, 2409–2413.
28. (*a*) H. Akdas, L. Bringel, E. Graf, M. W. Hosseini, G. Mislin, J. Pansanel, A. De Cian and J. Fischer, *Tetrahedron Lett.*, 1998, **39**, 2311–2314; (*b*) N. Iki, C. Kabuto, T. Fukushima, H. Kumagai, H. Takeya, S. Miyanari, T. Miyashi and S. Miyano, *Tetrahedron*, 2000, **56**, 1437–1443; (*c*) A. Bilyk, A. K. Hall, J. M. Harrowfield, M. W. Hosseini, B. W. Skelton and A. H. White, *Inorg. Chem.*, 2001, **40**, 672–686; (*d*) J. Hong, C. Yang, Y. Z. Li, G. S. Yang, C. Jin, Z. J. Guo and L. G. Zhu, *J. Mol. Struct.*, 2003, **655**, 435–441.
29. S. Chen, H. Guo, F. Yang and X. Di, *Journal of Polymer Research*, 2016, **23**, 1–12.
30. A. B. Thompson, S. J. Cope, T. D. Swift and J. M. Notestein, *Langmuir*, 2011, **27**, 11990–11998.
31. X. Zhou, Y. Koizumi, M. Zhang, M. Natsui, S. Koyota, M. Yamada, Y. Kondo, F. Hamada and T. Sugiyama, *Cancer Sci.*, 2015, **106**, 635–641.

32. J. Hong and S. Ham, *Tetrahedron Lett*., 2008, **49**, 2393–2396.
33. A. I. Vovk, L. A. Kononets, V. Y. Tanchuk, A. B. Drapailo, V. I. Kalchenko and V. P. Kukhar, *J. Incl. Phenom. Macrocycl. Chem.*, 2010, **66**, 271–277.
34. M. R. Gandhi, M. Yamada, Y. Kondo, A. Shibayama and F. Hamada, *Hydrometallurgy*, 2015, **151**, 133–140.
35. O. A. Mostovaya, M. N. Agafonova, A. V. Galukhin, B. I. Khayrutdinov, D. Islamov, O. N. Kataeva, I. S. Antipin, A. I. Konovalov and I. I. Stoikov, *J. Phys. Org. Chem.*, 2014, **27**, 57–65.
36. M. Mackova, J. Miksatko, J. Budka, V. Eigner, P. Curinova and P. Lhotak, *New J. Chem.*, 2015, **39**, 1382–1389.
37. N. Iki, F. Narumi, T. Suzuki, A. Sugawara and S. Miyano, *Chem. Lett.*, 1998, 1065-1066.
38. H. Tomiyasu, J.-L. Zhao, X.-L. Ni, X. Zeng, M. R. J. Elsegood, B. Jones, C. Redshaw, S. J. Teate and T. Yamato, *Rsc Adv.*, 2015, **5**, 14747–14755.
39. (*a*) P. Jiang, Z. Guo, *Coord. Chem. Rev.*, 2004, **248**, 205–229; (*b*) J. S. Kim, D. T. Quang, *Chem. Rev.*, 2007, **107**, 3780–3799; (*c*) Z. Xu, J. Yoon, D. R. Spring, *Chem. Soc. Rev.*, 2010, **39**, 1996–2006; (*d*) P. Kaur, K. Singh, *RSC Adv.*, 2014, **4**, 11980–11999.
40. M. Narita, Y. Higuchi, F. Hamada and H. Kumagai, *Tetrahedron Lett.*, 1998, **39**, 8687–8690.
41. Q. Sun, L. Mu, X. Zeng, J. Zhao, T. Yamato and J. Zhang, *Sci. China Chem.*, 2015, **58**, 539–544.
42. S. M. Darjee, D. R. Mishra, K. D. Bhatt, D. J. Vyas, K. M. Modi and V. K. Jain, *Tetrahedron Lett.*, 2014, **55**, 7094–7098.
43. K. Y. Kim, S. Park, S. H. Jung, S. S. Lee, K.-M. Park, S. Shinkai and J. H. Jung, *Inorg. Chem.*, 2014, **53**, 3004–3011.
44. M. Kumar, R. Kumar, V. Bhalla, P. R. Sharma, T. Kaurb and Y. Qurishi, *Dalton Trans.*, 2012, **41**, 408–412.
45. (*a*) *Unconventional Computing: From Cellular Automata to Wetware*, ed. C. Teuscher and A. Adamatzky and C. Luniver Press, Beckington, UK, 2005; (*b*) *Molecular Machines (special issue),* Acc. Chem. Res., 2001, **34**, 409–522.

46. (*a*) M. Kumar, R. Kumar and V. Bhalla, *Org. Biomol. Chem.*, 2011, **9**, 8237–8245; (*b*) Y. Li, W. Yang, Y. Chen and S. Gong, *CrystEngComm*, 2011, **13**, 259–268; (*c*) B.-T. Zhao, Z. Zhou and Z.-N. Yan, *J. Chem. Sci.*, 2009, **121**, 1047–1052; (*d*) O. Kasyan, V. Rudzevich, M. Bolte and V. Bohmer, *J. Chem. Crystallogr.*, 2011, **41**, 332–337; (*e*) F. Hamada, M. Yamada, Y. Kondo, S. Ito and U. Akiba, *CrystEngComm*., 2011, **13**, 6920–6922; (*f*) J. Sykora, M. Himl, I. Stibor, I. Cısarova and P. Lhotak, *Tetrahedron*, 2007, **63**, 2244–2248.
47. (*a*) D. Margulies, C. E. Felder, G. Melman and A. Shanzer, *J. Am. Chem. Soc.*, 2007, **129**, 347–354; (*b*) M. Kumar, A. Dhir and V. Bhalla, *Org. Lett.*, 2009, **11**, 2567–2570; (*c*) M. Kumar, R. Kumar and V. Bhalla, *Chem. Commun.*, 2009, 7384–7386; (*d*) M. Kumar, R. Kumar and V. Bhalla, *RSC Adv.*, 2011, **1**, 1045–1049; (*e*) M. Kumar, R. Kumar and V. Bhalla, *Org. Lett.*, 2011, **13**, 366–369.
48. N. Sharma, S. I. Reja, V. Bhalla and M. Kumar, *Dalton Trans.*, 2014, **43**, 15929–15936.
49. F. Yang, H. Guo, Z. Jiao, C. Li and J. Ye, *J. Iran. Chem. Soc.*, 2012, **9**, 327–332.
50. G. Castillo, I. Lamberti, L. Mosiello, T. Hianik, *Electroanal.*, 2012, **24**, 512–520.
51. G. Evtugyn, A. Porfireva, R. Sitdikov, V. Evtugyn, I. Stoikov, I. Antipin and T. Hianik, *Electroanal.*, 2013, **25**, 1847–1854.
52. G. A. Evtugyn, S. V. Belyakova, R. V. Shamagsumova, A. A. Saveliev, A. N. Ivanov, E. E. Stoikova, N. N. Dolgova, I. I. Stoikov, I. S. Antipin and H. C. Budnikov, *Talanta*, 2010, **82**, 613–619.
53. H. Zhao, J. Zhan, Z. Zou, F. Miao, H. Chen, L. Zhang, X. Cao, D. Tian and H. Li, *Rsc Adv.*, 2013, **3**, 1029–1032.
54. C. Tu, G. Li, Y. Shi, X. Yu, Y. Jiang, Q. Zhu, J. Liang, Y. Gao, D. Yan, J. Sun and X. Zhu, *Chem. Commun.*, 2009, 3211–3213.
55. C. Desroches, S. Parola, D. Cornu, P. Miele, P. L. Baldeck and C. Lopes, *Organic and Polymeric Materials and Devices*, eds. P. W. M. Blom, N. C. Greenham, C. D. Dimitrakopoulos and C. D. Frisbie, 2003, **771**, 237–242.

Chapter 2

An Efficient Cu^{2+} Fluorescent Probe Based on Thiacalix[4]arene Armed with Pyrene Group

This chapter focused on the synthesis, structure and complexation behavior of 1,3-alternate-1,2,3-triazole based on thiacalix-[4]arene probe, which was capable of acting as an efficient ratiometric fluorescent chemosensor at low ion concentration or as a fluorescence quenching type chemosensor in high ionic strength solution.

2.1 Introduction

Of the many application of thiacalix[4]arene derivatives, fluorescent probe based on thiacalix[4]arene is of special interest due to the high sensitivity and selectivity. Especially for the high selectivity which is possibly attribute to the shielding effect from thiacalix[4]arene platform. Thus, we firstly investigated the application of thiacalix[4]arene derivative as a fluorescent probe in this chapter.

Copper is the third most abundant essential trace element in the human body and plays a critical role in various biological processes.[1] For instance, copper is a catalytic cofactor for a variety of metalloenzymes, including cytochrome oxidase, superoxide dismutase and tyrosinase.[1,2] However, it can often be toxic to some biological systems when the amount of Cu^{2+} exceed cellular needs. Excess levels of the Cu(II) ion in the human body can cause gastrointestinal problems, kidney damage and Wilson's disease,[3] and are associated with brain diseases such as Parkinson's, Alzheimer's, Huntington's and prion diseases.[1c,4] Hence, the U.S. Environmental Protection Agency has set the limit of copper to be 1.3 ppm (~20 μM) in drinking water. Also, the average concentration of blood copper is 100–150 μg/dL (15.7–23.6 μM) in the normal group.[5]

In view of the importance of the Cu(II) ion, a lot of Cu^{2+} selective sensors have been developed recently.[6,7] Of those sensors, fluorescent probes appear to be particularly attractive over the other methods due to their specificity, high selectivity, high sensitivity and real-time monitoring with fast response times.[7] However, Cu^{2+} presents an inherent problem for fluorescent sensing due to the preferential quenching of the fluorescence by mechanisms inherent to paramagnetic species.[8] Most of the conventional Cu^{2+} probes generally show low sensitivity, and even more, low selectivity.[9] Additionally, most of the probes are based on single emission intensity changes such as fluorescence quenching[10] or enhancement,[11] which tend to be affected by a lot of uncontrollable factors such as instrument efficiency, probe molecule concentration, and micro-environment.[12]

In order to overcome these disadvantages, ratiometric fluorescent probes have been well developed in recent years.[13] Ratiometric fluorescent measurements observe changes in the ratio of the intensities of the emission at two wavelengths. In other words, ratiometric fluorescent probes have unique features that can be employed to provide a built–in correction

for environmental effects.[12] Among the various fluorophores, pyrene exhibits monomer–excimer dual emission wavelength fluorescence,[14] and the fluorescence intensity ratio of the excimer to monomer emission (I_{Ex}/I_M) is sensitive to conformational changes of the pyrene–functionalized system.[8a,15] Additionally, pyrene possesses photophysical properties that make it appropriate for such purposes due to its high fluorescence quantum yield, chemical stability, and long fluorescence lifetime.[16] Thus, pyrene has been employed as fluorophore in this chapter.

Based on our previous research,[17] a good fluorescent probe not only contains an efficient fluorophore, but also needs to consider the geometry of the coordination sites for a specific cation (or anion). In general, copper ion can be coordinated with soft heteroatoms, such as electron donors nitrogen and sulfur.[18] Thiacalix[4]arenes are widely exploited as a molecular platform for many fluorescent probes in the construction of selective binding sites given its structural tunableness, various conformations and given that it allows for the facile introduction of fluorophores.[19] Recently, we have reported that a pyrenyl-linked triazole-modified thiacalix[4]arene fluorescent probe displayed high affinity toward silver ion by changing the monomer and excimer emission. However, other heavy metal ions, especially Cu^{2+} and Hg^{2+} can also strongly quench both the monomer and excimer emission of pyrene.[20] We have also reported fluorescent probe with similar structures namely, pyrenyl-linked triazole-modified homooxacalix[3]arene. It is noteworthy to point out that the fluorescent probe possessing acetate groups (–CH_2COO–) linking the triazole groups to the homooxacalix[3]arene exhibite a higher selectivity than the other in which the triazole groups are directly linked to the lower rim oxygen atoms.[21] Therefore, we hypothesized that by analogy, introducing similar acetate group-linkages between the triazolyl-pyrenyl groups and the thiacalix[4]arene should help to improve the selectivity.

In this chapter, we report on the synthesis, crystal structures and complexation properties of fluorescent probe **L** based on thiacalix[4]arene scaffold armed with pyrene as a fluorophore.

2.2 Results and Discussion

2.2.1 Syntheses of fluorescent probe L

The synthetic route of fluorescent probe **L** is shown in Scheme 1. The synthesis of the parent compound **1**, **2** and **3** were carried out according to the reported procedure.[22] Recently, we reported the synthesis of hexahomotrioxacalix[3]arene triacetic acid with propargyl alcohol, obtained by the Steglich esterification reaction with 1,3-dicyclohexylcarbodiimide (DCC) as a coupling reagent and 4-(*N*,*N*-dimethylamino)pyridine (DMAP) as a catalyst.[21] However, following the above-mentioned method, we found that the reaction of the thiacalix[4]arene derivative **3**, even with a large excess of propargyl alcohol, only leads to the expected product **4** in a very low yield. Fortunately, an alternative, an efficient route was found by using propargyl bromide in the presence of K_2CO_3 as base, and we successfully obtained product **4** in high yield (73%). Following this, the click reaction, *i.e.* Cu(I)-catalysed azide–alkyne cycloaddition, was used to synthesize the new fluorescent probe **L**.

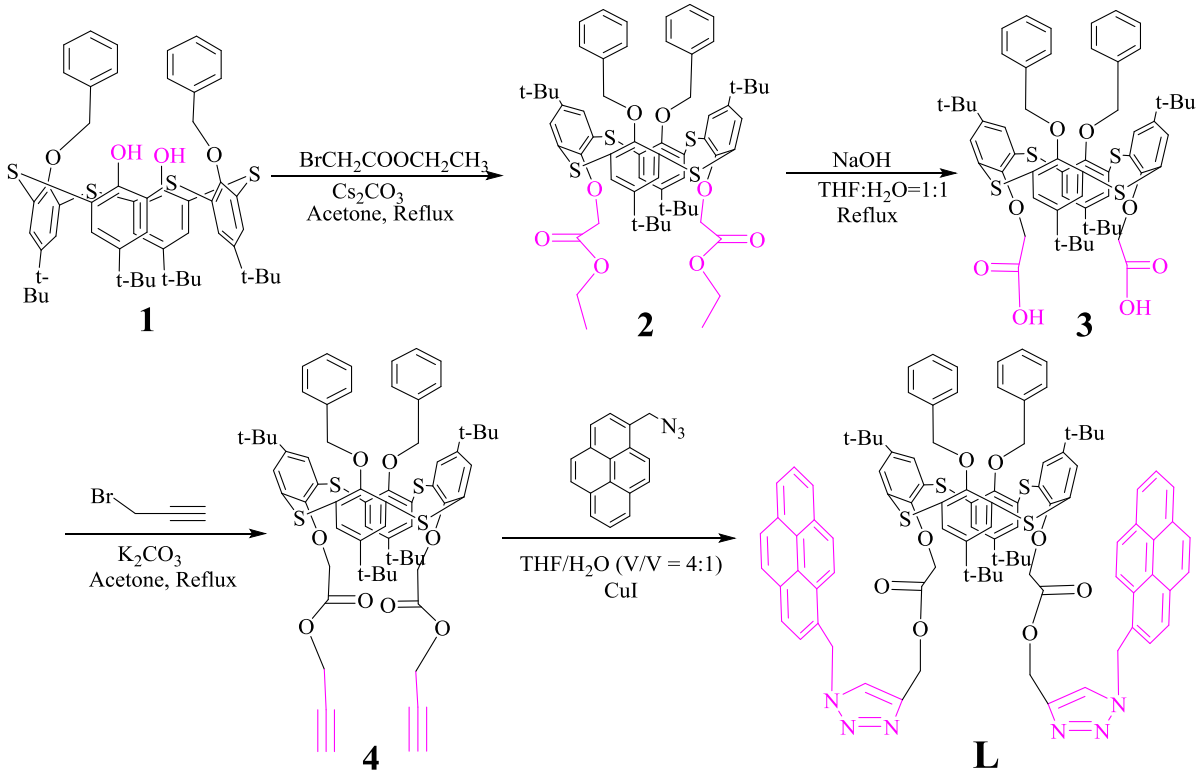

Scheme 1. The synthetic route of fluorescent probe **L**.

The intermediate **4** and fluorescent probe **L** were fully characterized by IR, ^{1}H NMR, ^{13}C NMR spectroscopy and mass spectrometry. The ^{1}H NMR spectrum of compound **4** exhibits two singlets for the *tert*-butyl protons at up field, *viz* δ 0.84 and 1.26 ppm; two singlets for the aromatic protons at δ 7.15 ppm and 7.52 ppm, respectively, all of which are indicative of a C_2-symmmetric structure for the 1,3-*alternate* conformer. One terminal triple bond proton signal is found at δ 2.47 ppm, which suggests that the propargyl group has been successfully introduced. In fluorescent probe **L**, the proton signal of the propargyl hydrogens has disappeared, whilst a new singlet appearing at about δ 7.40 ppm is attributed to the protons of the newly formed triazole skeleton. And a new singlet appearing at about δ 6.23 which is attributed to the protons of the newly formed methylene group (triazole*CH*$_2$Pyrene, Figure 1).

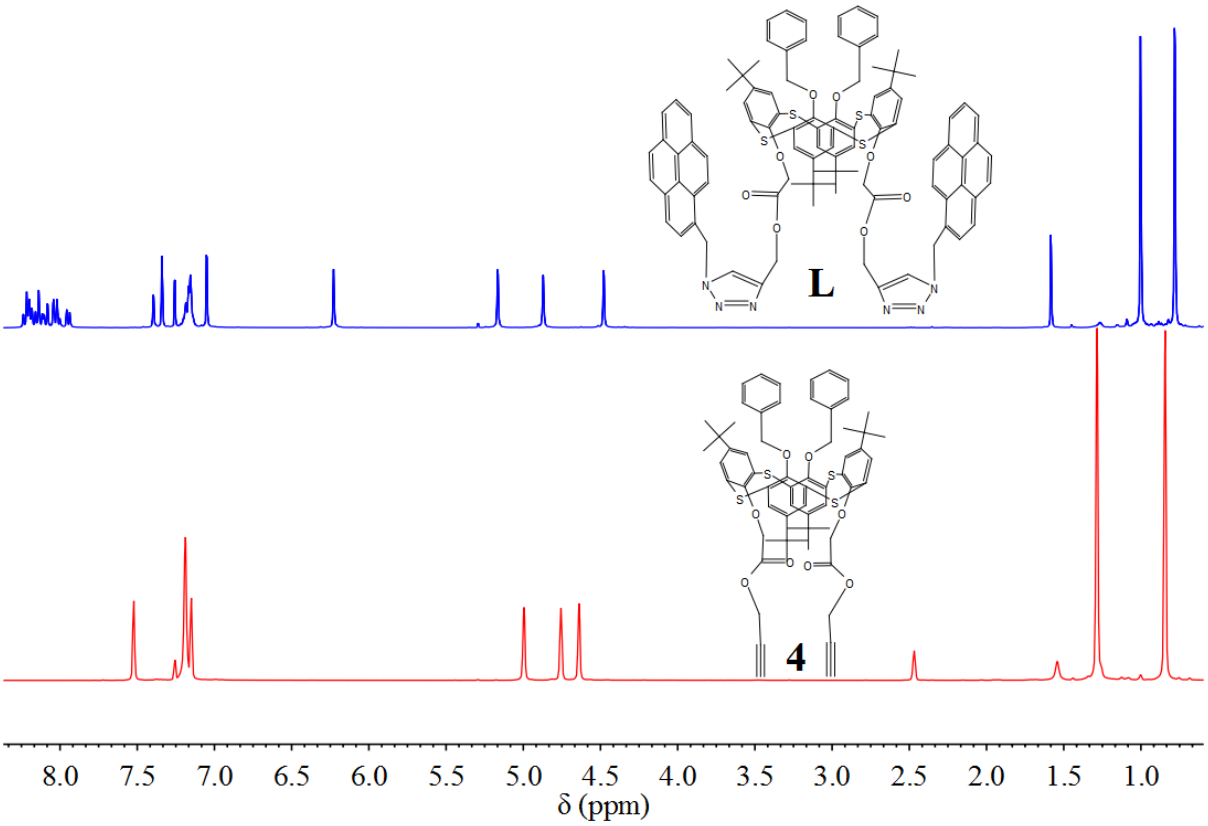

Figure 1. ^{1}H–NMR spectrum of compound **4** and **L** (400 MHz, $CDCl_3$, 293 K).

2.2.2 Crystal structures of fluorescent probe L

X-ray quality pale yellow crystals of fluorescent probe **L** were obtained by recrystallization from a MeOH/$CHCl_3$ solution. ORTEP representations of the molecular

structure of **L** are shown in Figure 2. It is clear that **L** adopts the 1,3-*alternate* conformation. There is a crystallographic twofold symmetry axis normal to the S_4 mean-plane, passing down the centre of the thiacalix[4]arene cage. Phenyl moieties, on the opposing site, related by this symmetry, are essentially parallel with their normals only 0.14(9) and 1.16(12) ° apart. These normals lie almost parallel to the S_4 plane, *i.e.* at angles of 89.93(7) and 89.42(6) ° to the normal of that plane. There are turns in the long substituent chain on O(1) [and O(1')] so that the triazole ring lies nearly parallel to the S_4 mean-plane, and the pyrene group is folded back to form an outer sheath around the cage.

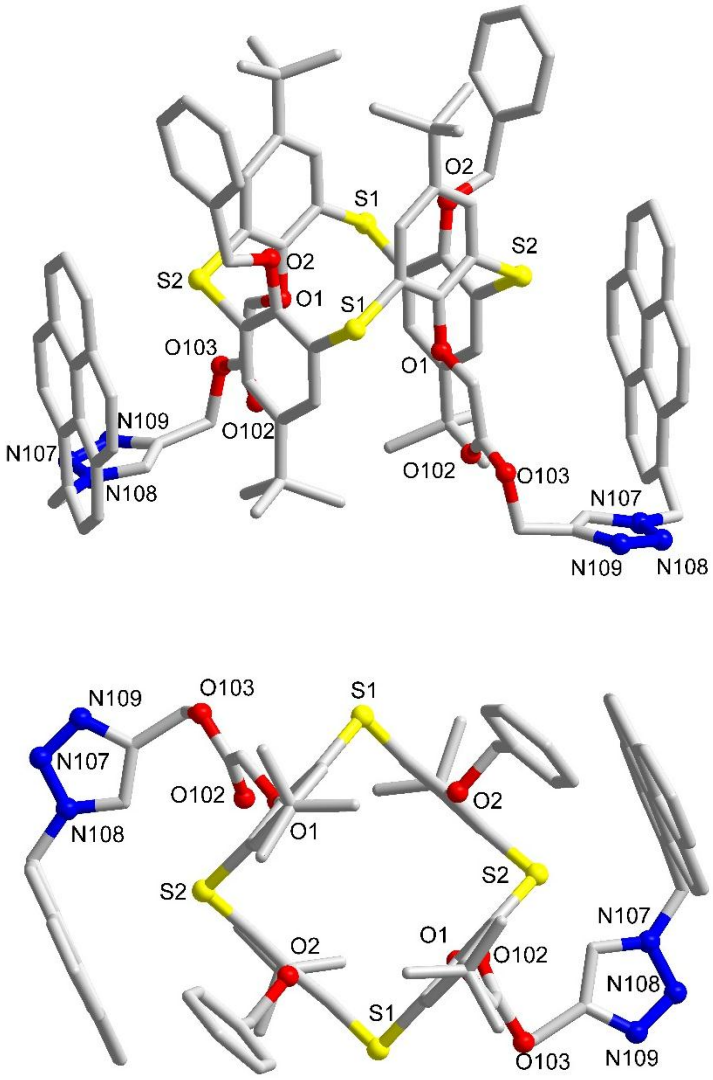

Figure 2. X-ray structure of **L**. (up) side view, (bottom) top view. Hydrogen atoms and the solvent water molecules have been omitted for clarity. Thermal ellipsoids are drawn at the 50% probability level.

2.2.3 Fluorescence spectroscopy study

The fluorescence spectra of probe **L** exhibited a stronger excimer emission at 484 nm and weaker monomer emissions at 379 and 397 nm (λ_{ex} = 344 nm), with an intensity ratio of monomer to excimer emission (I_{M379}/ I_{E484}) = 0.54. Among the various metal ions (Li^+, Na^+, K^+, Cs^+, Ag^+, Co^{2+}, Zn^{2+}, Ni^{2+}, Hg^{2+}, Pb^{2+}, Cu^{2+}, $Fe^{2+}$and Fe^{3+} as their perchlorate salts), fluorescent probe **L** displayed highly selective ratiometric changes upon the addition of Cu^{2+} (Figure 3). As expected, the pyrene moiety successfully serves as a source of these ratiometric changes. The formation of an excimer band at 484 nm indicated a strong face-to-

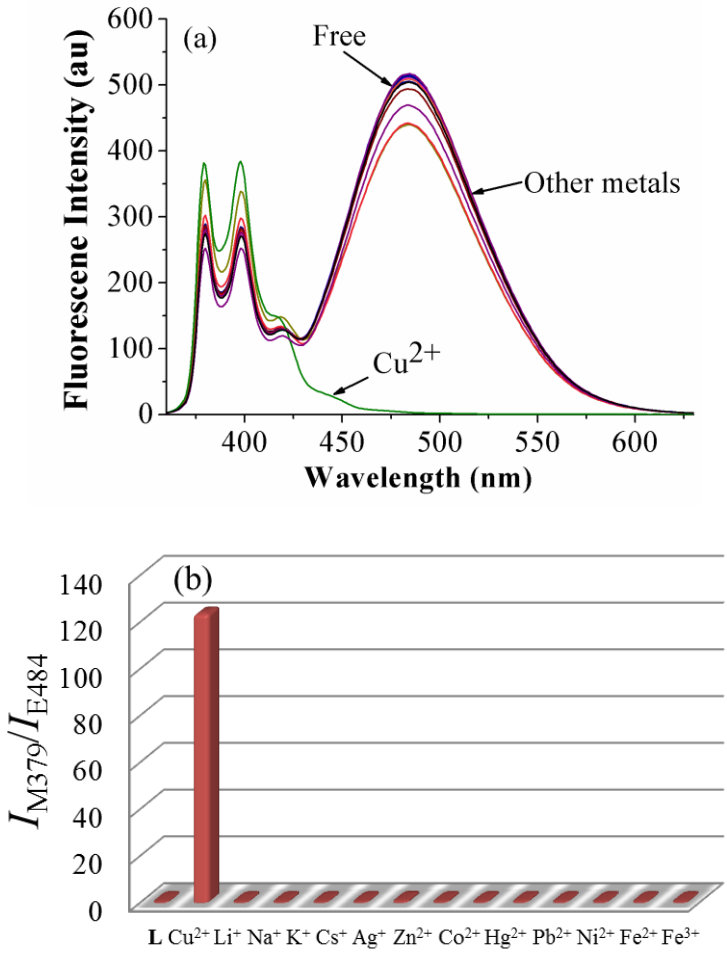

Figure 3. Fluorescence spectra of the fluorescent probe **L** (1.5 μM) on addition of various metal ions (Li^+, Na^+, K^+, Cs^+, Ag^+, Co^{2+}, Zn^{2+}, Hg^{2+}, Cu^{2+}, Pb^{2+}, Ni^{2+}, $Fe^{2+}$and Fe^{3+}, 20 equiv.) in EtOH solution at room temperature; (b) Ratiometric (I_{M379}/I_{E484}) selectivity of probe **L** upon addition of various metal ions (20 equiv.) as their EtOH solutions. λ_{ex} = 344 nm.

face π–π stacking between the two pyrene moieties. The relative intensity ratio of monomer to excimer emission (I_{M379}/ I_{E484}) of the blank probe **L** was 0.54 and it was increased 228–fold to 123 upon the addition of 20 equiv. of Cu^{2+} (Figure 3b) with the formation of an **L**–Cu^{2+} complex. We postulate that the excimer quenching in probe **L** is due to a conformational change which occurs during the binding of a Cu^{2+} ion between the nitrogen atoms of the triazole ring and the adjacent oxygen atoms. In this altered conformation, the coordination forces the pyrenyl groups to move away from one another thereby inhibiting the π–π stacking of the pyrene moieties which is necessary for the generation of the excimer emission.

Fluorescent titration experiments were carried out to further investigate more detailed complexation information for probe **L** with the copper ion. Interestingly, when we gradually increased the amounts of Cu^{2+} concentration from 0 to 4 equiv., the fluorescence intensity of the excimer emission of **L** was gradually decreased and accompanied by an enhancement of the monomer emission in EtOH solution (Figure 4a). However, when the concentration of Cu^{2+} was further increased more than 4 equiv. (5 equiv. to 45 equiv.), the fluorescence intensity of the monomer emission exhibited an unexpected decrease (Figure 4b). These unique phenomena can also be visualized by the solution color changes under UV light irradiation (Figure 4b inset). To the best of our knowledge, this is the first such case observed in thiacalixarene chemistry. A similar phenomenon was observed by Dabestani *et al.* in calix[4]arene chemistry.[23] They pointed out that the gradual quenching of the emission from

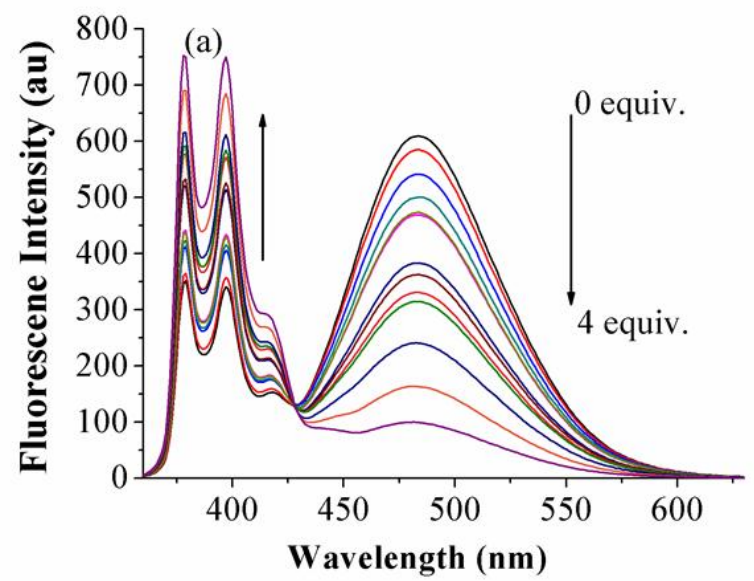

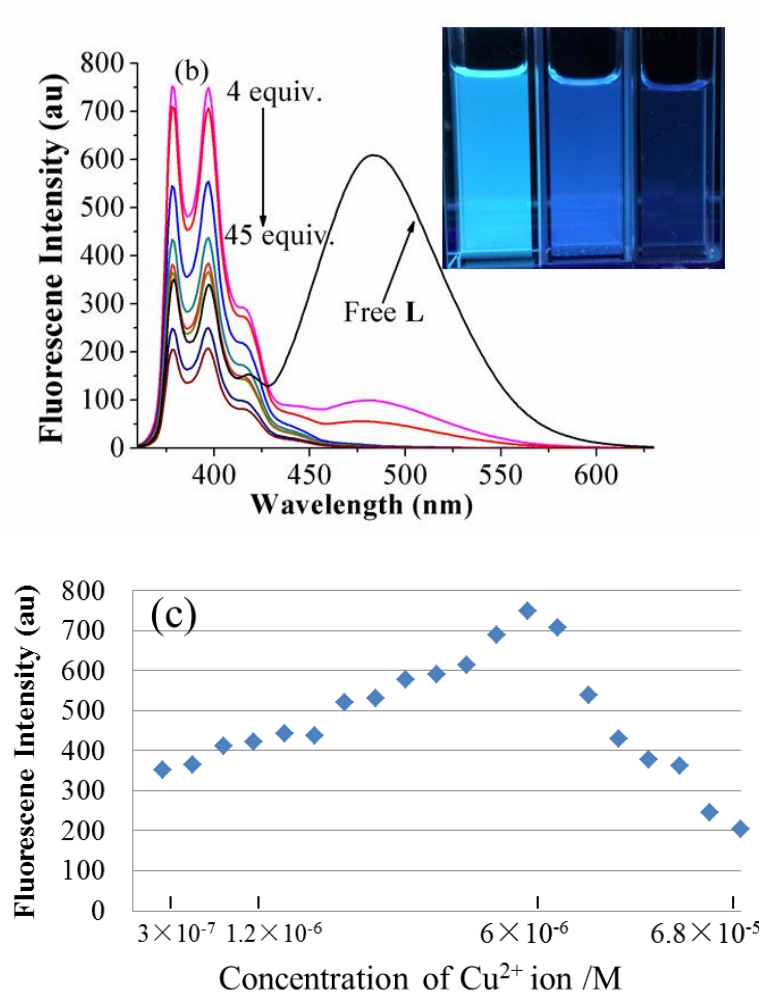

Figure 4. Fluorescence intensity changes of **L** (1.5 μM) upon addition of increasing concentrations of Cu^{2+} in EtOH solution (0–4 equiv.); (b) (4–45 equiv.) at 298 K with an excitation at 344 nm; (c) Changes in the emission spectra (379 nm) of **L** (1.5 μM) in EtOH upon addition of Cu^{2+} ion (EtOH solution).

L observed at high concentrations of Cu^{2+} (Figure 4c) may be attributable to a heavy metal effect caused by the higher ionic strength of the solution. Additionally, the fluorescence intensity of monomer emission quenching by the heavy atom (Cu^{2+}) in the chemosensor **L** generally can be attributed to a reverse Photoinduced Electron Transfer (PET)[24] from the pyrene moiety to the nitrogen atom of triazole group or to a heavy atom effect.[25] In other words, the probe **L** acted as an ratiometric fluorescent probe at low ion concentration or as a fluorescence quenching type probe due to the PET and heavy atom effect at high ionic strength of the solution.

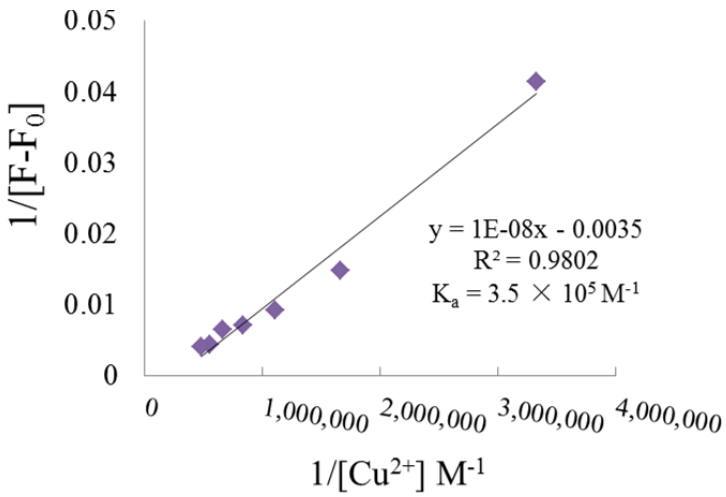

Figure 5. Bensei-Hilderbrand plot of probe **L** for various concentrations of Cu^{2+} ion at 298 K. The associate constant (*K*a) was calculated to be 3.5 $\times 10^5$ M^{-1}.

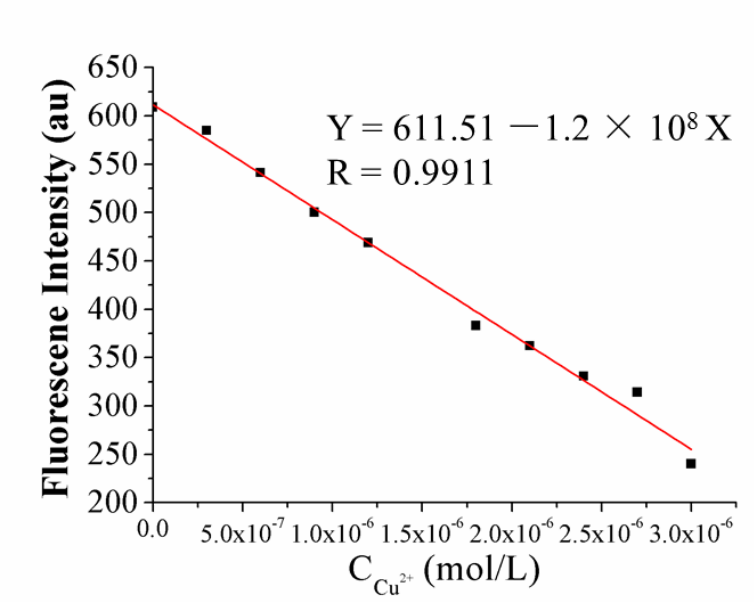

Figure 6. Plot of fluorescence intensity change (484 nm) of probe **L** with varied concentrations of Cu^{2+} at 298 K, the limit of detection of Cu^{2+} was calculated to be 1.45×10^{-7} M by the formula (3σ/K).

On the basis of the fluorescence titration experiments, the association constant (K_a)[26] for **L**·Cu^{2+} complex was determined to be 3.5 $\times 10^5$ M^{-1} by using a Benesi–Hildebrand plot (Figure 5). The detection limit of the probe **L** was calculated to be 1.44 $\times 10^{-7}$ M by the formula of 3σ/K (Figure 6). A Job's plot[27] for the complexation revealed a 1:1 stoichiometry

(Figure 7). All of the observed results are strongly suggested that probe **L** possesses a high sensitivity and high selectivity toward Cu^{2+}.

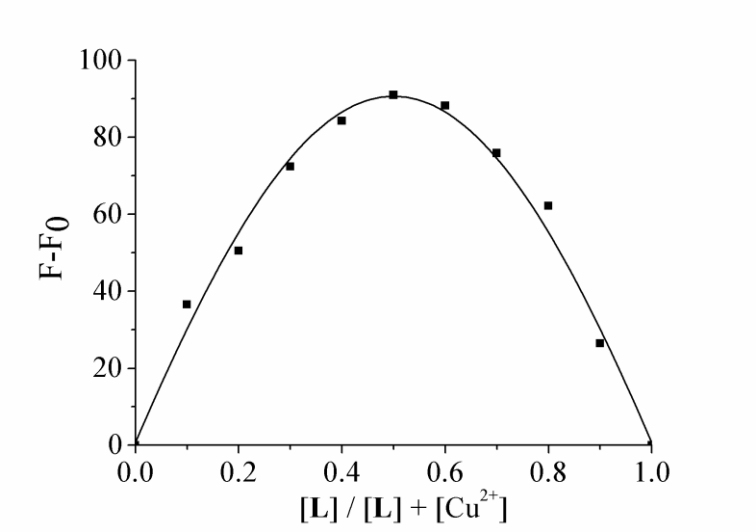

Figure 7. Job's plot for complexation of **L** with Cu^{2+}.

To further investigate the practical applicability of the probe **L** as a Cu^{2+} ion selective fluorescent sensor, competitive experiments were carried out in the presence of Cu^{2+} ion (30 μM) mixed with Li^{+}, Na^{+}, K^{+}, Cs^{+}, Ag^{+}, Co^{2+}, Zn^{2+}, Ni^{2+}, Hg^{2+}, Pb^{2+}, Fe^{2+}, Fe^{3+} at 30 μM. As shown in Figure 8, no obvious interference to the selective response of probe **L** to Cu^{2+} in the presence of most of the other tested metal ions. Accordingly, these observations suggested

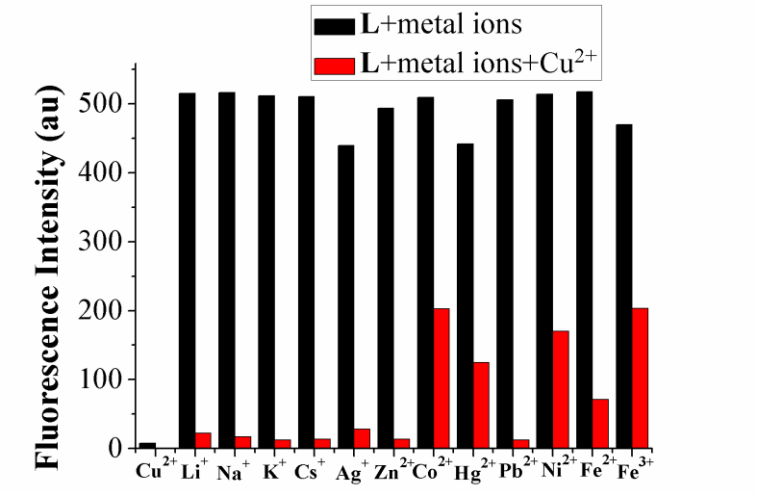

Figure 8. Fluorescence intensity responses (484nm) of probe **L** (1.5 μM) to 30 μM various tested ions (black bar) and to the mixture 30 μM tested cations with 30μM Cu^{2+} (red bar) at 298 K. λ_{ex} = 344 nm.

that probe **L** can be used as a selective fluorescent probe for the Cu^{2+} ion in the presence of most competitive metal ions.

2.2.4 Proton NMR Studies

Furthermore, in order to look further into the binding properties of probe **L** with Cu^{2+}, ^1H NMR titration experiments were carried out in the mixture of $CDCl_3/CD_3CN$ (V/V = 10 : 1) solution. The chemical shift changes for probe **L** on complexation with Cu^{2+} are shown in Figure 9. The proton signals of H_a, H_b, H_c, H_d and H_e completely disappeared once 0.25 equiv. of Cu^{2+} were added, and the signals of the benzyl protons (H_f) and pyrene ring protons (H_j) were blurred; this may be attributed to the paramagnetic effect of Cu^{2+}.[8] The chemical shift of protons H_g (–OCH_2Benzyl) were shifted to downfield with 0.31ppm. This may be due to the protons H_g of free **L** experiencing in the ring current shielding effect which is operating in the two thiacalixarene benzene rings (See the single-crystal structure of **L**, Figure 2a). However, when the **L**·Cu^{2+} complex was formed, the conformation of **L** would be changed which lead to the ring current shielding effect being diminished. This affected the protons H_g downfield shift back to the normal benzyl protons chemical shift (5.49ppm).[28]

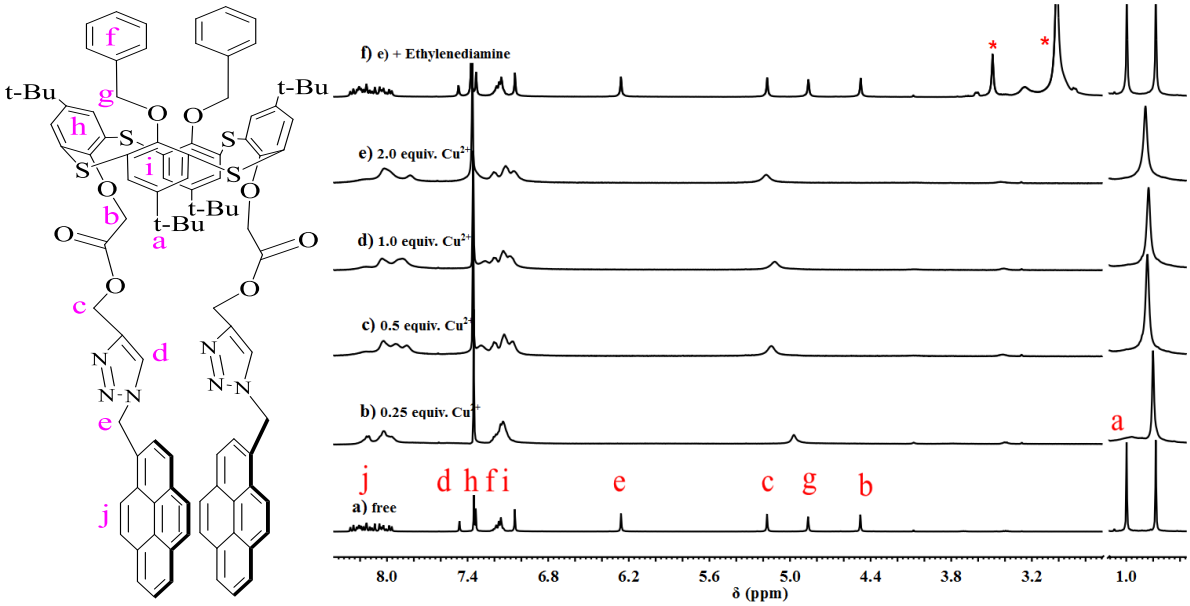

Figure 9. ^1H NMR spectral changes of Chemosensor **L** (4×10^{-3} M) on addition of $Cu(ClO_4)_2$ (400 MHz, $CDCl_3$:CD_3CN = 10 : 1). (a) Free **L**; (b) in the presence of 0.25 equiv. of $Cu(ClO_4)_2$; (c) in the presence of 0.5 equiv. of $Cu(ClO_4)_2$; (d) in the presence of 1.0 equiv. of $Cu(ClO_4)_2$; (e) in the presence of 2.0 equiv. of $Cu(ClO_4)_2$; (f) added 3 equiv. ethylenediamine to the solution of (e) * denoted the ethylenediamine peaks.

Proton signals corresponding to the thiacalixarene benzene rings (H_h and H_i) underwent a slight chemical shift, which can be attributed to both the paramagnetic effect of the Cu^{2+} and the conformation changes (Figure 9). All of the observed evidence strongly suggested that the 1,2,3-triazole moiety and the adjacent oxygen were directly involved in coordinating with Cu^{2+}. There was no significant change in the signal positions on addition of 1.0 to 2.0 equiv. concentration of Cu^{2+} to probe **L**, confirming a 1:1 binding stoichiometry for **L** and Cu^{2+}. Interestingly, it was observed that upon addition of 1.1 equiv. ethylenediamine to the **L**·Cu^{2+} complex solution, all of the disappeared peaks were immediately recovered (Figure 4f). This indicated that the complexation behaviour between **L** and Cu^{2+} ion was reversible.

2.2.5 IR Studies

IR titration spectroscopy further supported the possible complexation mode. The IR spectra of the complex (**L·Cu^{2+}**) *vs.* the free host (**L**) are shown in Figure 10. In the spectrum of free **L**, there are two relatively strong absorptions (bands at 1770 and 1740 cm^{-1}) which

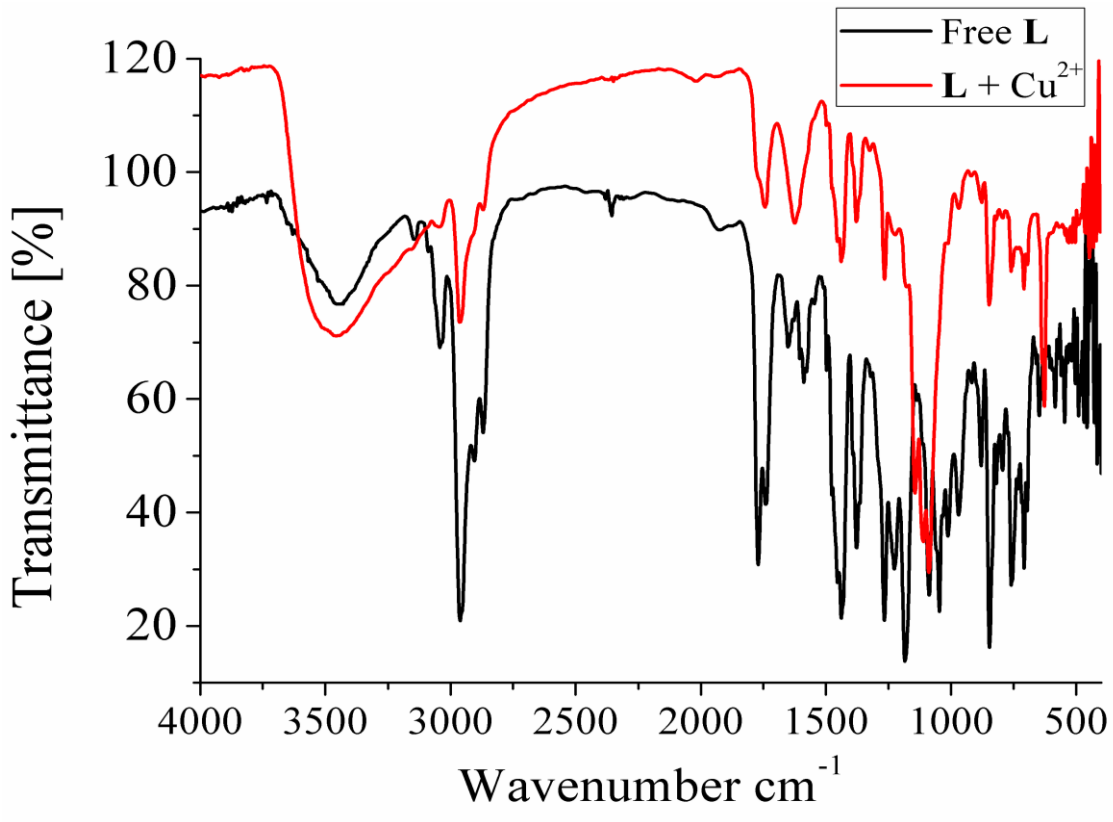

Figure 10. IR spectra of the complex (**L**·$Cu^{2+,}$ red line) vs. the free host (**L**, black line).

correspond to the –COO– group. After complexation with Cu^{2+}, they are dramatically changed to a weak absorption (band at 1743 cm^{-1}). A similar phenomenon also has been observed for the triazole group, bands at 1604 and 1588 cm^{-1} would be disappeared after complexation with Cu^{2+}. All of these evidences strongly indicate that Cu^{2+} is captured by these groups. The concept of **L**·Cu^{2+} complexation is proposed in Figure 11. Once the Cu^{2+} is captured by the nitrogen and oxygen atoms, the protons which are located in the adjacent area of the Cu^{2+} would be affected strongly by the inherent paramagnetism of Cu^{2+}, which led to the adjacent protons disappearing.

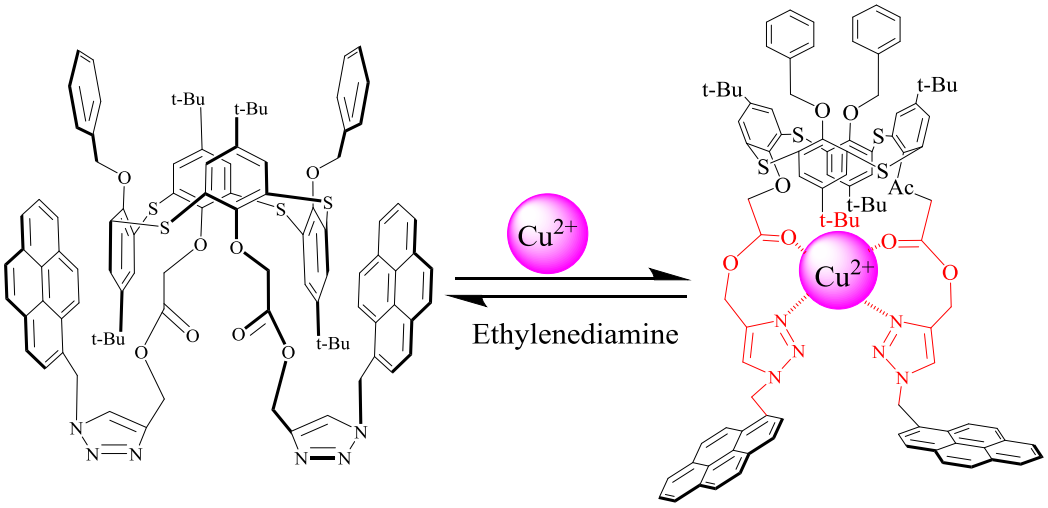

Figure 11. Plausible binding model of **L**·Cu^{2+} complex.

2.2.6 Density functional theory (DFT) computational studies

To better understand the binding properties of probe **L** with Cu^{2+}, density functional theory (DFT) computational studies were carried out to determine the geometry-optimized energies of probe **L** with Cu^{2+} ion. The starting structure was generated from the X-ray structure of **L**. In the DFT-optimized structures the large distance between the nitrogen atoms of the triazole rings shown by the X-ray structure of the ligand **L** prevented effective binding, between the Cu^{2+} and the two triazole units, as evidenced by the ^1H NMR data (Fig. 9). The structure for **L** was therefore modified, using SpartanPro'10,[29] for the putative DFT binding or complexation study with Cu^{2+}, was modified using SpartanPro'10.[29a] The generated structure of the ligand **L** was then imported into *Gaussian*-09 *rev D.01*[29b] and the geometry optimizations using the B3LYP/6-31G(d) basis set were first conducted in the gas phase (Fig.

14) and then with chloroform-corrected geometry-optimization. Significant conformational changes were observed for the pyrene ring moieties of **L** after the complexation with Cu^{2+}, which induced the excimer quenching in probe **L**. The conformation changes for **L** upon complexation with Cu^{2+} can be seen in Figure 14~15. Figure 14~15 bottom showed the proposed structure of the **L** ⊃ Cu^{2+} complex. The optimized molecular geometry suggested that the Cu^{2+} binds in accord with the IR and ^1H NMR titration study. Cu^{2+} ion was located in the centre of the fluorophore site, and the signal of the protons which surrounded Cu^{2+} ion will be strongly interfered due to the paramagnetic effect of the Cu^{2+}. In the **L** ⊃ Cu^{2+} complex, Cu^{2+} revealed an optimized distorted tetrahedral geometry (Figure 12) in the gas phase as well as with the $CHCl_3$ solvent correction (Figure 13). The DFT B3LYP/6-31G (d) calculated apparent binding (or interaction) energies of modified **L** with Cu^{2+} were -1808 KJ/mol for the gas-phase and -677 kJ/mol in the $CHCl_3$ solvent system, respectively. The N--N distance between the triazole ring nitrogens in **L** decreases from 9.845 Å to 2.948 Å and 11.178 Å to 3.107 (Å) since the nitrogen atoms moved inwards after complexing **L** with Cu^{2+} in the gas phase. The O—O distance of the acetate group carbonyl oxygen's decreases from 5.925 Å to 2.769 Å after complexing **L** with Cu^{2+} in the gas phase.

The binding energies of the complexes were based upon the following equation:

$$\mathbf{\Delta E = E_{Complex} - \Sigma(E_{thiacalix[4]arene} + E_{Cu^{2+}})}$$

Table 1. The geometry optimised binding energies of the fluorescent probe **L**(X-ray) and **L**(modified) complexes with Cu^{2+} ion in gas phase and chloroform solvent system at B3LYP/6-31G(d) basis set.

Parameter	**L**(X-ray)⊃Cu^{2+} (KJ/mol)	**L**(modified)⊃Cu^{2+} (KJ/mol)
Gas phase	-1794.21	-1808.28
Chloroform solvent	-667.22	-677.34

Table 2. The calculated distance for selected parameters for the backbones of the fluorescent probe **L** and complexes with Cu^{2+} ion in gas phase at B3LYP/6-31G(d) basis set (Distance in Å).

Parameter	**L (**From X-ray) in gas phase Distance **(**Å)	**L** (Modified) in gas phase Distance **(**Å)	**L** ⊃ Cu^{2+} in gas phase Distance **(**Å)
N_7-N_{83}	15.662	9.845	2.948
N_{83}-N_{182}	16.600	11.178	3.107
N_{83}-O_{77}	6.528	3.997	2.924
N_7-O_{181}	4.647	3.776	2.839
O_{77}-O_{181}	9.063	5.925	2.769
H_{190}-H_{2192}	10.473	15.893	8.697
N_7-Cu^{2+}	-	-	1.963
N_{82}-Cu^{2+}	-	-	1.960
O_{77}-Cu^{2+}	-	-	1.974
O_{181}-Cu^{2+}	-	-	1.997

Table 3. The calculated distances for selected parameters for the backbones of the fluorescent probe **L** and complexes with Cu^{2+} ion in Chloroform solvent system at B3LYP/6-31G(d) basis set (Distance in Å).

Parameter	**L** (From X-ray) in chloroform Distance (Å)	**L** (Modified) in chloroform Distance (Å)	**L** ⊃ Cu^{2+} in chloroform Distance (Å)
N_7-N_{83}	15.226	10.360	2.868
N_{82}-N_{182}	16.259	11.732	2.743
N_{83}-O_{77}	4.575	4.098	2.832
N_7-O_{181}	4.574	4.374	2.711
O_{77}-O_{181}	6.599	6.6293	2.874
H_{190}-H_{2192}	10.339	16.416	8.475
N_7-Cu^{2+}	-	-	2.009
N_{82}-Cu^{2+}	-	-	2.046
O_{77}-Cu^{2+}	-	-	1.9836
O_{1817}-Cu^{2+}	-	-	1.942

Table 4. The calculated angles in degrees (°) for selected parameters for the backbones of the fluorescent probe **L** and complexes with Cu^{2+} ion in gas phase and chloroform solvent system at B3LYP/6-31G(d) basis set.

Parameter	**L**⊂Cu^{2+} in gas phase bond angles in degree(°)	**L**⊂Cu^{2+} in $CHCl_3$ bond angles in degree(°)
N_7-Cu^{2+}-N_{83}	97.39	90.04
N_7-Cu^{2+}-O_{181}	91.62	86.63
N_{83}-Cu^{2+}-O_{77}	96.02	89.31
O_{77}-Cu^{2+}-O_{181}	88.41	94.11

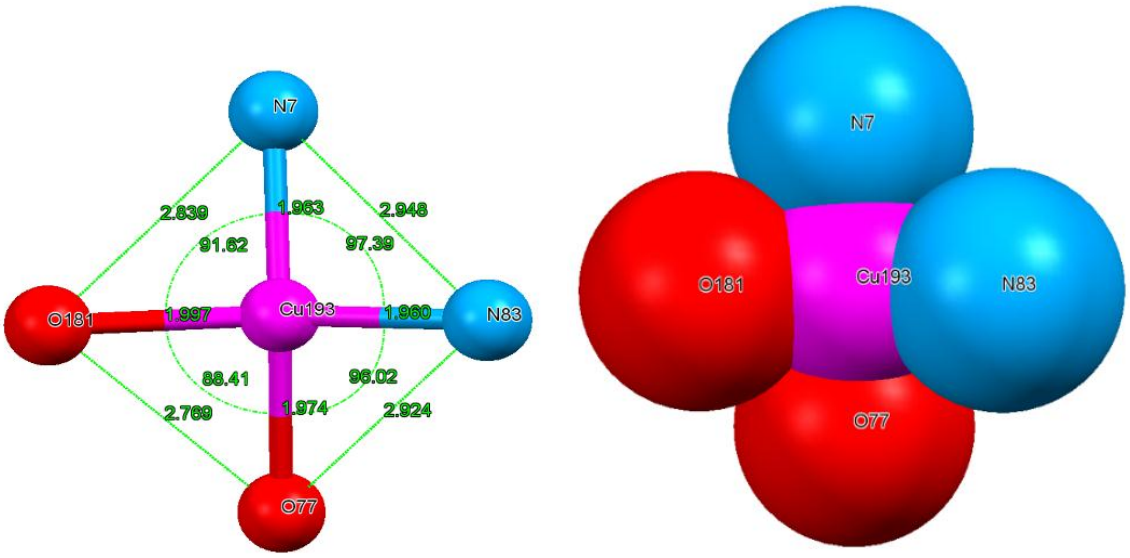

Figure 12. Geometry-optimized structures (in gas phase) of: *Left*: **L** ⊃ Cu^{2+} complex (ball-and-stick), and *Right*: The **L** ⊃ Cu^{2+} complex (space fill). Cu^{2+} shows the distorted tetrahedral geometry. Colour code: Cu^{2+} = magenta, nitrogen = light blue and oxygen atom = red.

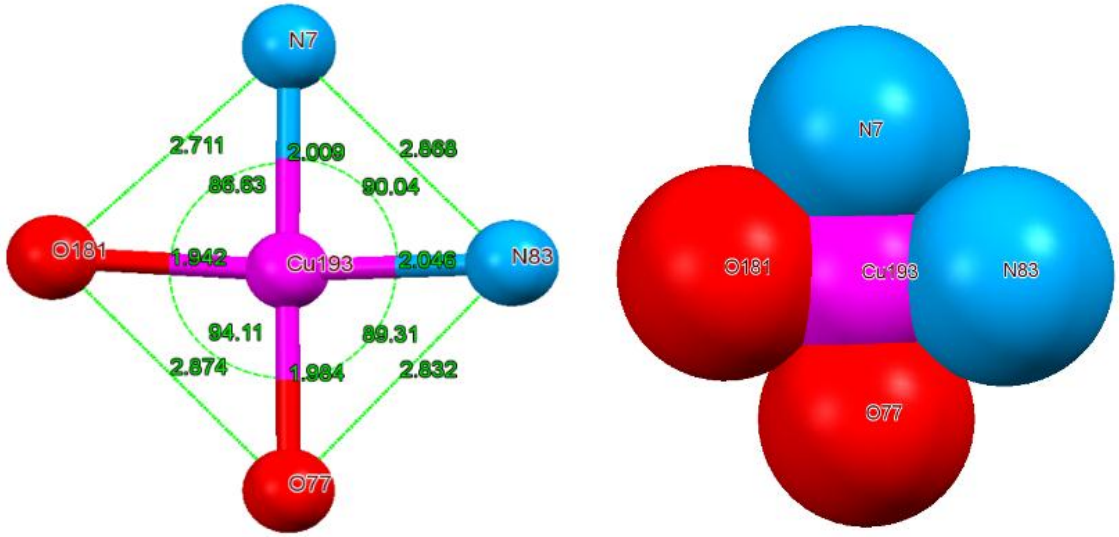

Figure 13. Geometry-optimized structures (in chloroform) of: *Left*: **L** ⊃ Cu^{2+} complex (ball-and-stick), and *Right* The **L** ⊃ Cu^{2+} complex (space fill). Cu^{2+} shows the distorted tetrahedral geometry. Colour code: Cu^{2+} = magenta, nitrogen = light blue and oxygen atom = red.

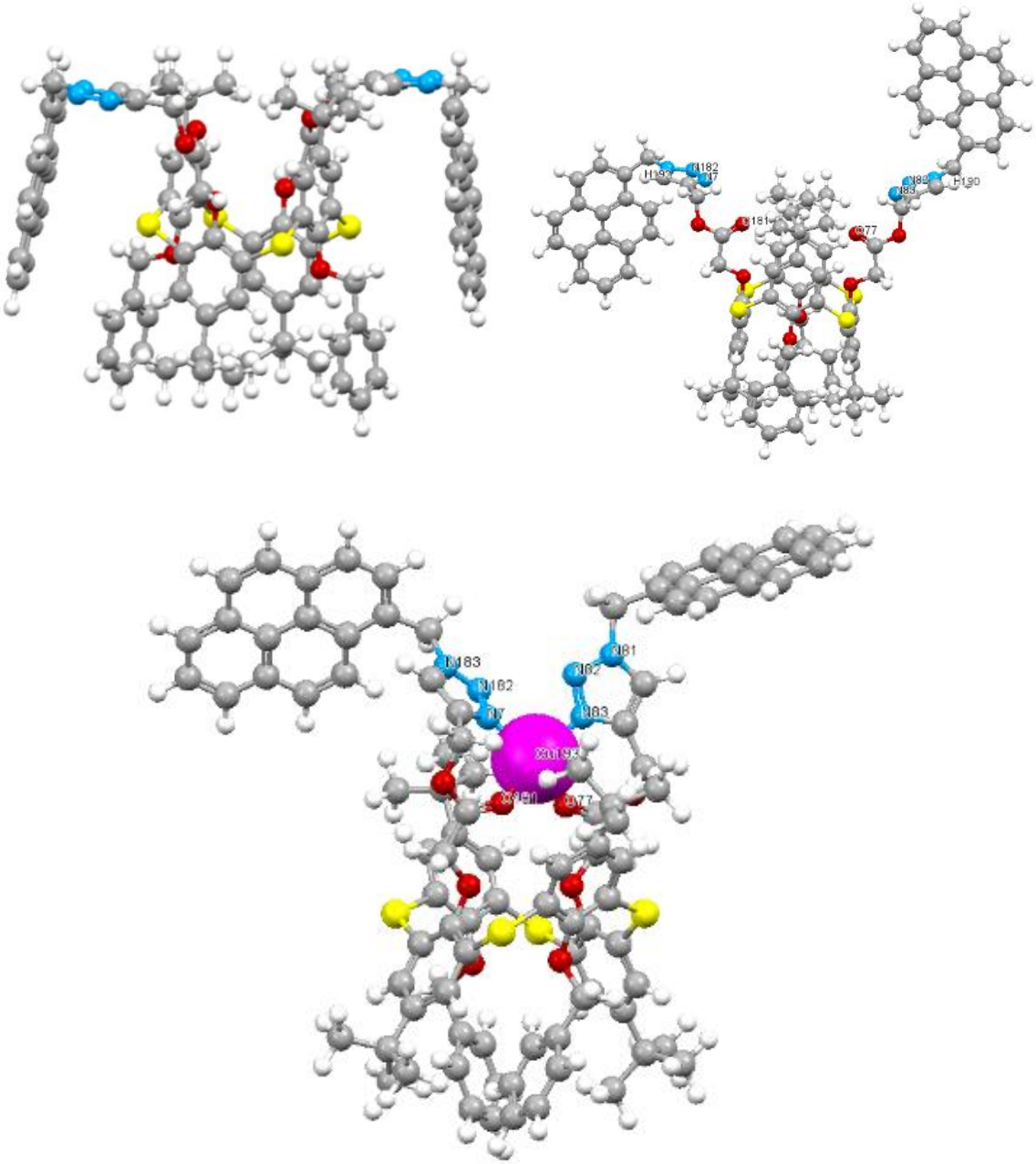

Figure 14. Geometry-optimized (ball-and-stick) structures (in gas phase) of: *Left (Up)*: Free ligand **L** (from X-ray); *Right (Up)*: Modified structure of the free ligand **L** used for the binding study; and *Bottom*: **L** ⊃ Cu^{2+}. Colour code: Cu^{2+} = magenta, nitrogen = light blue, sulphur = yellow, hydrogen = white, carbon = dark grey and oxygen atom = red.

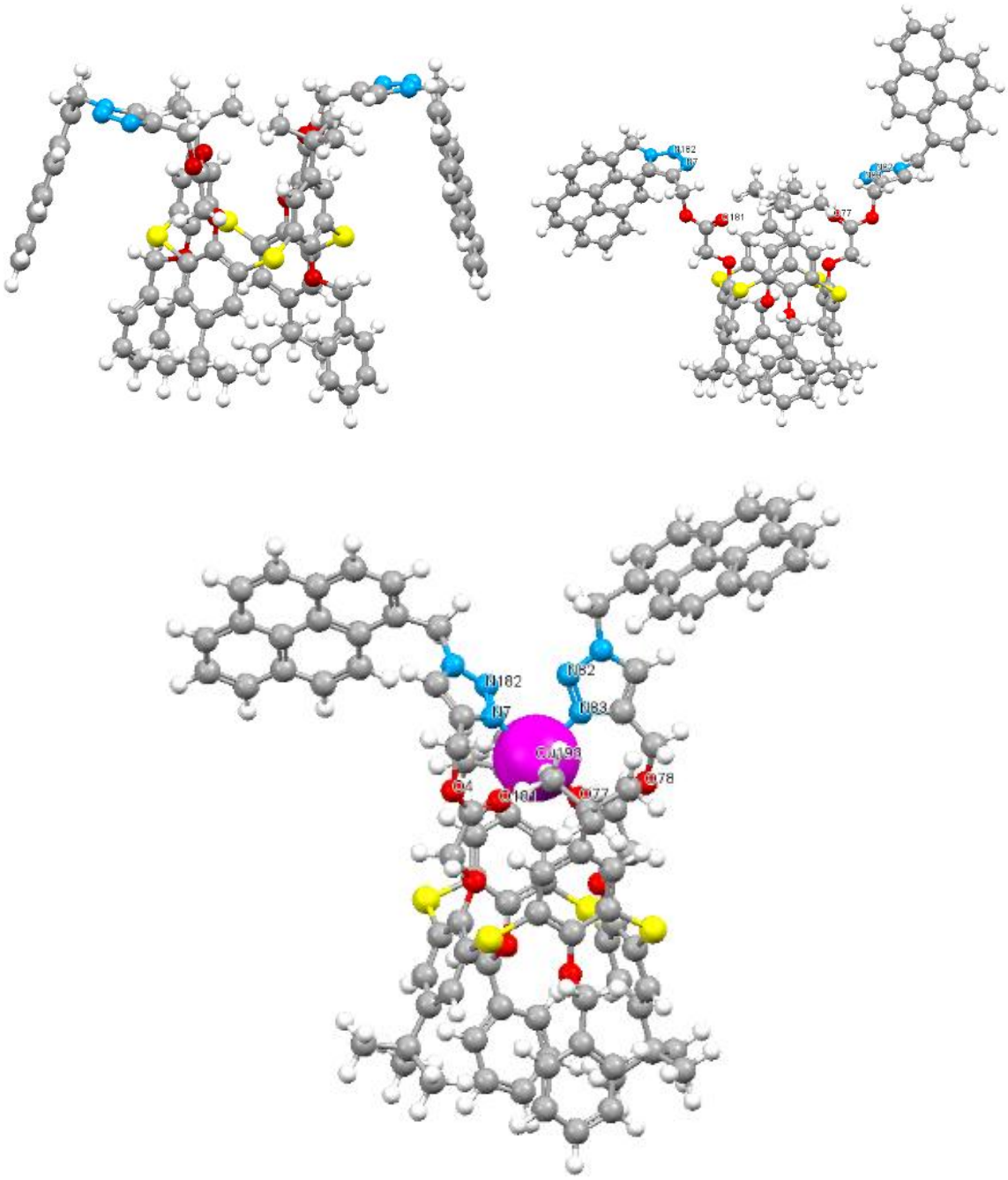

Figure 15. Geometry-optimized (ball-and-stick) structures (in $CHCl_3$) of: *Left*: Free ligand **L** (from X-ray); *Middle*: Modified structure of the free ligand **L** used for the binding study; and *Right*: **L**⊃Cu^{2+}. Colour code: Cu^{2+} = magenta, nitrogen = light blue, sulphur = yellow, hydrogen = white, carbon = dark grey and oxygen atom = red.

2.3 Conclusions

In summary, we have synthesized a new type of selective and sensitive fluorescent probe bearing triazole rings as the binding sites on the lower rim of a thiacalix[4]arene scaffold in a 1,3-*alternate* conformation. The selective binding behaviour of fluorescent probe **L** has been investigated by fluorescence spectra, IR and ^{1}H NMR spectroscopic analysis. The observed results suggested that fluorescent probe **L** acted as an ratiometric fluorescent probe at low ion concentration or as a fluorescence quenching type fluorescent probe due to the PET and heavy atom effect at high ionic solution strength. All the results suggested that fluorescent probe **L** exhibited highly selective and sensitive toward Cu^{2+}.

2.4 Experimental Section

2.4.1 General

Unless otherwise stated, all reagents used were purchased from commercial sources and were used without further purification. Compound **1**, **2**, and **3**[19] was prepared following the reported procedures. All used solvents were dried and distilled by the usual procedures prior to use. All melting points (Yanagimoto MP-S1) are uncorrected. ^{1}H NMR and ^{13}C NMR spectra were recorded on a Varian-400MR-vnmrs400 with $SiMe_4$ as an internal reference: J-values are given in Hz. IR spectra were measured for samples as KBr pellets on a Nippon Denshi JIR-AQ2OM spectrophotometer. Mass spectra were obtained with a Nippon Denshi JMS-HX110A Ultrahigh Performance mass spectrometer at 75 eV using a direct-inlet system. Fluorescence spectroscopic studies of compounds in solution were performed in a semimicro fluorescence cell (Hellma®, 104F-QS, 10 × 4 mm, 1400 μL) with a Varian Cary Eclipse spectrophotometer.

2.4.2 Materials.

2.4.2.1. Synthesis of compound **4**.

A suspension of **3** (203 mg, 0.2 mmol) and K_2CO_3 (400 mg, 2.9 mmol) was heated at reflux for 1 h in dry acetone (20 mL), and a solution of propargyl bromide (345 mg, 2.9 mmol) in dry acetone (10 mL) was added. The reaction mixture was refluxed for 24 h. The

solvents were evaporated and the residue partitioned between 10% HCl and CH_2Cl_2. The organic layer was separated and dried ($MgSO_4$) and the solvents were evaporated. The residue was dried to afford the solid crude product. The residue eluted from a column chromatography column of silica gel with $CHCl_3$ gave the target product **4** (180 mg, 72.7%) as a white solid. M.p.: 267–268 ℃. IR ν_{max} (KBr)/cm^{-1}: 3292, 3065, 3033, 2961, 2906, 2869, 2131, 1778, 1746, 1576 and 1498. ^{1}H NMR (400 MHz, $CDCl_3$) δ = 0.84 (18 H, s, t*Bu*), 1.28 (18H, s, t*Bu*), 2.47 (2H, s, *HC*C), 4.64 (4H, s, HCC*CH*$_2$O–), 4.76 (4H, s, –O*CH*$_2$COO–), 4.99 (4H, s,–O*CH*$_2$Benzyl), 7.15 (4H, s, Ar*H*), 7.19 (10H, s, Ph*H*) and 7.52 (4H, s, Ar*H*) ppm. ^{13}C NMR (100 MHz) δ 29.8, 30.2, 32.8, 33.2, 51.0, 65.7, 72.0, 74.1, 126.1, 126.5, 127.0, 127.2, 127.5, 129.8, 131.8, 136.9, 145.1, 145.3, 155.0, 157.2 and 166.1 ppm. HRMS (ESI-TOF): calcd for $C_{64}H_{68}O_8S_4$ $[M + H]^+$ *m/z* = 1093.3875; found 1093.3961 $[M + H]^+$.

***2.4.2.2. Synthesis of receptor* L**.

Copper iodide (20 mg) was added to a mixture of **4** (150 mg, 0.14 mmol) and 1-(azidomethyl)pyrene (108 mg, 0.42 mmol) in 25 mL THF/H_2O (4:1) and refluxed for 24 h. The resulting solution was cooled and diluted with water and extracted with CH_2Cl_2. The organic layer was separated and dried ($MgSO_4$) and evaporated to give the solid crude product. The residue eluted from a column chromatography column of silica gel with $CHCl_3$ gave the desired product, **L** (170 mg, 76.1%) as colourless prisms. Mp: 231–232 ℃. IR ν_{max} (KBr)/cm^{-1}: 3450, 3043, 2962, 2904, 2869, 1770, 1740, 1651, 1604, 1588 and 1497. ^{1}H NMR (400 MHz, $CDCl_3$) δ = 0.78 (18H, s, t*Bu*), 1.00 (18H, s, t*Bu*), 4.48 (4H, s, –O*CH*$_2$COO–), 4.87 (4H, s, –O*CH*$_2$Benzyl), 5.17 (4H, s, –Triazole*CH*$_2$O–), 6.23 (4H, s, –*CH*$_2$Pyrene), 7.05 (4H, s, Ar*H*), 7.16–7.18 (10H, m, Ph*H*), 7.34(4H, s, Ar*H*), 7.40 (2H, s, Triazole-*H*) and 7.94–8.24 (18H, m, Pyrene-*H*) ppm. ^{13}C NMR (100 MHz) δ 30.8, 30.9, 33.8, 34.0, 52.5, 57.8, 66.9, 73.1, 121.8, 123.6, 124.5, 125.0, 125.1, 125.9, 126.0, 126.4, 126.5, 127.1, 127.2, 127.4, 127.7, 127.9, 128.2, 128.4, 128.4, 129.2, 129.3, 130.5, 130.9, 131.2, 132.2, 133.0, 137.9, 142.9, 145.9, 146.0, 156.0, 158.1 and 167.7 ppm. HRMS (ESI-TOF): calcd for $[M + H]^+$ *m/z* = 1608.5815; found 1608.6492 $[M + H]^+$. Anal. Calcd for $C_{98}H_{90}N_6O_8S_4 \cdot 2H_2O$: C, 71.62; H, 5.72; N, 5.11. Found: C, 71.95; H, 5.64; N, 4.96.

2.4.3 Crystallography

Crystallographic Data for L: $C_{98}H_{90}N_6O_8S_4 \cdot H_2O$, M = 1626.0. Monoclinic, space group P2/n (equiv. to no. 13), a = 17.4815(6), b = 13.9971(5), c = 18.1134(6) Å, β = 109.991(3)°, V = 4165.1(2) $Å^3$. Z = 2, Dc = 1.297 g cm^{-3}, F(000) = 1716, T = 140(1) K, μ(Mo-Kα) = 1.8 cm^{-1}, λ(Mo-Kα) = 0.71069 Å.

Crystals are pale yellow, rectangular prisms. One, *ca* 0.43 x 0.14 x 0.10 mm, was mounted on a glass fibre and fixed in the cold nitrogen stream on an Oxford Diffraction Xcalibur-3/Sapphire3-CCD diffractometer, equipped with Mo-Kα radiation and graphite monochromator. Intensity data were measured by thin-slice ω- and φ-scans. Total no. of reflections recorded, to θmax = 22.5°, was 44921 of which 5417 were unique (R_{int} = 0.086); 3169 were 'observed' with $I > 2\sigma_I$.

Data were processed using the CrysAlisPro-CCD and -RED [19] programs. The structure was determined by the direct methods routines in the SHELXS program[30] and refined by full-matrix least-squares methods, on F^2's, in SHELXL.[30] The non-hydrogen atoms were refined with anisotropic thermal parameters. Hydrogen atoms were included in idealised positions and their U_{iso} values were set to ride on the U_{eq} values of the parent carbon atoms. At the conclusion of the refinement, wR_2 = 0.092 and R_1 = 0.086[30] for all 5417 reflections weighted $w = [\sigma^2(Fo^2) + (0.0478P)^2]^{-1}$ with $P = (Fo^2 + 2Fc^2)/3$; for the 'observed' data only, R_1 = 0.041. In the final difference map, the highest peak (*ca* 0.43 $eÅ^{-3}$) was close to the water molecule, O(9).

Scattering factors for neutral atoms were taken from reference.[31] Computer programs used in this analysis have been noted above, and were run through WinGX[32] on a Dell Precision 370 PC at the University of East Anglia.

Crystallographic data for this structure have been deposited with the Cambridge Crystallographic Data Centre with code number CCDC 1063255. Copies of the data can be obtained, free of charge, on application to CCDC, 12 Union Road, Cambridge CB2 1EZ, UK [fax: 144-1223-336033 or e-mail: deposit@ccdc.cam.ac.uk].

2.5 References

1 (*a*) E. L. Que, D. W. Domaille and C. J. Chang, *Chem. Rev.*, 2008, **108**, 1517–1548; (*b*) E. Pontiki, D. Hadjipavlou-Litina, A. T. Chaviara and C. A. Bolos, *Bioorg. Med. Chem. Lett.*, 2006, **16**, 2234–2237; (*c*) E. Gaggelli, H. Kozlowski, D. Valensin and G. Valensin, *Chem. Rev.*, 2006, **106**, 1995–2044.

2 H. Tapiero, D. M. Townsend, K. D. Tew, *Biomed. Pharmacother.*, 2003, **57**, 386–398.

3 (*a*) M. Schaefer, J. D. Gitlin, *Am. J. Physiol. Gastrointest. Liver Physiol.*, 1999, **276**, 311–314; (*b*) D. Huster, *Ann. N. Y. Acad. Sci.*, 2014, **1314**, 37–44.

4 (*a*) W. I. Vonk, V. Kakkar, P. Bartuzi, D. Jaarsma, R. Berger, M. H. Hofker, L. W. Klomp, C. Wijmenga, H. H. Kampinga and B. van de Sluis, *PLoS One*, 2014, **9**, e92408; (*b*) G. Xiao, Q. Fan, X. Wang and B. Zhou, *Proc. Natl. Acad. Sci.U. S. A.*, 2013, **110**, 14995–15000; (*c*) M. G. Savelieff, S. Lee, Y. Liu and M. H. Lim, *ACS Chem. Biol.*, 2013, **8**, 856–865; (*d*) A. J. McDonald, J. P. Dibble, E. G. Evans and G. L. Millhauser, *J. Biol. Chem.*, 2014, **289**, 803–813.

5 (*a*) W. T. Tak and S. C. Yoon, *Korean J Nephrol.*, 2001, **20**, 863–871; (*b*) W. Cao, X. J. Zheng, D. C. Fang and L. P. Jin, *Dalton Trans.*, 2015, **44**, 5191–5196.

6 (*a*) L. Quan, T. T. Sun, W. H. Lin, X. G. Guan, M. Zheng, Z. G. Xie and X. B. Jing, *J. Fluoresc.*, 2014, **24**, 841–846; (*b*) S. Chematea and N. Sekar, *RSC Adv.*, 2015, **5**, 27282–27289; (*c*) P. G. Sutariya, A. Pandya, A. Lodha and S. K. Menon, *Analyst*, 2013, **138**, 2531–2535.

7 (*a*) P. Jiang and Z. Guo, Coord. Chem. Rev., 2004, **248**, 205–229; (*b*) J. S. Kim and D. T. Quang, *Chem. Rev.*, 2007, **107**, 3780–3799; (*c*) Z. Xu, J. Yoon and D. R. Spring, *Chem. Soc. Rev.*, 2010, **39**, 1996–2006; (*d*) P. Kaur and K. Singh, *RSC Adv.*, 2014, **4**, 11980–11999.

8 (*a*) A. P. d. Silva; H. Q. N. Gunaratne, T. Gunnlaugsson, A. J. M. Huxley, C. P. McCoy, J. T. Rademacher and T. E. Rice, *Chem. Rev.*, 1997, **97**, 1515–1566; (*b*) Z. Hu, J. Hu, Y. Cui, G. Wang, X. Zhang, K. Uvdal and H. W Gao, *J. Mater. Chem. B*, 2014, **2**, 4467–4472; (*c*) J. A. Cotruvo, Jr., A. T. Aron, K. M. Ramos-Torresa and C. J. Chang, *Chem. Soc. Rev.*, 2015, **44**, 4400-4414.

9 (*a*) X. L. Ni, X. Zeng, C. Redshaw and T. Yamato, *Tetrahedron*, 2011, **67**, 3248–3253; (*b*)

S. Patra, R. Lo, A. Chakraborty, R. Gunupuru, D. Maity, B. Ganguly and P. Paul, *Polyhedron*, 2013, **50**, 592–601; (*c*) P. Chavez-Crooker, N. Garrido and G. A. Ahearn, *J. Exp. Biol*., 2001, **204**, 1433–1444.

10 (*a*) J. Wang, L. Long, D. Xie and X. Song, *Sensor. Actuat. B: Chem.*, 2013, **177**, 27–33; (*b*) B. Tang, T. Yue, J. Wu, Y. Dong, Y. Ding and H. Wang, *Talanta*, 2004, **64**, 955–960.

11 (*a*) S. Wu, K. Zhang, Y. Wang, D. Mao, X. Liu, J. Yu and L. Wang, *Tetrahedron Lett*., 2014, **55**, 351–353; (*b*) L. Ma, W. Cao, J. Lin, M. Zhang, L. Yang, *Sensor. Actuat. B: Chem.*, 2013, **181**, 782–786.

12 Y. S. Wu, C. Y. Li, Y. F. Li, J. L. Tang and D. Liu, *Sensor. Actuat. B: Chem.*, 2014, **203**, 712–718.

13 (*a*) P. Thirupathi and K. H. Lee, *Bioorg. Med. Chem. Lett*, 2013, **23**, 6811–6815; (*b*) S. Das, A. Sahana, A. Banerjee, S. Lohar, D. A. Safin, M. G. Babashkina, M. Bolte, Y. Garcia, I. Hauli, S. K. Mukhopadhyay and D. Das, *Dalton Trans.*, 2013, **42**, 4757–4763; (*c*) S. A. Ingale and F. Seela, *J. Org. Chem.*, 2012, **77**, 9352–9356.

14 Birks, J. B., *Rep. Prog. Phys.*, 1975, **38**, 903−974.

15 (*a*) F. M. Winnik, *Chem. Rev.*, 1993, **93**, 587−614; (*b*) S. Karuppannan and J. C. Chambron, *Chem. Asian J.*, 2011, **6**, 964–984.

16 (*a*) F. M. Winnik, *Chem. Rev.*, 1993, **93**, 587−614; (*b*) C. Yao, H. B. Kraatz and R. P. Steer, *Photochem. Photobiol. Sci.*, 2005, **4**, 191−199.

17 (*a*) H. Tomiyasu, J. L. Zhao, X. L. Ni, X. Zeng, M. R. J. Elsegood, B. Jones, C. Redshaw, S. J. Teat and T. Yamato, *RSC Adv.*, 2015, **5**, 14747−14755; (*b*) C. C. Jin, H. Cong, X. L. Ni, X. Zeng, C. Redshaw and T. Yamato, *RSC Adv.*, 2014, **4**, 31469−31475; (*c*) H. Tomiyasu, C. C. Jin, X. L. Ni, X. Zeng, C. Redshaw and T. Yamato, *Org. Biomol. Chem.*, 2014, **12**, 4917−4923; (*d* Q. Sun, L. Mu, X. Zeng, J. L. Zhao, T. Yamato and J. X. Zhang, *Sci. China Chem.*, 2015, **58**, 539−544.

18 (*a*) Z.-T. Jiang, R.-R. Deng and L. Tang, *Sensors Actuators B*, 2008, **135**, 128–132; (*b*) Y.-Q. Weng, F. Yue, Y.-R. Zhong and B.-H. Ye, *Inorg. Chem.*, 2007, **46**, 7749–7755; (*c*) I. S. Cho, H. Han, J. H. Shim, J. S. Lee, J. H. Shin, G. S. Cha and B. H. Kim, *Tetrahedron Lett.*, 2010, **51**, 2835–2839; (*d*) S. Goswami, D. Sen and N. K. Das, *Org. Lett.*, 2010, **12**, 856–859.

19 (*a*) N. Morohashi, F. Narumi, N. Iki, T. Hattori and S. Miyano, *Chem. Rev.*, 2006, **106**,

5291–5316; (*b*) R. Kumar, Y. O. Lee, V. Bhalla, M. Kumar and J. S. Kim, *Chem. Soc. Rev.*, 2014, **43**, 4824–4870; (*c*) M. Song, Z. Sun, C. Han, D. Tian, H. Li and J. S. Kim, *Chem.– Asian J.*, 2014, **9**, 2344–2357; (*d*) J. L. Zhao, H. Tomiyasu, X. L. Ni, X. Zeng, M. R. J. Elsegood, C. Redshaw, S. Rahman, P. E. Georghiou, S. J. Teat and T. Yamato, *Org. Biomol. Chem.*, 2015, **13**, 3476−3483; (*e*) J. L. Zhao, H. Tomiyasu, X. L. Ni, X. Zeng, M. R. J. Elsegood, C. Redshaw, S. Rahman, P. E. Georghiou and T. Yamato, *New J. Chem.*, 2014, **38**, 6041−6049.

20 (*a*) X.-L. Ni, X. Zeng, C. Redshaw and T. Yamato, *Tetrahedron*, 2011, **67**, 3248-3253; (*b*) X.-L. Ni, X. Zeng, D. L. Hughes, C. Redshaw and T. Yamato, *Supramol. Chem.*, 2011, **23**, 689-695.

21 (*a*) X. L. Ni, X. Zeng, C. Redshaw and T. Yamato, *J. Org. Chem.*, 2011, **76**, 5696–5702; (*b*) X. L. Ni, S. Wang, X. Zeng, Z. Tao and T. Yamato, *Org. Let.*, 2011, **13**, 552–555.

22 C. Perez-Casas, S. Rahman, N. Begum, X. Zeng and T. Yamato, *J. Inclusion Phenom. Macrocyclic Chem.*, 2008, **60**, 173–185.

23 (*a*) H. F. Ji, G. M. Brown and R. Dabestani, *Chem. Commun.*, 1999, 609–610; (*b*) H. F. Ji, R. Dabestani, G. M. Brown and R. L. Hettich, *J. Chem. Soc., Perkin Trans. 2*, 2001, 585–591.

24 (*a*) K. C. Chang, I. H. Su, A. Senthilvelan and W. S. Chung, *Org. Lett.*, 2007, **9**, 3363–3366; (*b*) A. Ojida, Y. Mito-oka, M. A. Inoue and I. Hamachi, *J. Am. Chem. Soc.*, 2002, **124**, 6256–6258; (*c*) M. Choi, M. Kim, K. D. Lee, K. N. Han, I. A. Yoon, H. J. Chung, and J. Yoon, *Org. Lett.*, 2001, **3**, 3455–3457.

25 M. Y. Chae, X. M. Cherian and A. W. Czarnik, *J. Org. Chem.*, 1993, **58**, 5797–5801.

26 (*a*) H. A. Benesi and J. H. Hildebrand, *J. Am. Chem. Soc.*, 1949, **71**, 2703–2707; (*b*) O. Stern and M. Volmer, *Phys. Z.*, 1919, **20**, 183–188.

27 P. Job, *Ann. Chim.*, 1928, **9**, 113–203.

28 T. Yamato, C. P. Casas, H. Yamamoto, M. R. J. Elsegood, S. H. Dale, C. Redshaw, *J. Inclusion Phenom. Macrocyclic Chem.*, 2005, **54**, 261–269.

29 (*a)* Initial molecular modeling calculations using MMFF94 were performed using the *PC Spartan'10* software from Wavefunction Inc., Irvine CA.M.; (*b*) M. J. Frisch, G. W. Trucks, H. B. Schlegel, G. E. Scuseria, M. A. Robb, J. R. Cheeseman, G. Scalmani, V. Barone, B. Mennucci, G. A. Petersson, H. Nakatsuji, M. Caricato, X. Li, H. P. Hratchian,

A. F. Izmaylov, J. Bloino, G. Zheng, J. L. Sonnenberg, M. Hada, M. Ehara, K. Toyota, R. Fukuda, J. Hasegawa, M. Ishida, T. Nakajima, Y. Honda, O. Kitao, H. Nakai, T. Vreven, Jr. J. A. Montgomery, J. E. Peralta, F. Ogliaro, M. Bearpark, J. J. Heyd, E. Brothers, K. N. Kudin, V. N. Staroverov, T. Keith, R. Kobayashi, J. Normand, K. Raghavachari, A. Rendell, J. C. Burant, S. S. Iyengar, J. Tomasi, M. Cossi, N. Rega, J. M. Millam, M. Klene, J. E. Knox, J. B. Cross, V. Bakken, C. Adamo, J. Jaramillo, R. Gomperts, R. E. Stratmann, O. Yazyev, A. J. Austin, R. Cammi, C. Pomelli, J. W. Ochterski, R. L. Martin, K. Morokuma, V. G. Zakrzewski, G. A. Voth, P. Salvador, J. J. Dannenberg, S. Dapprich, A. D. Daniels, O. Farkas, J. B. Foresman, J. V. Ortiz, J. Cioslowski, D. J. Fox. *Gaussian 09, Revision D.01*; Gaussian, Inc., Wallingford CT, 2013.

30 G. M. Sheldrick, SHELX-97 – programs for crystal structure determination (SHELXS) and refinement (SHELXL), *Acta Crystallogr.,* 2008, **A64**, 112–122 and 2015, **C71**, 3-8

31 *International Tables for X-ray Crystallography*, ed. A. J. C. Wilson, Kluwer Academic Publishers, Dordrecht, 1992, vol. C, pp. 500, 219 and 193.

32 L. J. Farrugia, *J. Appl. Crystallogr.*, 2012, **45**, 849–854.

Chapter 3

A di-topic hard/soft receptor for K^+/Ag^+ and Na^+/Ag^+ with negative allosteric effect and a mono-topic receptor as a reusable extractant for dichromate anions based on thiacalix[4]arene

*This chapter described two novel receptors possessing imidazole moieties based on thiacalix[4]arene. The exclusive formation of mononuclear complexes of di-topic hard/soft receptor **L1** with metal cations is of particular interest revealing a negative allosteric effect. Liquid-liquid extraction experiments indicate that synthesized mono-topic receptor **L2** can be utilized as an efficient reusable extractant for dichromate anion by controlling the pH of the aqueous solution.*

3.1 Introduction

We have further explored the potential application of thiaclaix[4]arene derivatives in allosteric regulation and extraction for the dichromate anion in this chapter.

Allosteric regulation between subunits within a receptor system is one of nature's elegant strategies for precisely regulating and controlling the diverse functions in biological systems.[1] The chemists used the allosteric regulation to control molecular function by external stimuli to transduce chemical signals, and to obtain chemical feedback regulation.[2] Given that, much effort has been devoted in supramolecular chemistry to construct artificial systems to achieve analogous functions such as signal amplification and molecular recognition.

Two or more binding subunits within the same macrocyclic structure have been named as di- or poly-topic receptors.[3] Such systems are suitable candidates for the allosteric regulation of host-guest interactions with guests.[1d,4] Thiacalix[4]arenes are macrocyclic molecules which possess unlimited possibilities for functionalization on the low rim, up rim, bridging sulfur atoms and benzene scaffold. In particularly, the unique 1,3-*alternate* conformation is capable of arrangement the binding subunits in two opposite sides of the molecule, and is thus a potentially ideal structure for allosteric regulation.[5] Hence, we have been interested in being able to incorporate two different binding properties subunits into a 1,3-*alternate* conformation thiacalix[4]arene. This would therefore permit the construction of a di-topic receptor system which should possess allosteric features.

The development of systems for the fast separation, removal and estimation of precious metal silver (soft metal), the use of Ag^+ complexes in cancer radioimmunotherapy and their potential use in photographic materials has attracted the attention of supramolecular chemists towards designing high affinity Ag^+-selective receptors.[6] According to the reported literatures, the synthesis and evaluation of homotrioxacalix[3]arene and thiacalix[4]arene ligands as Ag^+ ionophores and found that by introducing imidazole groups at the lower rim of the calixarene skeleton resulted in a high affinity for Ag^+.[7] On the other hand, it has been reported that the introduction of ester groups at its lower or upper rim, the thiacalix[4]arene derivative can selectively complex alkali metal cations (hard metals), such as Na^+ and K^+.[8] Thus, we designed an potential di-topic receptor by introducing imidazole groups onto the

thiacalix[4]arene framework as one binding subunit and introducing ester groups on the opposite side as the other binding subunit. Such a di-topic system with two binding subunits which was expected for both hard (Na^+ and K^+) and soft (Ag^+) cations, and with possible switching of complexation preferences.

In this chapter, a novel di-topic receptor **L1** which have two different binding subunits based on a thiacalix[4]arene in the 1,3-*alternate* conformation has been synthesized and characterized. The allosteric effect of receptor **L1** has been investigated by ^1H NMR spectroscopies. In order to further understand the allosteric effects, the mono-topic receptor **L2**, with a similar structure, was also introduced. Given the amphoteric nature of the imidazole group which can be functioned not only as an effective cation but also as an anion receptor under appropriate conditions. And also, as a continuation of our previously research for dichromate anion extractants based on thiacalixarene derivatives,[7,13] the extraction efficiency of the systems described herein towards dichromate anion was conducted by liquid-liquid extraction experiments.

3.2 Results and Discussion

3.2.1 Syntheses of receptors L1 and L2

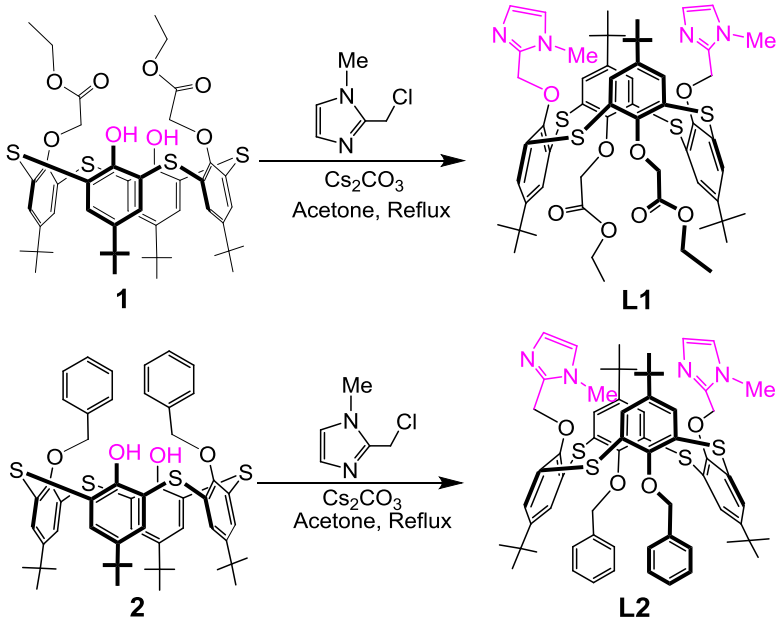

Scheme 1. The synthetic routes to compounds **L1** and **L2**.

The preferential formation of the 1,3-*alternate* conformer of thiacalix[4]arene occurs in the presence of a cesium cation which size is compatable with that of the thiacalix[4]arene cavity and thus contributes significantly to the cation-π interaction.[5] Di-topic receptor **L1** with two different binding sites could therefore be obtained in 55% yield by the stereoselective *O*-alkylation of **1**[10] with 2-chloromethyl-1-methyl-1*H*-imidazole[9] in the presence of Cs_2CO_3 in dry acetone (Scheme 1). Similarly, mono-topic receptor **L2** was also obtained in 44% yield by the stereoselective *O*-alkylation of **2**[11] with 2-chloromethyl-1-methyl-1*H*-imidazole in the presence of Cs_2CO_3 in dry acetone (Scheme 1).

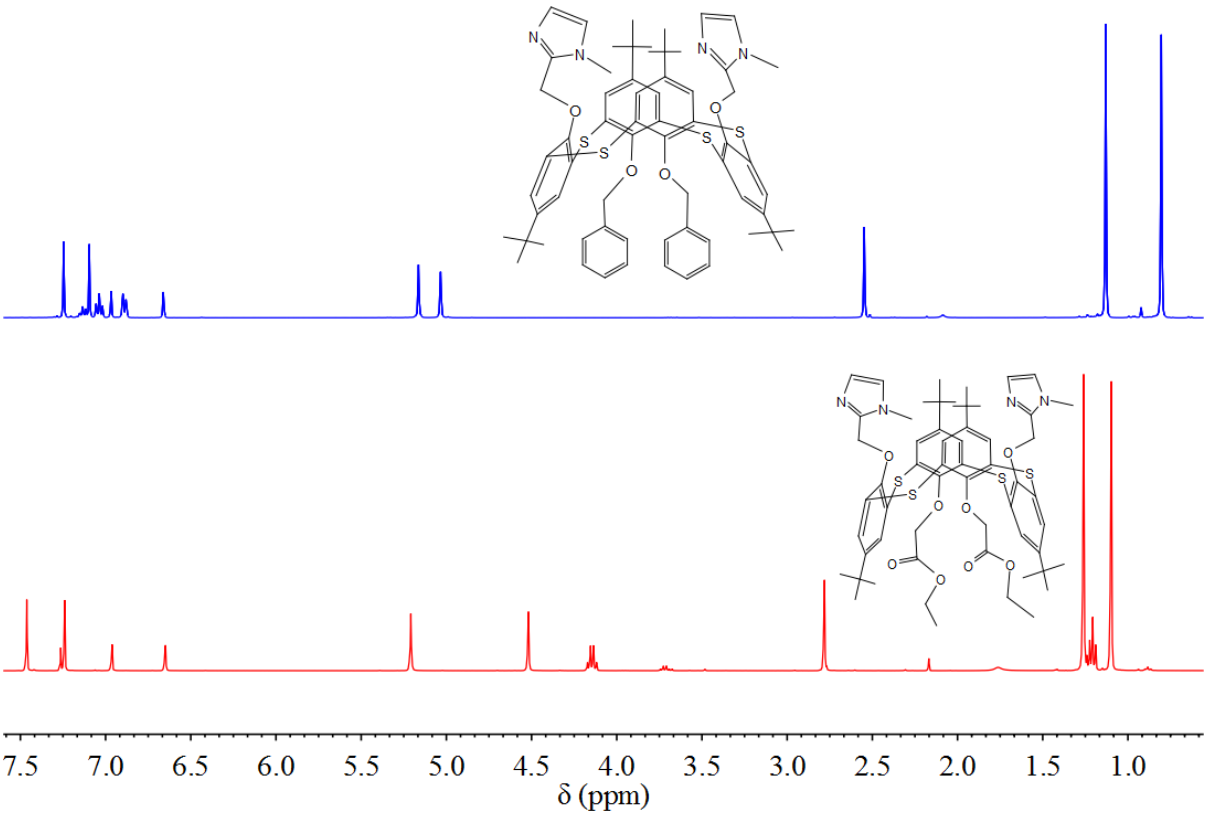

Figure 1. ^{1}H–NMR spectrum of compound **L1** and compound **L2** (400 MHz, $CDCl_3$, 293 K).

The ^{1}H NMR spectra of **L1** exhibited two singlets for the *tert*-butyl protons at up-field positions, *viz* δ 1.10 and 1.26 ppm; two singlets for the benzene ring protons at δ 7.24 ppm and 7.46 ppm (Figure 1), all of which was indicative of a C_2-symmmetric structure for the 1,3-*alternate* conformation. Obviously, receptor **L2** was also in the 1,3-*alternate* conformation revealing two singlets for the *tert*-butyl protons (δ 0.82 and 1.15 ppm) and two

singlets for the benzene ring protons (δ 7.12 and 7.27 ppm, Figure 1). Surprisingly, remarkable shielding effects were observed for the N-*Me* protons of **L1** and **L2** (Table 1), compared with the reference compound **L3**,[7] which was prepared by *O*-alkylation of 4-*tert*-butyl-2,6-dimethylphenol **3**[12] with 2-chloromethyl-1-methyl-1*H*-imidazole in the presence of NaH (Scheme 2). It strongly suggested that the imidazole groups for both of **L1** and **L2** were exposed to the ring current shielding effect area operating between two of the thiacalixarene benzene rings.[7,13]

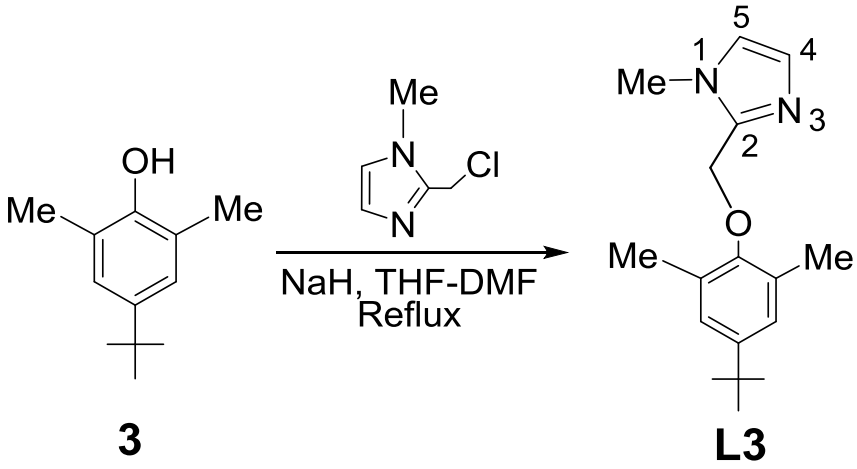

3 **L3**

Scheme 2. The synthetic route of reference compound **L3**.

Table 1. Partial **c**hemical shifts of **L1**, **L2** and reference compound **L3**.[a]

Compound	Chemical shifts, δ (ppm)		
	-N-*CH*$_3$	*H*$_4$	*H*$_5$
L1	2.78	6.65	6.96
L3	3.70	6.82	6.94
L2	2.57	6.68	6.99
$\Delta\delta_{\mathbf{L1}}$[b]	–0.92	–0.17	+0.02
$\Delta\delta_{\mathbf{L2}}$[b]	–1.13	–0.14	+0.05

[a] Δδ value is the difference of the chemical shift between **L1**, **L2** and reference compound **L3** in $CDCl_3$ at 27 ℃. [b] A plus sign (+) denotes a shift to lower magnetic field, whereas, a negative sign (–) denotes a shift to higher magnetic field.

3.2.2 Crystal Structures of L1 and L2

The molecular structure of **L1** and **L2** were further confirmed by X–ray crystallographic analysis as shown in Figure 2. Both **L1** (Fig. 2a) and **L2** (Fig. 2c) were in the 1,3-*alternate* conformation. The imidazole ring containing N(1) and C(45) of **L1** and **L2** were pointing into the thiacalix[4]arene cavity (Fig.2b and Fig.2d) which were consistent with the significant up-field shift for the N-CH_3 group in the ^{1}H NMR spectra. Receptor **L1** exhibited a slightly distorted square (Fig. 2b, S1 ··S2 = 5.636 Å, S2 ··S3 = 5.562 Å, S3 ··S4 = 5.546 Å and S4 ··S1 = 5.579 Å); however, an approximate square was observed for receptor **L2** (Fig. 2d, S1 ··S2 = 5.559 Å, S2 ··S3 = 5.552 Å, S3 ··S4 = 5.535 Å and S4 ··S1 = 5.558 Å). The observed results indicated that the cavity size of receptor **L1** was a little larger than receptor **L2** based on the sum of the S ··S distances.

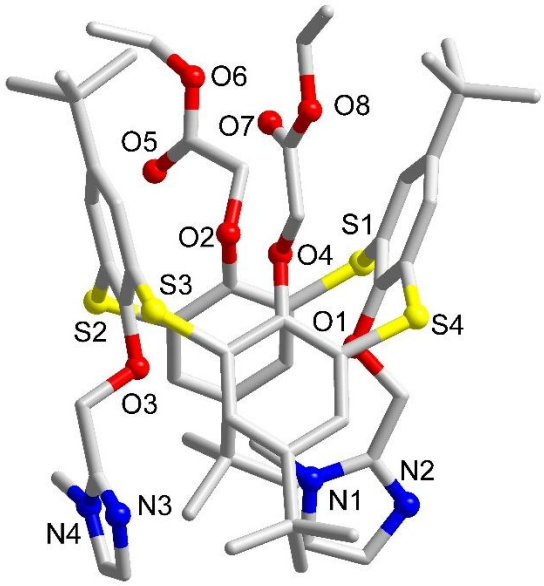

(a)

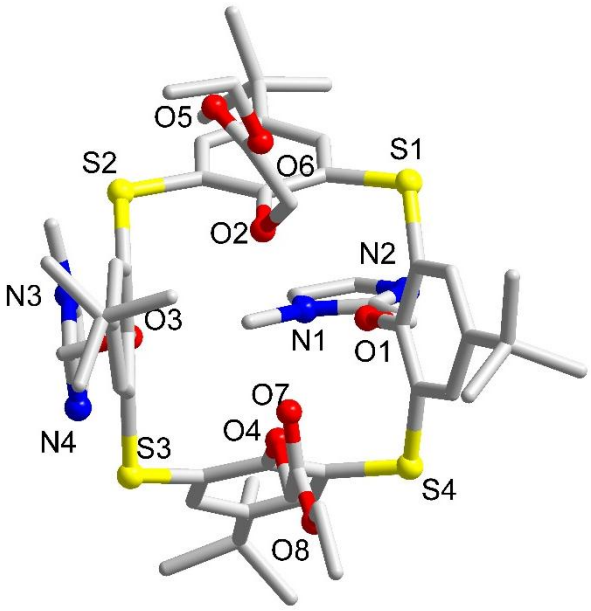

(b)

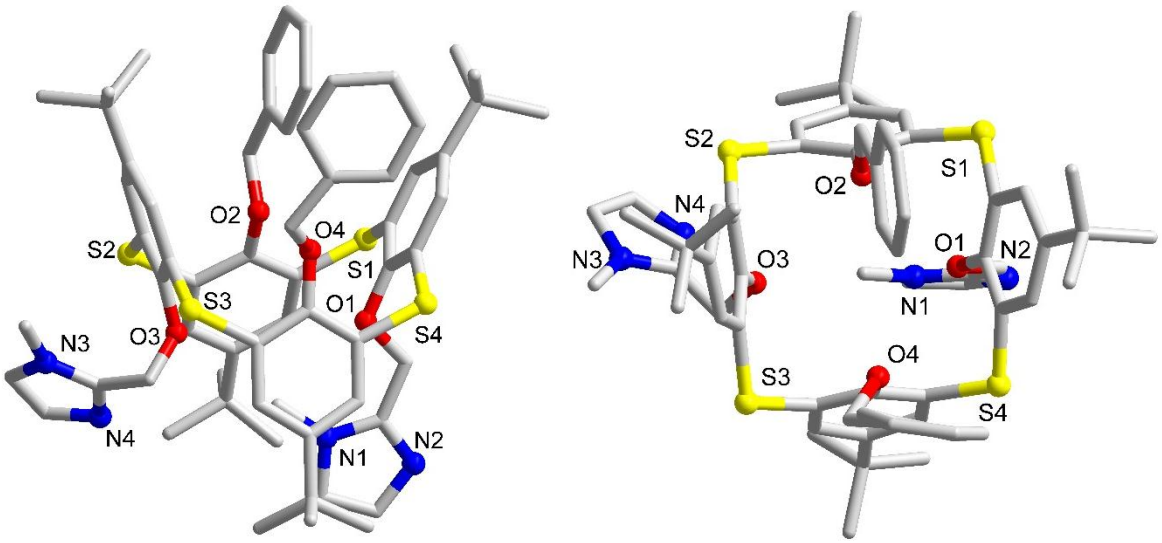

(c) (d)

Figure 2. Single-crystal structure of **L1** and **L2** showing: (a) the side view of **L1** (b) the top view of **L1**; (c) the side view of **L2** (d) the top view of **L2**. Hydrogen atoms and water molecules as solvent of crystallization, and minor disorder components have been omitted for clarity.

3.2.3 Complex behavior studies

At the onset of the study, it was anticipated that the di-topic receptor **L1** should possess multi-recognition for both hard metals (Na^+, K^+) and soft metals (Ag^+). This was due to the presence of the two ester moieties[8] at one side of the thiacalix[4]arene cavity and the two imidazole moieties[7] at the opposite side. The binding affinities of **L1** and **L2** toward metal cations were therefore evaluated by ^1H NMR titration experiments ($CDCl_3$:CD_3CN = 10:1, v/v).

3.2.3.1 ^1H NMR titration studies

Both **L1** and **L2** possess imidazole moieties which would preferentially exhibit higher affinity towards Ag^+ ion. Consequently, we carried out the ^1H NMR titration experiments of **L1** and **L2** with CF_3SO_3Ag. The addition of 1.0 equiv. Ag^+ to the solution of receptor **L1** resulted in a dramatically downfield shift ($\Delta\delta$ = +0.86 ppm) for the imidazole-N-*Me* protons at δ 3.68 ppm (Figure 3). It was noteworthy to point out that δ 3.68 ppm was almost the same chemical shift for the Imid-N-*Me* protons (δ 3.70 ppm, Table 1) of the reference compound **L3**. It strongly revealed that the Imid-N-*Me* group of **L1** was released from the shielding area

to the deshielding area upon Ag^+ was captured by receptor **L1**. Subsequently, the adjacent Imid- proton H_4 was also affected by the change in the position of the N-CH_3 group, and exhibited a downfield shift to δ 7.14 ppm (Δδ = +0.46 ppm). In contrast, the methylene protons of OCH_2Imid were also significantly up-field shifted to δ 5.04 ppm (Δδ = –0.15 ppm). This unusual chemical shift change may be attributed to the OCH_2Imid methylene protons being folded into the shielding area of the parent thiacalix[4]arene-cavity in order to form an efficient complex with Ag^+. All of the evidence strongly suggested that Ag^+ was well complexed by the nitrogen atoms of the imidazole moieties via N···Ag^+ interactions.

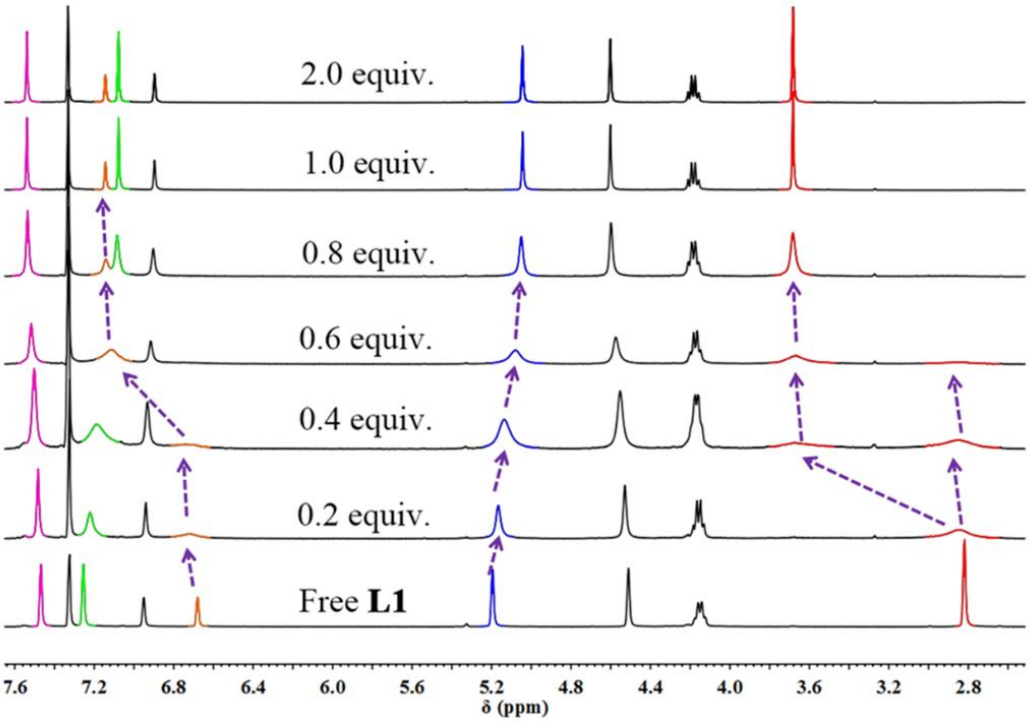

Figure 3. Partial ^{1}HNMR spectra of **L1** (5.0mM) and increasing concentrations of Ag^+ in $CDCl_3/CD_3CN$(10:1, v/v) at 298K.

Similar phenomena were observed for the titration experiments of **L2** with Ag^+ (Figure 4). The proton signals of N-*Me* and H_4 in the imidazole rings were gradually shifted to downfield by the addition of Ag^+ ions which could be attributed to the formation of **L2**·Ag^+ complex with a concomitant deshielding effect. The methylene protons of OCH_2Imid were slightly shifted up-field after complexing with 1.0 equiv. Ag^+, which may also be attributed

to the O*CH*$_2$Imid methylene protons being folded into the shielding field of the parent thiacalix[4]arene-cavity. Both **L1** and **L2** exhibited slight chemical shift changes of the

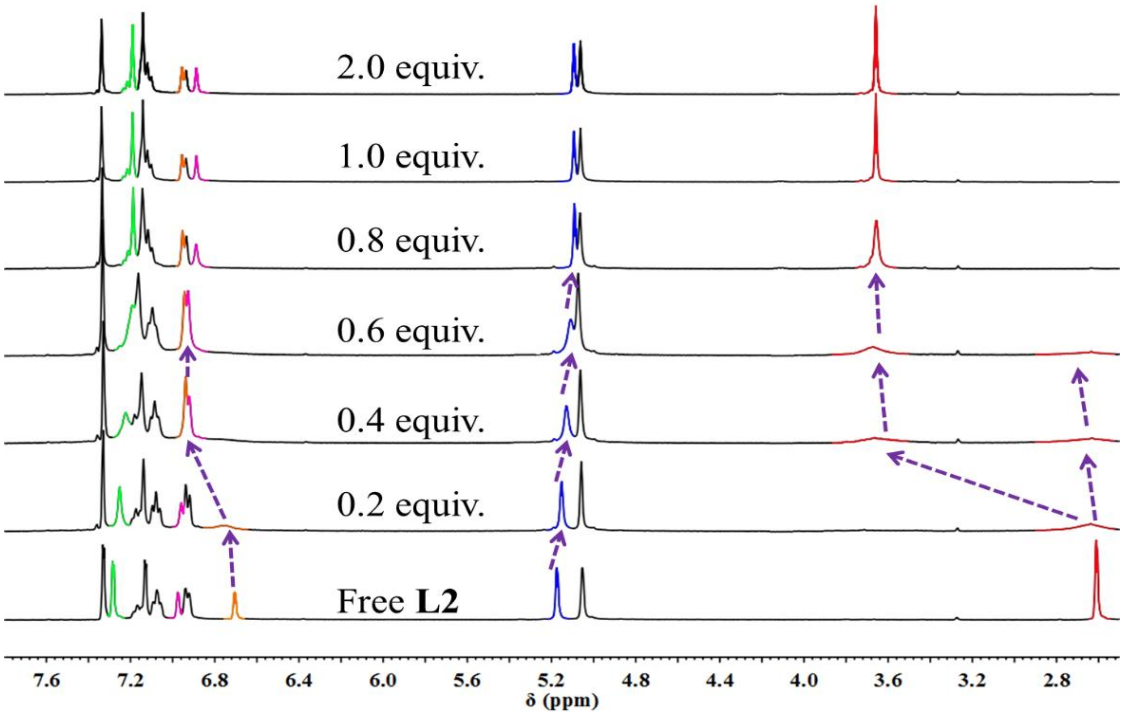

Figure 4. Partial ^{1}HNMR spectra of **L2** (5.0mM) and increasing concentrations of Ag^+ in $CDCl_3/CD_3CN$(10:1, v/v) at 298K.

benzene ring protons which were also attributed to the conformational changes upon complexation. On increasing the titration concetration of Ag^+ to 2.0 equiv., no further significant changes were observed for both of **L1** and **L2**. According to the corresponding titration curve, the association constants were calculated to be 44 M^{-1} and 83 M^{-1} by Bensei-Hilderbrand plot, respectively (Figure 5 and 6). And based upon Thordarson's global analysis for 1:1 complexation (http://app.supramolecular.org/bindfit/), the association constants values could be determined to **L1**+Ag^+ = 441 ±50 % M^{-1} and **L2**+Ag^+ = 683 ±37% M^{-1}. All of the observed results strongly suggested that receptors **L1** and **L2** possess higher affinity towards Ag^+ ion via N···Ag^+ interactions.

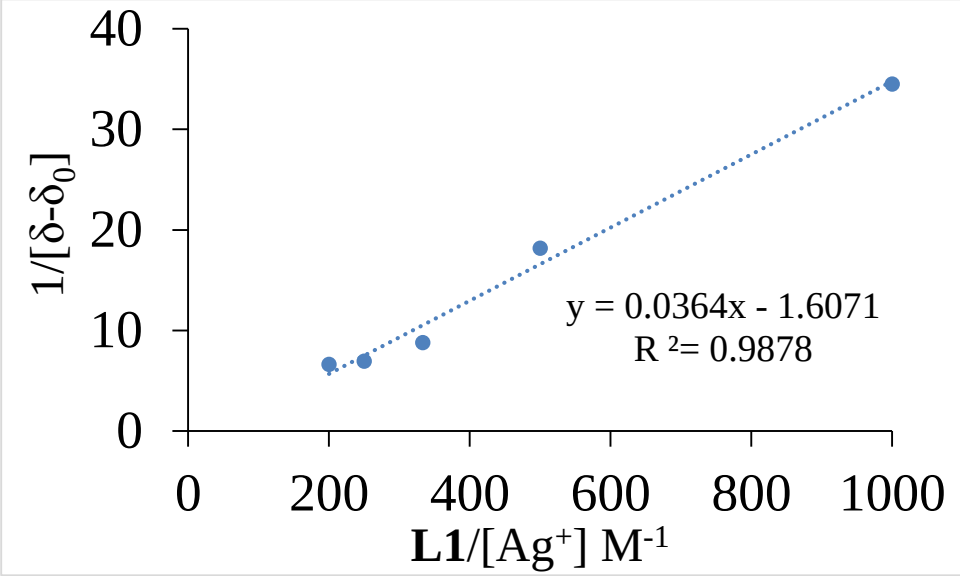

Figure 5. Bensei-Hilderbrand plot of **L1** for various concentrations of Ag^+ ion at 298 K. The associate constant (K_a) was calculated to be 44 M^{-1}.

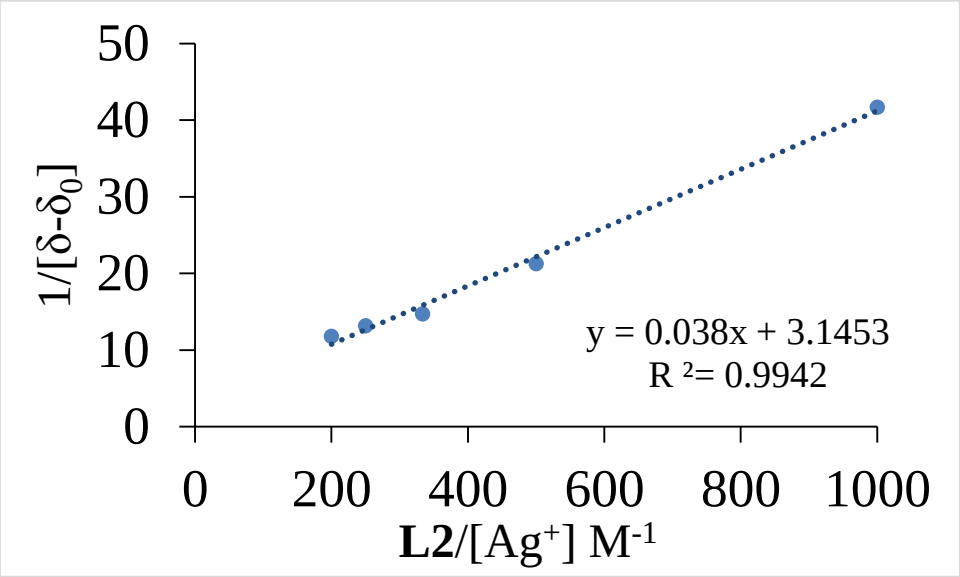

Figure 6. Bensei-Hilderbrand plot of **L2** for various concentrations of Ag^+ ion at 298 K. The associate constant (K_a) was calculated to be 83 M^{-1}.

The affinity towards alkali metal cations was also investigated, given that K^+ and Na^+ ions were known to interact with the ester moiety.[8] ^1H NMR titration experiments toward CF_3SO_3K, CF_3SO_3Na and CF_3SO_3Li were carried out. The addition of one equiv. of K^+ cation to the solution of di-topic receptor **L1** caused immediate complexation as

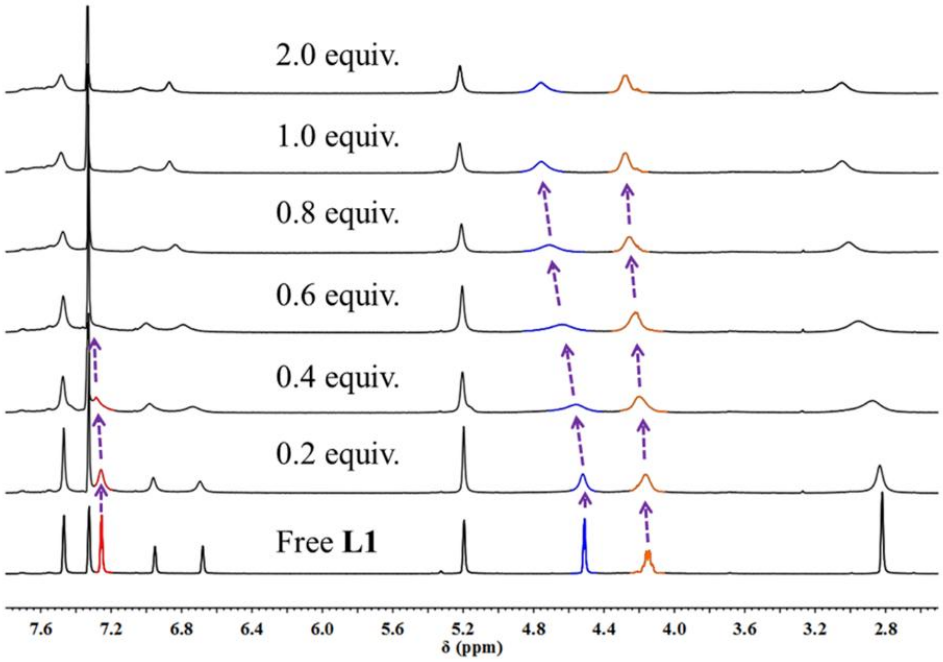

Figure 7. Partial ^{1}HNMR spectra of **L1** (5.0mM) and increasing concentrations of K^+ in $CDCl_3/CD_3CN$(10:1, v/v) at 298K.

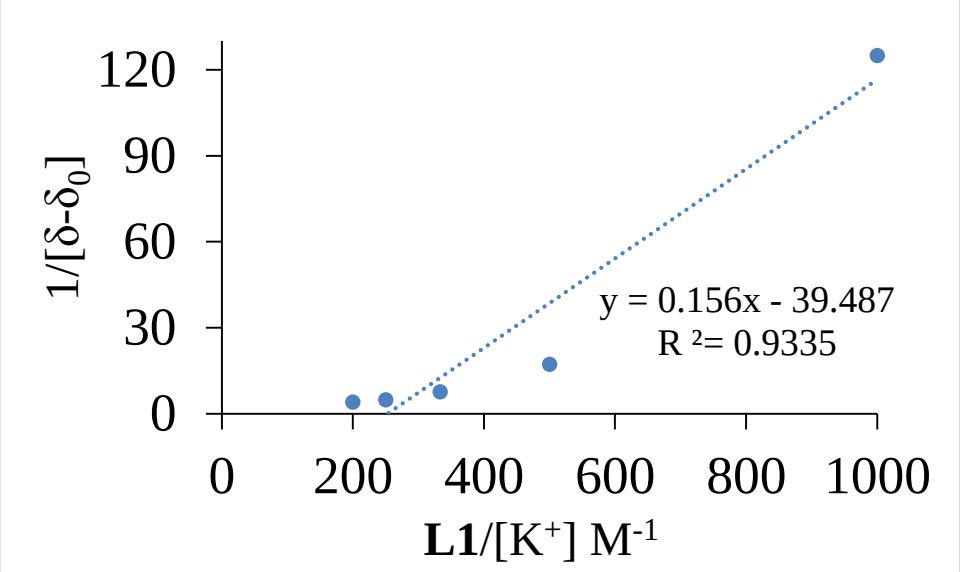

Figure 8. Bensei-Hilderbrand plot of **L1** for various concentrations of K^+ ion at 298 K. The associate constant (K_a) was calculated to be 253 M^{-1}.

demonstrated by the downfield shifts for the ester ethyl group signals (COO*CH*$_2$, Δδ = +0.12 ppm and O*CH*$_2$CO, Δδ = +0.25 ppm Figure 7) for the 1:1 complex of **L1** with an association constant of 253 M^{-1} (Figure 8). The slightly downfield shifts of the thiacalixarene benzene

protons may be attributed to the diminished shielding effect operating in two of the thiacalixarene benzene rings upon the ester moieties complex with K^+. The signals of the imidazole group's protons were broadened, indicating slow ligand exchange on the NMR time scale. A similar phenomenon was observed for the ester groups in the presence of one equiv. of Na^+ (O*CH*$_2$CO, $\Delta\delta$ = +0.15; COO*CH*$_2$, $\Delta\delta$ = +0.07 ppm, Figure 9) which formed a 1:1 complex of **L1** with an association constant of 92 M^{-1} (Figure 10). The addition of Li^+ did not cause detectable spectral changes for **L1** due to the small atom radius which could not form an efficient complex (Figure 11). According to the corresponding association constants for the complex processes, it suggests that complex ability for alkali metal cations directly follow the radius of the alkali metal cations: K^+ > Na^+ > Li^+ which reflects the size recognition ability of receptor **L1**.

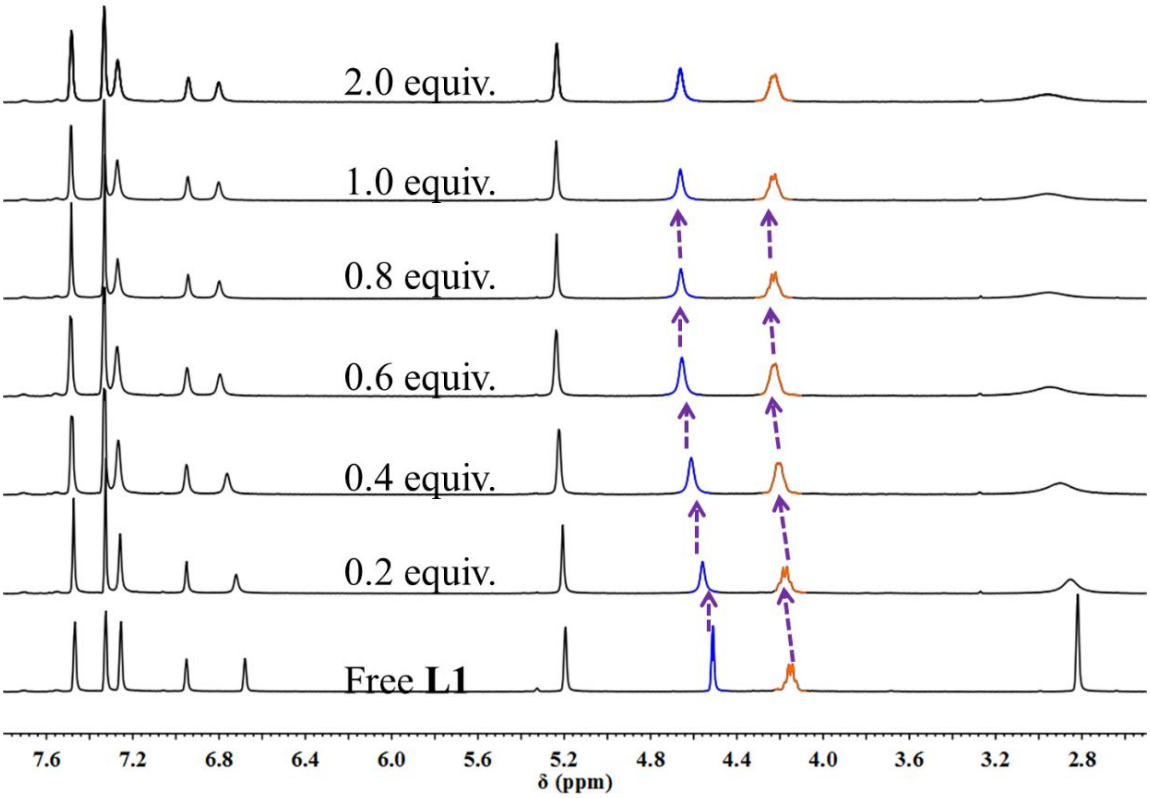

Figure 9. Partial ^{1}HNMR spectra of **L1** (5.0mM) and increasing concentrations of Na^+ in $CDCl_3/CD_3CN$(10:1, v/v) at 298K.

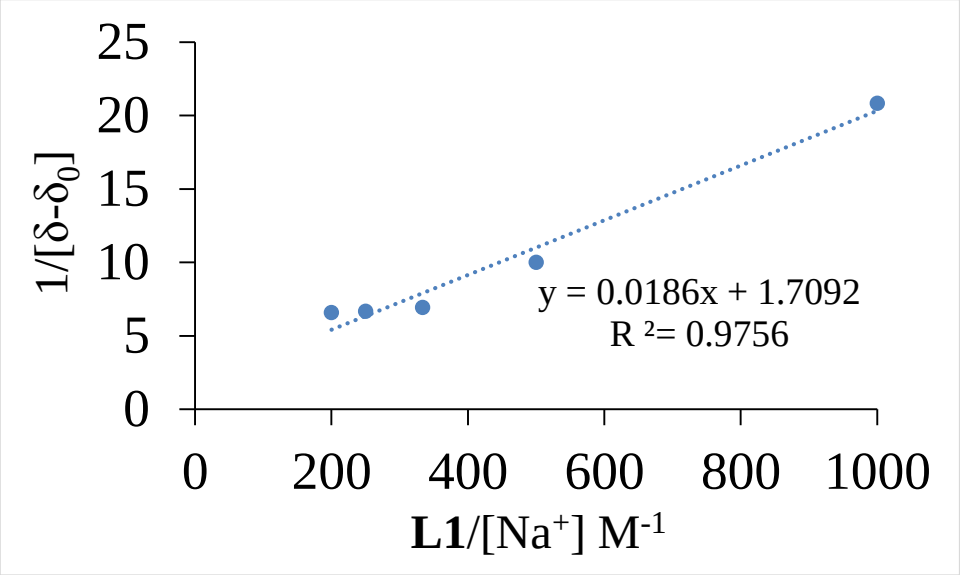

Figure 10. Bensei-Hilderbrand plot of **L1** for various concentrations of Na^+ ion at 298 K. The associate constant (K_a) was calculated to be 92 M^{-1}.

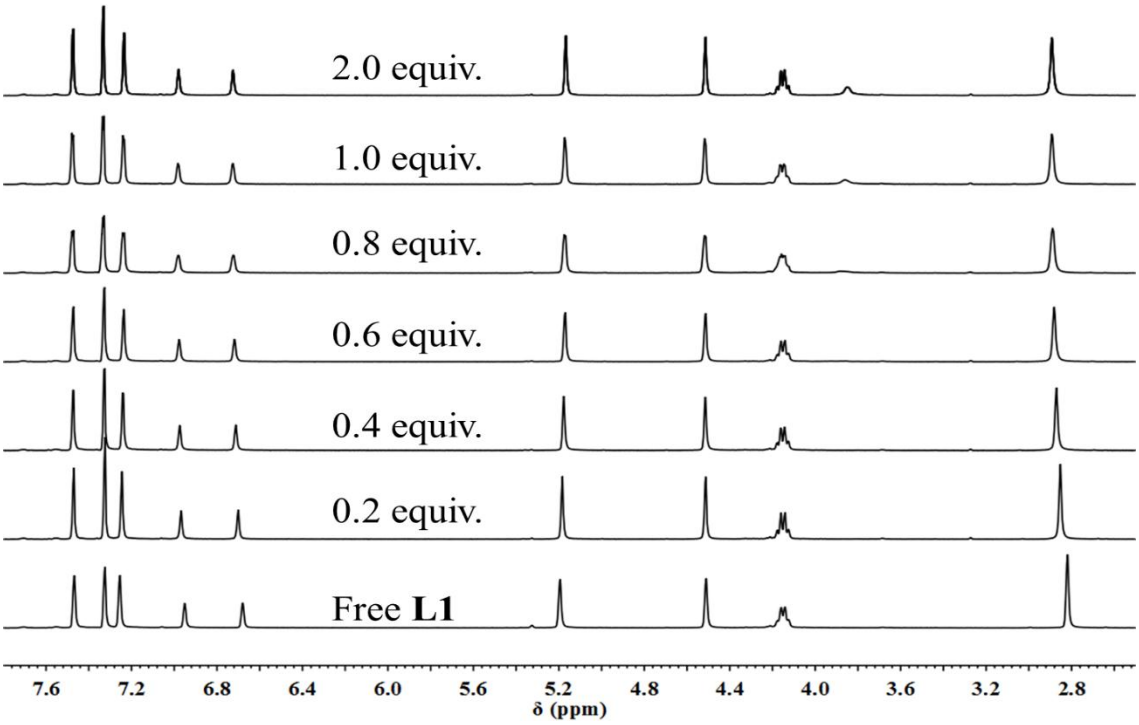

Figure 11. Partial ^{1}HNMR spectra of **L1** (5.0mM) and increasing concentrations of Li^+ in $CDCl_3/CD_3CN$(10:1, v/v) at 298K.

Given the fact that receptor **L2** was unable to bind alkali metal cations due to the presence of phenyl moieties, which are inactive for recognition of alkali metal cations, as expected, no

significant changes were observed during the ^{1}H NMR titration experiments with various alkali metal cations. The chemical shift change of the methylene (*CH*$_2$) groups of receptor **L1** and **L2** plotted against the amount of cations (Ag^+, K^+ and Na^+) were shown in Figure 12. The Δδ value increased in proportion to the amount of cations and became almost constant after the addition of one equiv. of cations, which indicated the 1:1 stoichiometry formation of the receptors–cations complex.

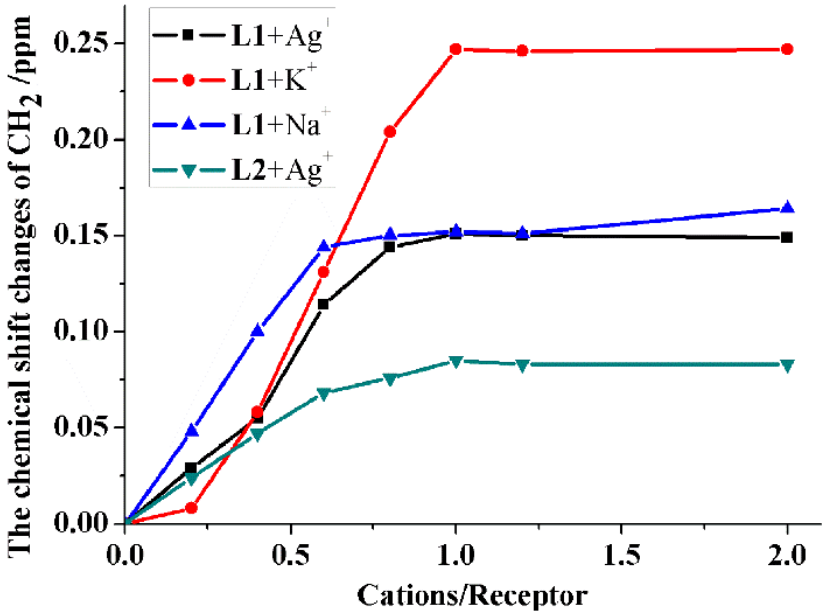

Figure 12. ^{1}H NMR shift of CH_2 groups in **L1** with Ag^+, K^+, Na^+ and **L2** with Ag^+. [In the presence of 0.2, 0.4, 0.6, 0.8, 1.0, 1.2, 2.0 equiv. of cations in $CDCl_3/CD_3CN$(10:1, v/v), respectively.]

Mass titration data further supported the formation of a stable 1:1 host–guest complex. As shown in Figure 13 ~ 15, the mass spectra of **L1** with cations exhibited peaks at 1187.123, 1119.301 and 1103.285 which was corresponding to masses of [**L1** + Ag]$^+$, [**L1** + K]$^+$ and [**L1** + Na]$^+$, respectively. And the mass spectrum of **L2** with cation showed peak at 1195.107 which is corresponding to masses of [**L2** + Ag]$^+$ (Figure 16). Thus, the 1:1 stoichiometry complex between receptors and guest cations were unambiguously confirmed by Mass. Consequently, the proposed binding model and chemical shift changes (Δδ) of **L1** and **L2** with metal ions were summarized in Figure 17.

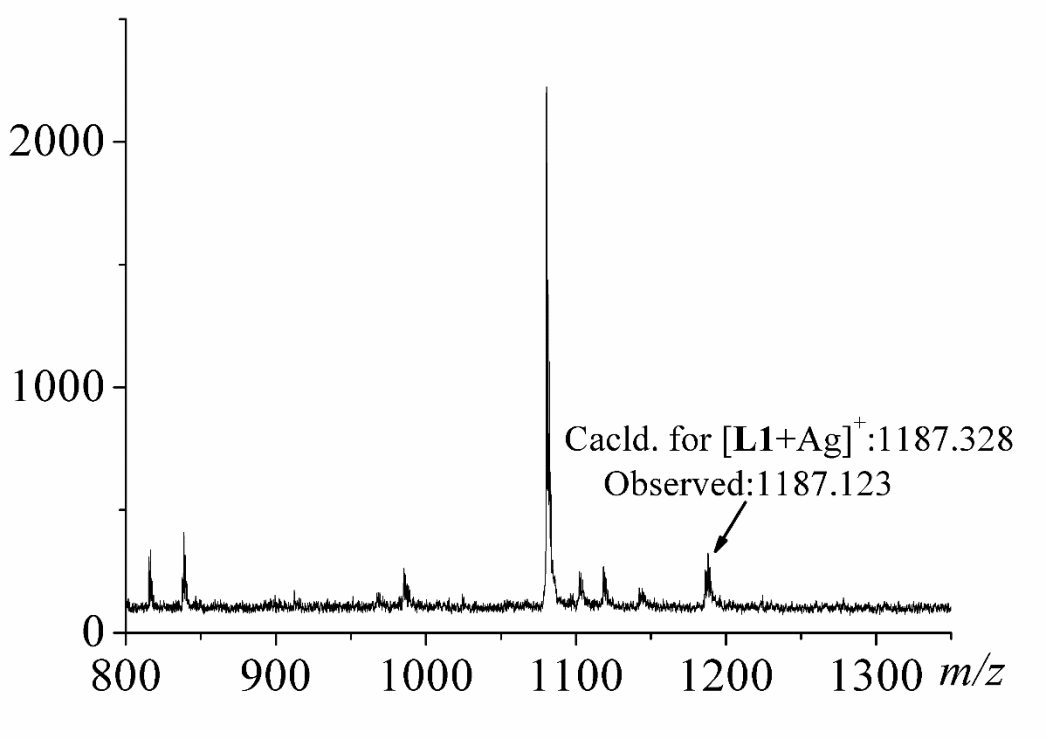

Figure 13. MALDI-TOF-MS spectra of [**L1**+Ag]$^+$ complex.

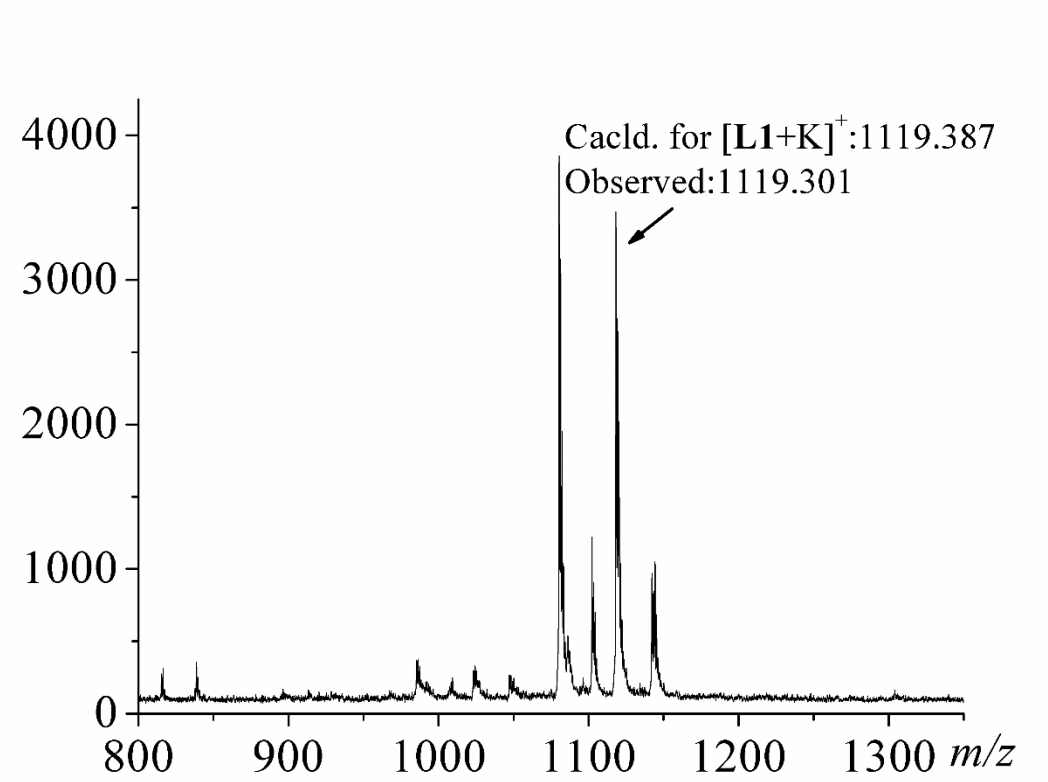

Figure 14. MALDI-TOF-MS spectra of [**L1**+K]$^+$ complex.

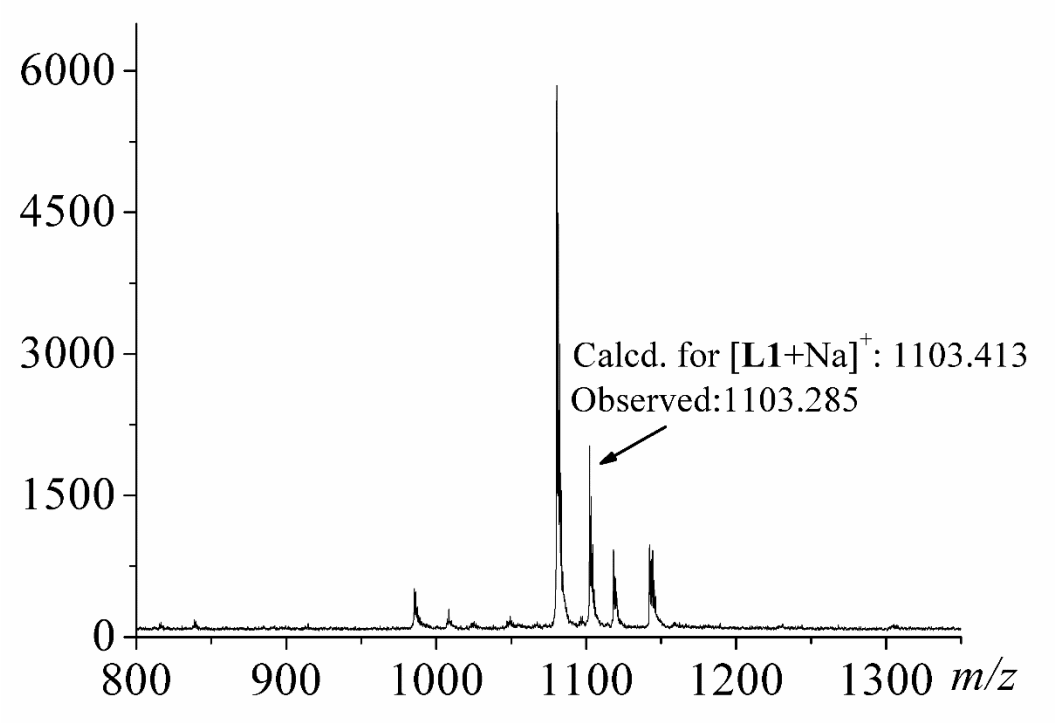

Figure 15. MALDI-TOF-MS spectra of [**L1**+Na]$^+$ complex.

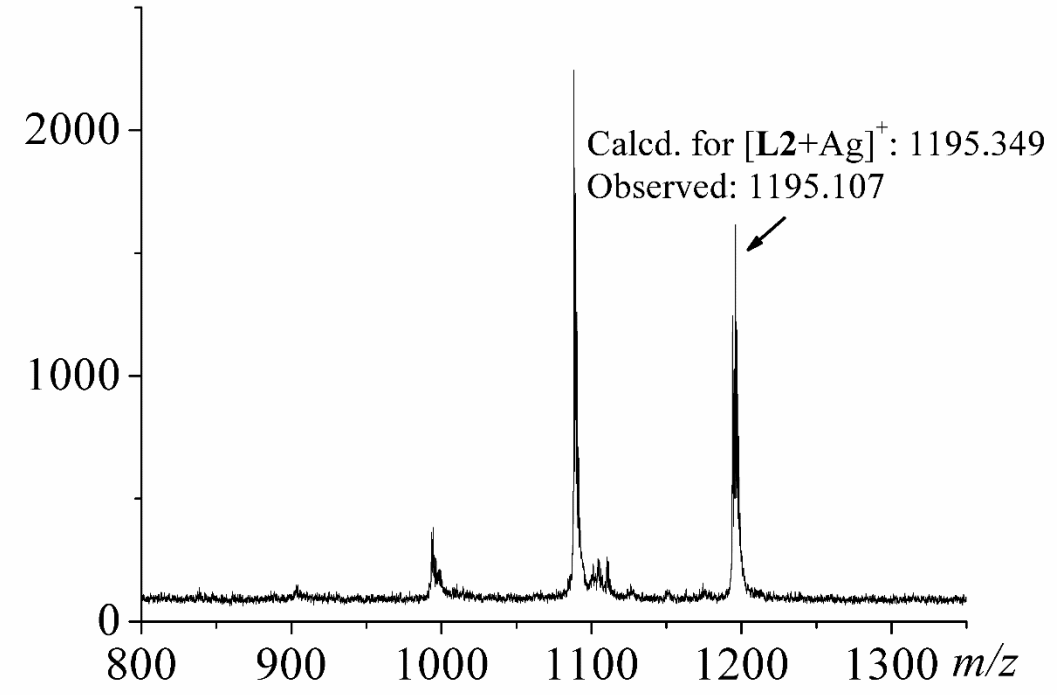

Figure 16. MALDI-TOF-MS spectra of [**L2**+Ag]$^+$ complex.

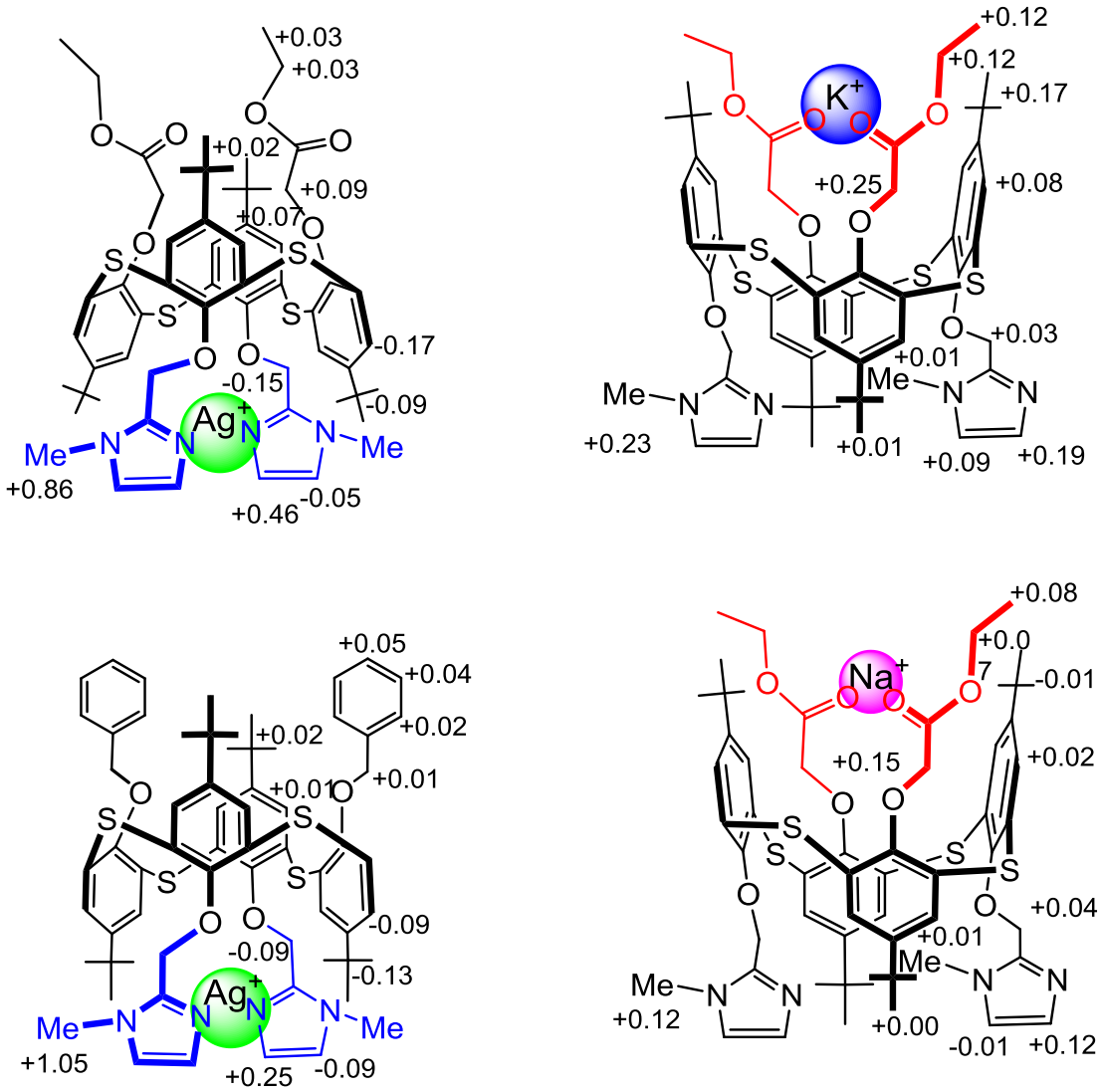

Figure 17. Chemical shift changes of **L1** and **L2** in the presence of different metal ions; (+) denotes the downfield shift and (–) denotes the up field shift.

3.2.3.2 Allosteric studies

The potential allosteric effect of **L1** was investigated by ^{1}H NMR titration experiments. Upon titration with one equiv. of Ag^{+} to the 1:1 $M^{+} \subset$ **L1** (M^{+} = K^{+}, Na^{+} or Li^{+}) complex solution, the corresponding proton signals were dramatically shifted back to the same chemical shift positions as were noted for the 1:1 $Ag^{+} \subset$ **L1** complex. This therefore implied that Ag^{+} was bound to the imidazole site and induced the decomplexation of hard metal cations (K^{+}, Na^{+} or Li^{+}) from the ester moities (Figure 17). In the other hands, the 1:1 $Ag^{+} \subset$ **L1** complex was titrated with one equiv. of M^{+} cations (M^{+} = K^{+}, Na^{+} or Li^{+}). None of the

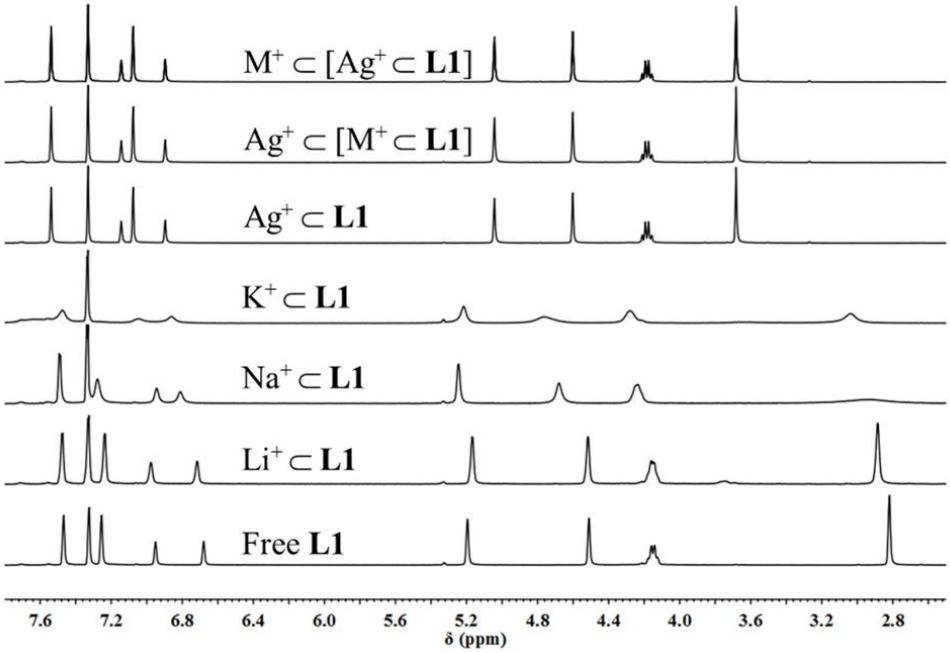

Figure 17. Partial ^{1}H NMR spectra of receptor **L1** (5.0 mM) in $CDCl_3/CD_3CN$ (10:1, v/v) complex with an equiv. of various metal ions; M^+ denoted the alkali metal cations (M^+ = Li^+, Na^+ or K^+).

spectral patterns of $K^+ \subset [Ag^+ \subset \mathbf{L1}]$, $Na^+ \subset [Ag^+ \subset \mathbf{L1}]$ and $Li^+ \subset [Ag^+ \subset \mathbf{L1}]$ complexes showed any detectable signal changes. These results indicated that the complexation of Ag^+ completely suppressed the recognition of Li^+, Na^+ or K^+ by the ester moiety. The concept of a negative allosteric effect by receptor **L1** with hard and soft cations were given in Figure 18.

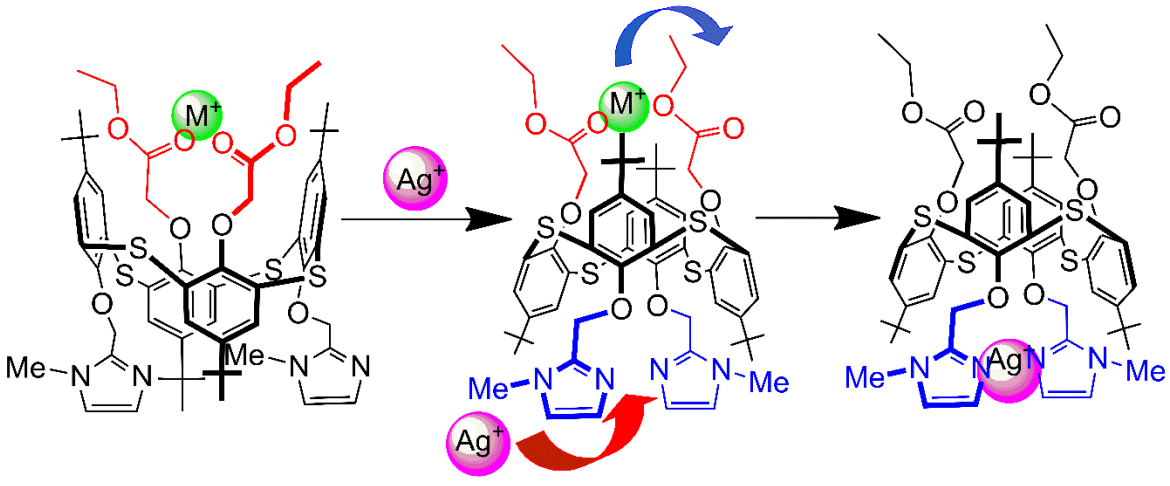

Figure 18. Proposed negative allosteric effect of di-topic recptor **L1**. M^+ denotes the alkali metal cations (M^+ = K^+, Na^+ or Li^+).

3.2.3.3 Two-phase solvent extraction

Chromium and its derivatives are widely used in our daily life, such as., leather dyes, tanning, plating, and in the photographic industry, all of which will produce large quantities of toxic pollutants.[21] However, the presence of hexavalent chromium (VI) ion is toxic to the human body, due to it can diffuse as $HCr_2O_7^-$ or $Cr_2O_7^{2-}$ through cell membranes and oxidize biological molecules.[22] Thus, selective treatment of pollutional water containing Cr (VI) prior to discharge is very important. The dichromate ($HCr_2O_7^-$ and $Cr_2O_4^{2-}$) ions are anions with oxide functionalities at their periphery. These oxide moieties are potential sites for hydrogen bonding to the complexant. Imidazole group, among such heterocyclic units, the imidazole ring can be served as an excellent hydrogen bond donor moiety in synthetic anion receptor systems, and the acidity of the NH proton of the imidazole can be tuned by changing the electronic properties of the imidazole substituents.[14] Thus, the introduction of a imidazole moiety to thiacalix[4]arene would potentially lead to an effective extractant for dichromate anions.

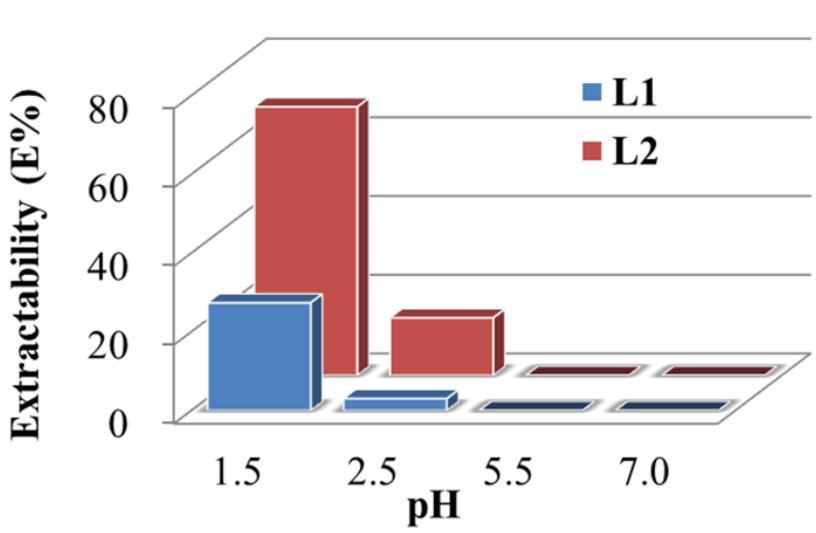

Figure 19. E% values of dichromate anion with ionophores **L1** and **L2** (2.0×10^{-4} M, 2 h at 25 ℃) at pH 1.5–7.0 (H_2O/CH_2Cl_2:10/10 (v/v); $K_2Cr_2O_7 = 1 \times 10^{-4}$ M).

To further investigate the applicability of the receptors **L1** and **L2** which possess imidazole groups, liquid-liquid extraction experiments were carried out to examine the extraction ability of **L1** and **L2** toward dichromate anions from the aqueous phase into the organic phase over the range of pH 1.5–7.0. It has been clearly demonstrated that, for both of

L1 and **L2**, the lower the pH, the higher the extractability(Figure 19). It could be attributed to the fomation of an ion-pair (hydrogen bonded) complex in the two-phase extraction system following proton transfer to the nitrogen atoms of the imidazole units in extractants **L1** and **L2** and then complexation with $Cr_2O_7^{2-}/HCr_2O_7^-$.[7] Interestingly, according to the reported reports,[7] the reference extractant **L3** showed almost no significant binding of dichromate anions even at the low pH. It strongly suggested that the thiacalix[4]arene platform played an important role in confirming cooperative participation of the peripheral imidazole groups. Furthermore, the extraction results also indicated that extractant **L2** was more effective than extractant **L1** for the extraction of dichromate anions. This could be ascribed to extractant **L2** maybe provided a more ideal mutual distance needed for hydrogen bonding between two imidazole groups to extract dichromate anions.

The imidazole moieties are 'proton-switchable' binding sites, which can be protonated at low pH.[15] The protonated forms of **L1** and **L2** are more effective at complexing with dichromate anion through hydrogen bonds. In contrast, there is no efficeint complex when the pH over 5.5. In other words, the extraction of dichromate anion by extractants **L1** and **L2** only occurs when the aqueous phase is acidic, especially at lower pH, in order to form efficient hydrogen bonds. Thus, a possible reusable extractant concept for extractant **L2** by controlling the pH of the aqueous solution is shown in Figure 20.

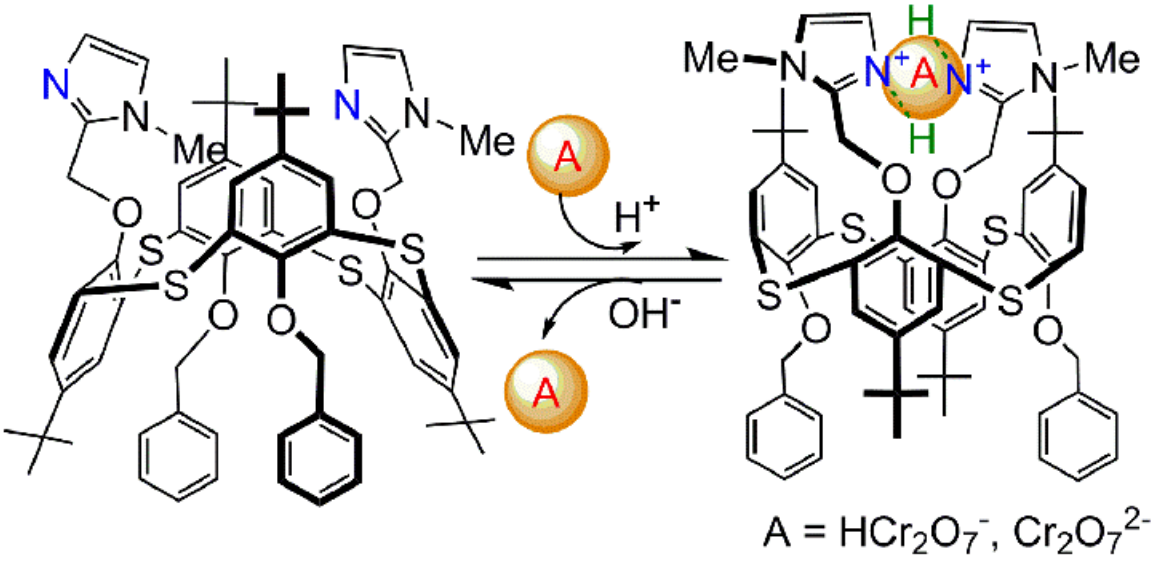

Figure 20. A proposed reusable extractant concept of **L2** with dichromate anions.

3.3 Conclusions

Two new thiacalix[4]arene receptors **L1** and **L2** which possess imidazole moieties have been synthesized and characterized. The structures for both **L1** and **L2** have been further confirmed by X-ray analysis. The binding behaviour towards Na^+, K^+ and Ag^+ ions have been evaluated by ^1H NMR titration experiments. The di-topic receptor **L1** showed affinity not only toward hard alkali metal cations but also toward soft metal Ag^+ cations, owing to the presence of ester moieties and imidazole moieties based on thiacalix[4]arene. However, the mono-topic receptor **L2** only showed affinity toward Ag^+ due to its lack of the ester groups. The exclusive formation of mononuclear complexes of **L1** with metal cations is of particular interest with respect to negative allosteric effects in the thiacalix[4]arene family. Due to the amphoteric nature of imidazole ring which can function as an effective cation and/or anion receptor system. Furthermore, the extraction abilities of **L1** and **L2** toward dichromate anion were investigated by a liquid-liquid extraction method. The extraction results indicated that the synthesized extractant **L2** can be served as a reusable extractant by control of the pH of the aqueous solution.

3.4 Experimental Section

3.4.1 General

Unless otherwise stated, all reagents used were purchased from commercial sources and were used without further purification. All solvents used were dried and distilled by the usual procedures prior to use. All melting points (Yanagimoto MP-S1) are uncorrected. ^1H NMR and ^{13}C NMR spectra were recorded on a Varian-400MR-vnmrs 400 with $SiMe_4$ as an internal reference: *J*-values are given in Hz. Mass spectra were obtained with a Nippon Denshi JMS-HX110A Ultrahigh Performance mass spectrometer at 75 eV using a direct-inlet system. Elemental analyses were performed by Yanaco MT-5. UV-vis spectra were recorded using a Shimadzu UV-3150UV-vis-NIR spectrophotometer.

3.4.2 Materials

2-Chloromethyl-1-methyl-*1H*-imidazole hydrochloride,[9] 5,11,17,23 -tetra-*tert*-butyl-25,27-bis[(ethoxycarbonyl)methoxy]-26,28-dihydro-xy-2,8,14,20-tetrathiacalix[4]arene **1**[10] and

25,27-dibenzyloxy-5,11, 17,23-tetra-*tert*-butyl-2,8,14,20-tetra thiacalix[4]arene-26,28-diol **2**[11] were prepared according to the reported procedures.

3.4.2.1. Synthesis of 5,11,17,23-tetra-tert-butyl-25,27-bis[(ethoxycarbonyl)-methoxy]-26,28-bis-[1-methyl-(imidazole)-methoxy]-2,8,14,20-tetra-thiacalix[4]arene (L1)

A mixture of compound **1** (200 mg, 0.224 mmol) and Cs_2CO_3 (728 mg, 2.24 mmol) in dry acetone (30 mL) was heated at reflux for 1 h under nitrogen. Then 2-chloromethyl-1-methyl-*1H*-imidazole hydrochloride (372 mg, 2.24 mmol) was added and the mixture was heated at reflux for another 20 h. After cooling the reaction mixture to room temperature, it was acidified with 1 M HCl (15 mL) and extracted with CH_2Cl_2 (20 mL × 3). The combined extracts were washed with water (30 mL × 2) and then brine (30mL × 1), and dried with Mg_2SO_4. The organic solvent was removed under reduced pressure and the crude product was purified by column chromatography with chloroform–ethyl acetate (1:1) as an eluent to give **L1** (133 mg, 55%) as colourless prisms, M.p. 239–241 ℃. ^{1}H NMR (400 MHz, $CDCl_3$): δ = 1.10 (s, 18 H, *t*-Bu), 1.21 (t, 6 H, *J* = 7.1 Hz, CH_2CH_3), 1.26 (s, 18 H, *t*-Bu), 2.78 (s, 6 H, Imid-CH_3), 4.14 (q, 4 H, *J* = 7.1 Hz, $COOCH_2$), 4.52 (s, 4 H, OCH_2COO), 5.21 (s, 4 H, OCH_2Imme), 6.65 (s, 2 H, Imid-H_4), 6.96 (s, 2 H, Imid-H_5), 7.24 (s, 4H, Ar-*H*) and 7.46(s, 4 H, Ar-*H*) ppm. ^{13}C NMR (100 MHz, $CDCl_3$): δ = 31.0, 31.1, 33.0, 34.1, 34.2, 60.3, 65.1, 65.9, 121.8, 127.5, 127.6, 128.4, 129.3, 131.9, 143.5, 146.6, 146.8, 155.4, 156.8 and 167.7 ppm. FABMS: *m/z*: $[M+H]^+$ Calcd for $C_{58}H_{73}N_4O_8S_4$ 1081.4311; Found 1081.4319.

3.4.2.2. Synthesis of 5,11,17,23-tetra-tert-butyl-25,27-bis[(benzyl)metho-xy]-26,28-bis-[1-methyl-(imidazole)methoxy]-2,8,14,20-tetrathiacalix[4]arene (L2)

A mixture of compound **2** (200 mg, 0.221 mmol), Cs_2CO_3 (720 mg, 2.21 mmol) in dry acetone (30 mL) was heated at reflux for 1 h under nitrogen. Then a solution of 2-chloromethyl-1-methyl-*1H*-imidazole hydrochloride (369 mg, 2.21 mmol) was added and the mixture was heated at reflux for another 20 h. After cooling the reaction mixture to room temperature, it was acidified with 1 M HCl (15 mL) and extracted with CH_2Cl_2 (20 mL × 3). The combined extracts were washed with water (30 mL × 2) and then brine (30mL × 1), dried with (Mg_2SO_4). The organic solvent was removed under reduced pressure and the crude product was purified by column chromatography with chloroform as an eluent to give **L2**

(105 mg, 44%) as colourless prisms, M.p. 252–253 ℃. ^{1}H NMR (400 MHz, $CDCl_3$): δ = 0.82 (s, 18 H, t-Bu), 1.15 (s, 18 H, t-Bu), 2.57(s, 6 H, Imid-CH_3), 5.05 (s, 4 H, OCH_2Ph), 5.18 (s, 4 H, OCH_2Imid), 6.68(d, *J* = 0.7 Hz, 2 H, Imid-H_4), 6.91(d, *J* = 7.3 Hz, 4 H, Ph-*H*) 6.99(d, *J* = 0.9 Hz, 2 H, Imid-H_5), 7.06(t, *J* = 7.5 Hz, 4 H, Ph-*H*), 7.12 (s, 4 H, Ar-*H*), 7.16 (t, *J* = 7.3 Hz, 2 H, Ph-*H*) and 7.27 (s, 4 H, Ar-*H*) ppm. ^{13}C NMR (100 MHz, $CDCl_3$): δ = 30.7, 31.2, 32.8, 33.9, 34.3, 64.5, 70.7, 122.1, 126.9, 127.2, 127.4, 128.0, 128.6, 128.9, 129.3, 129.5, 137.3, 143.6, 146.8, 146.9, 156.2 and 156.6 ppm. FABMS: found 1089.35 $[M+H]^+$. Anal. calcd. For $C_{64}H_{73}N_4O_4S_4$ ($[M + H]^+$ *m/z* = 1089.45): C, 70.55; H, 6.66; N, 5.14 %, found: C, 70.44; H, 6.43; N, 5.10%.

3.4.2.3. Liquid-liquid extraction studies[17]

Two-phase solvent extraction was carried out between $K_2Cr_2O_7$ aqueous (10 mL, [dichromate anion] = 1.0×10^{-4} M) and host (10 mL, [host] = 2×10^{-4} M in CH_2Cl_2). A few drops of 0.01 M KOH/HCl solution were added in order to obtain the desired pH at equilibrium and maintain the ionic strength. The two phase mixture in a stoppered flask was immersed in a thermostated water bath at 25 °C which was shaken at 300 strokes per min for 4 h and then kept at the same temperature for 1 h, allowing the complete separation of the two phases. Each extraction experiment was repeated three times. The concentration of dichromate ion remaining in the aqueous phase was determined by UV spectroscopy. Blank experiments showed that no dichromate extraction occurred in the absence of thiacalix[4]arene derivatives **L1** and **L2**. The percent extraction (*E*%) has been calculated using the following expression:

$$E\% = (C_0 - C/C_0) \times 100$$

where C_0 and C are the initial and final concentrations of the metal dichromate before and after the extraction, respectively.

3.4.2.4. ^{1}H-NMR complexation experiments

To a $CDCl_3/CD_3CN$ (v/v 10:1, v/v) solution of **L1** and **L2** (5×10^{-3} M) in an NMR tube was gradually added 0.2 – 2.0 equivalent of the related metal perchlorates. The spectrum was recorded after the addition and the temperature of the NMR probe was kept constant at 27 °C.

The ^{1}H NMR data of the most representative complexes is given below:

$Ag^+ \subset$ **L1**(1:1), (400 MHz, $CDCl_3/CD_3CN$, 10:1): δ = 1.01 (s, 18 H, t-Bu), 1.24 (t, 6 H, *J* = 7.2 Hz, CH_2CH_3), 1.29 (s, 18 H, t-Bu), 3.68 (s, 6 H, Imid-CH_3), 4.18 (q, 4 H, *J* = 7.0 Hz, CO_2CH_2), 4.60 (s, 4 H, OCH_2CO_2), 5.04 (s, 4 H, OCH_2Imid), 6.90 (s, 2 H, Imid-H_5), 7.08 (s, 4 H, Ar-*H*), 7.14 (s, 2 H, Imid-H_4), 7.54 (s, 4 H, Ar-*H*).

$K^+ \subset$ **L1**(1:1), (400 MHz, $CDCl_3/CD_3CN$, 10:1): δ = 1.27 (s, 36 H, t-Bu), 1.34 (m, 6 H, CH_2CH_3), 3.05(s, 6 H, Imid-CH_3), 4.27(m, 4 H, CO_2CH_2), 4.76(s, 4 H, OCH_2CO_2), 5.22 (s, 4 H, OCH_2Imid), 6.87 (s, 2 H, Imid-H_4), 7.04 (s, 2 H, Imid-H_5), 7.34 (s, 4 H, Ar-*H*), 7.48 (s, 4 H, Ar-*H*).

$Na^+ \subset$ **L1**(1:1), (400 MHz, $CDCl_3/CD_3CN$, 10:1): δ = 1.09 (s, 18 H, t-Bu), 1.26 (s, 18 H, t-Bu), 1.30 (m, 6 H, CH_2CH_3), 2.94 (s, 6H, Imid-CH_3), 4.22 (m, 4 H, CO_2CH_2), 4.66 (s, 4 H, OCH_2CO_2), 5.23 (s, 4 H, OCH_2Imid), 6.80 (s, 2 H, Imid-H_4), 6.94 (s, 2 H, Imid-H_5), 7.27 (s, 4 H, Ar-*H*), 7.48 (s, 4 H, Ar-*H*) .

$Ag^+ \subset$ **L2** (1:1), (400 MHz, $CDCl_3/CD_3CN$, 10:1): δ = 0.85 (s, 18 H, t-Bu), 1.03 (s, 18 H, t-Bu), 3.66 (s, 3 H, Imid-CH_3), 5.06 (s, 4 H, OCH_2Ph), 5.09 (s, 4 H, OCH_2Imid), 6.89 (s, 2 H, Imid-H_5), 6.95 (d, J = 7.4 Hz, 4 H, Ph-*H*), 6.96 (s, 2H, Imid-H_4), 7.12 (m, 4H, Ph-H), 7.14 (s, 4 H, Ar-*H*) and 7.19 (s, 4 H, Ar-*H*), 7.22 (m, 2 H, Ph-*H*).

3.4.2.5. X-ray Crystallography

Diffraction data were collected on a Bruker APEX 2 CCD diffractometer equipped with graphite-monochromated Mo-Kα radiation for **L1·3EtOH·H$_2$O** and with synchrotron radiation for **L2·2.58EtOH**.[18] Data were corrected for Lorentz and polarisation effects and for absorption.[18] The structures were solved by charge flipping or direct methods algorithms and refined by full-matrix least-squares methods, on F^2.[19] In **L1·3EtOH·H$_2$O** Atom C(49) was modelled as 2-fold disordered with major component 55.1(13)%. One of the ethanol molecules was modelled as a region of diffuse electron denistry using the Platon Squeeze

procedure.[20] The water molecule was also 2-fold disordered and the minor component was modelled with Squeeze. In **L2 2.58EtOH** The non-integer amount of EtOH is a consequence of the nature of the imidazole disorder. The benzyl group containing C(58) > C(64) was modelled as disordered over two sets of positions with major site occupation factor of 54.9(12)%. The 1-methylimidazole group attached to C(53), and C(53) itself, were modelled as disordered over two sets of positions with major site occupation factor of 57.3(5)%. Both positions are pointing outside the calixarene cavity. The ethanol molecule containing O(5) was modelled as disordered over three sets of positions. Those containing O(5) and O(5Y) are present when the major disorder component of imidazole group containing C(53) is present and has the same occupation factor. That containing O(5X) is present when the minor imidazole disorder component containing C(53X) is present and has the same occupation factor of 42.7(5)%.

Table 2 Summary of crystal data for the receptors **L1**, and **L2**.

Complex	**L1**	**L2**
Empirical formula	$C_{58}H_{72}N_4O_8S_4$ 3EtOH H_2O	$C_{64}H_{72}N_4O_4S_4$ 2.58EtOH
Formula weight	1237.65	1208.05
Crystal system	Triclinic	Triclinic
Space group	$P\ \bar{1}$	$P\ \bar{1}$
a[Å]	13.9134(18)	14.6911(6)
b[Å]	15.4414(19)	14.8673(6)
c[Å]	17.086(2)	15.0303(7)
α[°]	103.616(2)	85.407(3)
β[°]	104.584(2)	86.152(3)
γ[°]	96.412(2)	79.641(3)
Volume[Å^3]	3395.2(7)	3214.3(2)
Z	2	2
Crystal size[mm^3]	0.88 × 0.42 × 0.20	0.11 × 0.09 × 0.01
λ[Å]	0.71073	0.7749
Dcalcd[Mg/m^3]	1.211	1.248
μ[mm^{-1}]	0.20	0.25
temperature [K]	150(2)	100(2)
Measured reflns	37601	22331
unique reflns	12465	8081
obsd reflns	8007	5494
parameters	815	942
R(int)	0.062	0.060
R[*I*> 2σ(*I*)][a]	0.069	0.087
wR2[all data][b]	0.193	0.256
GOF on F^2	1.03	1.05

[a] Conventional *R* on F_{hkl}: $\Sigma||F_o| - |F_c||/\sigma|F_o|$. [b] Weighted *R* on $|F_{hkl}|^2$: $\Sigma[w(F_o^2 - F_c^2)_2]/\Sigma[w(F_o^2)^2]^{1/2}$

Crystallographic data for the structures in this paper have been deposited with the Cambridge Crystallographic Data Centre as supplementary publication numbers CCDC 1445271 & 1445272. Copies of the data can be obtained, free of charge, on application to CCDC, 12 Union Road, Cambridge CB2 1EZ, UK [fax: 144-1223-336033 or e-mail: deposit@ccdc.cam.ac.uk].

3.5 References

1 (*a*) L. Stryer, *Biochemistry, 4th ed.*, W. H. Freeman, New York, 1995; (*b*) A. Livitzki, *Quantitative Aspects of Allosteric Mechanism*; Springer-Verlag, Berlin, 1978; (*c*) M. Takeuchi, M. Ikeda, A. Sugasaki and S. Shinkai, *Acc. Chem. Res.*, 2001, **34**, 865–873; (*d*) C. Kremer and A. Lützen. *Chem. Eur. J.*, 2013, **19**, 6162-6196.

2 (*a*) T. Endoh and N. Sugimoto, *Anal. Chem.*, 2015, **87**, 7628–7635; (*b*) A. M. Lifschitz, M. S. Rosen, C. M. McGuirk and C. A. Mirkin, *J. Am. Chem. Soc.*, 2015, **137**, 7252–7261; (*c*) L. Kovbasyuk and R. Kramer, *Chem. Rev.*, 2004, **104**, 3161-3187.

3 (*a*) T. Nabeshima, *Coord. Chem. Rev.*, 1996, **148**, 151–169; (*b*) B. Linton and A.D. Hamilton, *Chem. Rev.*, 1997, **97**, 1669–1680; (*c*) T. Nabeshima, S. Akine and T. Saiki, *Rev. Heteroatom Chem.*, 2000, **22**, 219–239; (*d*) N. Y. Edwards and A. L. Possanza, *Supramol. Chem.*, 2013, **25**, 446-463.

4 (*a*) T. Nabeshima, T. Saiki and S. Akine, *Tetrahedron Lett.*, 2004, **45**, 4719–4722; (*b*) T. Saiki, J. Iwabuchi, S. Akine and T. Nabeshima, *Tetrahedron Lett.*, 2004, **45**, 7007–7010; (*c*) T. Nabeshima, Y. Yoshihira, T. Saiki, S. Akine and E. Horn, *J. Am. Chem. Soc.*, 2003, **125**, 28–29; (*d*) P. D. Beer, J. P. Martin and M. G. B. Drew, *Tetrahedron*, 1992, **48**, 9917–9928.

5 (*a*) H. Tomiyasu, J. L. Zhao, X. L. Ni, X. Zeng, M. R. J. Elsegood, B. Jones, C. Redshaw, S. J. Teat and T. Yamato, *RSC Adv.*, 2015, **5**, 14747–14755; (*b*) H. Tomiyasu, C. C. Jin, X. L. Ni, X. Zeng, C. Redshaw and T. Yamato, *Org. Biomol. Chem.*, 2014, **12**, 4917–4923; (*c*) J.-L. Zhao, H. Tomiyasu, C. Wu, H. Cong, X. Zeng, S. Rahman, P. E. Georghiou, D. L. Hughes, C. Redshaw and T. Yamato, *Tetrahedron*, 2015, **71**, 8521-8527; (*d*) R. Kumar, Y. O. Lee, V. Bhalla, M. Kumar and J. S. Kim, *Chem. Soc. Rev.*,

2014, **43**, 4824–4870; (*e*) N. Morohashi, F. Narumi, N. Iki, T. Hattori and S. Miyano, *Chem. Rev.*, 2006, **106**, 5291–5316.

6 (*a*) S. Singha, D. Kim, H. Seo, S. W. Cho and K. H. Ahn, *Chem. Soc. Rev.*, 2015, **44**, 4367–4399; (*b*) X. Li, S. L. Gong, W. P. Yang, Y. Li, Y. Y. Chen and X. G. Meng, *J. Incl. Phenom. and Macrocycl. Chem.*, 2010, **66**, 179–184; (*c*) A. Melaiye, Z. Sun, K. Hindi, A. Milsted, D. Ely, D. H. Reneker, C. A. Tessier and W. J. Youngs, *J. Am. Chem. Soc.*, 2005, **127**, 2285–2291.

7 (*a*) J. L. Zhao, H. Tomiyasu, X. L. Ni, X. Zeng, M. R. J. Elsegood, C. Redshaw, S. Rahman, P. E. Georghiou and T. Yamato, *New J. Chem.*, 2014, **38**, 6041–6049; (*b*) X. L. Ni, C. C. Jin, X. K. Jiang, M. Takimoto, S. Rahman, X. Zeng, D. L. Hughes, C. Redshaw and T. Yamato, *Org. Biomol. Chem.*, 2013, **11**, 5435–5442.

8 (*a*) X. L. Ni, H. Cong, A. Yoshizawa, S. Rahman, H. Tomiyasu, U. Ray- han, X. Zeng and T. Yamato, *J. Mol. Struct.*, 2013, **1046**, 110–115; (*b*) E. G. Akgemci, H. Bingol, M. Ersoz, I. Stibor, *Electroanal.*, 2008, **20**, 1354–1360; (*c*) T. Yamato, C. P. Casas, M. R. J. Elsegood, S. H. Dale and C. Redshaw, *J. Incl. Phenom. Macrocycl. Chem.*, 2006, **55**, 31–36; (*d*) N. Iki, F. Narumi, T. Fujimoto, N. Morohashi and S. Miyano, *J. Chem. Soc. Perkin Trans. 2*, 1998, 2745–2750.

9 C. Liao, X. Zhu, X. G. Sun and S. Dai, *Tetrahedron Lett.*, 2011, **52**, 5308–5310.

10 M. Lamouchi, E. Jeanneau, R. Chiriac, D. Ceroni, F. Meganem, A. Brioude, A. W. Coleman and C. Desroches, *Tetrahedron Lett.*, 2012, **53**, 2088–2090.

11 T. Yamato, C. P. Casas, H. Yamamoto, M. R. J. Elsegood, S. H. Dale and C. Redshaw, *J. Incl. Phenom. Macrocycl. Chem.*, 2005, **54**, 261–269.

12 U. Svanholm and V. D. Parker, *J. Chem. Soc., Perkin Trans. 1*, 1973, **1**, 562–566.

13 J. L. Zhao, H. Tomiyasu, X. L. Ni, X. Zeng, M. R. J. Elsegood, C. Redshaw, S. Rahman, P. E. Georghiou, S. J. Teat and T. Yamato, *Org. Biomol. Chem.*, 2015, **13**, 3476−3483.

14 P. Molina, A. Tarraga and F. Oton, *Org. Biomol. Chem.*, 2012, **10**, 1711–1724.

15 (*a*) M. Tabakci, B. Tabakci and A. D. Beduk, *Tetrahedron*, 2012, **68**, 4182–4186; (*b*) A. Yilmaz, B. Tabakci and M.Tabakci, *Supramol. Chem.*, 2009, **21**, 435–441; (*c*) M. Tabakci, S. Memon and M. Yilmaz, *Tetrahedron*, 2007, **63**, 6861–6865; (*d*) A. Yilmaz, B. Tabakci, E. Akceylan and M. Yilmaz, *Tetrahedron*, 2007, **63**, 5000–5005.

16 (*a*) J. -P. E. Grolier and J. M. Del R ǿ, *J. Chem. Thermodynamics*, 2012, **55**, 193-202; (*b*) J. Makowska, K. Żamojć, D. Wyrzykowski, D. Uber, M. Wierzbicka, W. Wiczk and L. Chmurzyński, *Spectrochim. Acta A,* 2016, **153**, 451–456; (*c*) E. Freire, O. L. Mayorga and M. Straume, *Anal. Chem.*, 1990, **62**, 950A-959A.

17 (*a*) S. Sayin, F. Ozcan and M. Yilmaz, *Mat. Sci. Eng. C-Mater.*, 2013, **33**, 2433–2439; (*b*) A. Yilmaz, S. Memon and M. Yilmaz, *Tetrahedron*, 2002, **58**, 7735–7740.

18 APEX 2 & SAINT (2012), software for CCD diffractometers. Bruker AXS Inc., Madison, USA.

19 (*a*) G. M. Sheldrick, *Acta Crystallogr*. 2008, **A64**, 112-122; (*b*) G. M. Sheldrick, *Acta Cryst*. 2015, **A71**, 3–8; (*c*) G. M. Sheldrick, *Acta Cryst*. 2015, **C71**, 3–8.

20 A.L. Spek, *Acta Crystallogr*. 1990, **A46**, C34.

21 (*a*) C. Raji and T. S. Anirudhan, *Water Res.* 1998, **32**, 3772–3780; (*b*) N. Goyal, S. C. Jain and U. C. Banerjee, *Adv. Environ. Res.* 2003, **7**, 311–319.

22 P. G. Krishna, J. M. Gladis, U. Rambabu, T. P. Rao and G. R. K. Naidu, *Talanta,* 2004, **63**, 541–546.

Chapter 4

A Rare Photochemical Reaction Based on Thiacalix[4]arene Armed with Anthracene Moiety

This chapter described a new type of photochemical reaction based on thiacalix[4]arene. A rare and exclusive endoperoxide photoproduct was quantitatively obtained from a thiacalix[4]arene crown-shaped derivative upon irradiation at 365 nm.

4.1 Introduction

Photochemica reactions have found widespread utility in both bio- and polymer science given that the use of light as a "reagent" is considered an ideal external control element for in situ chemical manipulation, *i.e.* it is clean, inexpensive, acts as very invasive switching stimulus and there is no need to add external chemical species.[1] We firstly investigated the photochemical behavious of thiacalix[4]arene derivative in this chapter which expected that the present design strategy will help to extend applications of thiacalixarenes. Of the many photochemical reaction systems, anthracene and its derivatives are of special interest due to the possibility of [4π + 4π] reversible photodimerization.[2–5] However, the practical application of this system is limited due to these photochemical reactions are often non-selective, leading to a mixture and complicated photoproducts.[3] Even in one of the simplest systems, there are at least two possible photoproducts (tail–tail and tail–head photoproducts) after the photodimerization of the 9–substituted anthracene derivative [2c,4] whilst a multitude of photoproducts are isolated in more complex systems.[5] Additionally, it is noteworthy that such photochemical reactions not only form photodimerization products but also yield endoperoxide products in the presence of oxygen which tend to be overlooked by scientists due to their negligible yield.[6,8]

Thiacalix[4]arenes are widely used as a molecular platform as the unlimited possibilities for functionalization on the bridging sulfur atoms, upper-rim and lower-rim with various conformations.[9a] Here, we report the synthesis and characterization of a series novel thiacalix[4]arene derivatives (**T1**,**T2** and **T3**) which bearing anthracene moiety. The photochemical behavious were investigated by ^{1}H NMR, UV and fluorescent spectra. Among them, a crown–shaped thiacalix[4]arene derivative **T1** with 9,10–substituted anthracene group is special interest. The photochemical behaviour of **T1** in solution is leading to a rare and exclusive endoperoxide photoproduct. And the photoproduct is confirmed by X-ray analysis. To the best of our knowledge, this is a rare case in which a photoproduct is confirmed unequivocally in macrocyclic chemistry.[9b]

4.2 Results and Discussion

4.2.1 Synthesis and characterization

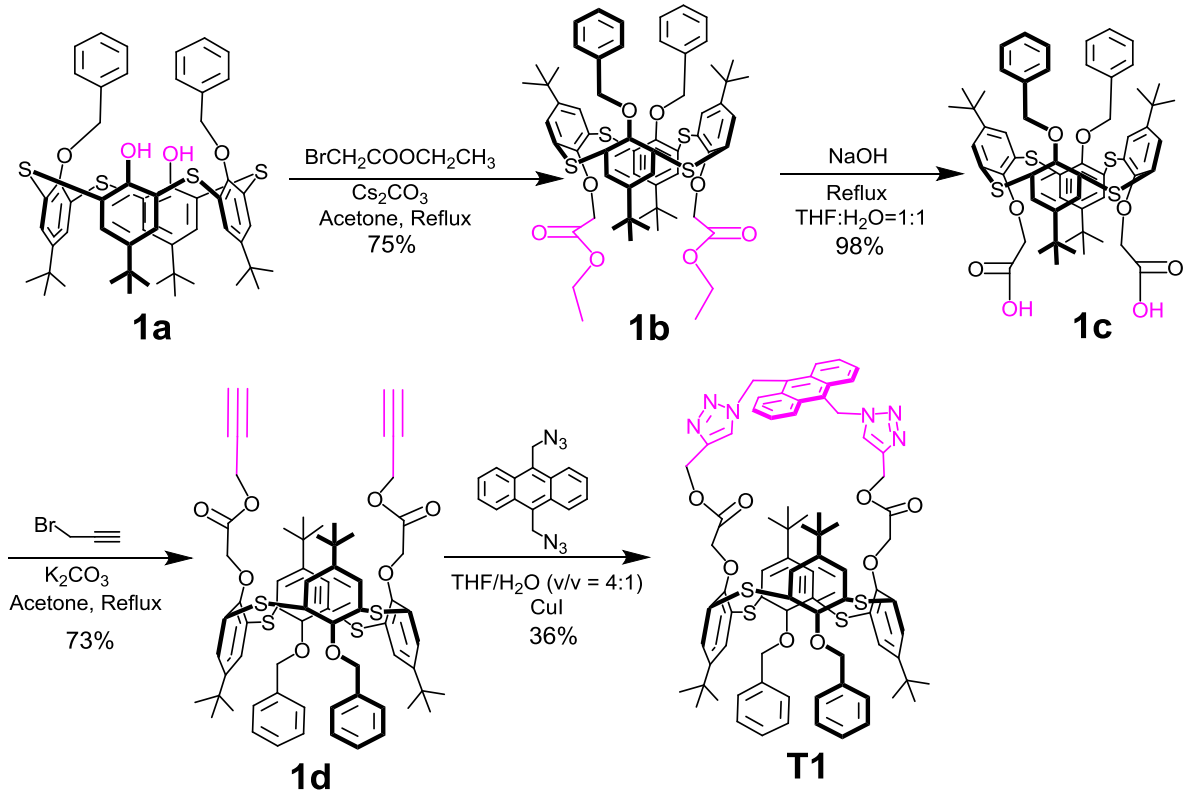

Scheme 1. The synthesis route of thiacalix[4]arene derivative **T1**.

The novel thiacalix[4]arene crown–shaped derivative **T1** was synthesized by Cu(I)–catalysed azide–alkyne cycloaddition click reaction in 36% yield (Scheme 1). As shown in the ^{1}H NMR spectrum of **T1** (Figure 1), the initial proton signal (δ 2.47 ppm) of the propargyl hydrogens of **1d**[10] had been disappeared, whilst a new singlet appearing at δ 7.40 ppm was attributed to the protons of the newly formed triazole skeleton. Two singlets for the *tert*-butyl protons are found in up field, *viz* δ 0.30 ppm and 0.79 ppm. One of the unusually up field shift of the *tert*-butyl pronts (δ 0.30 ppm) is attributed to the additional shielding effect of the anthracene moiety; two singlets for the aromatic protons at δ 7.09 and 7.29 ppm, all of which is indicative of a C_2–symmetric structure of **T1** in the 1,3-*alternate* conformation.

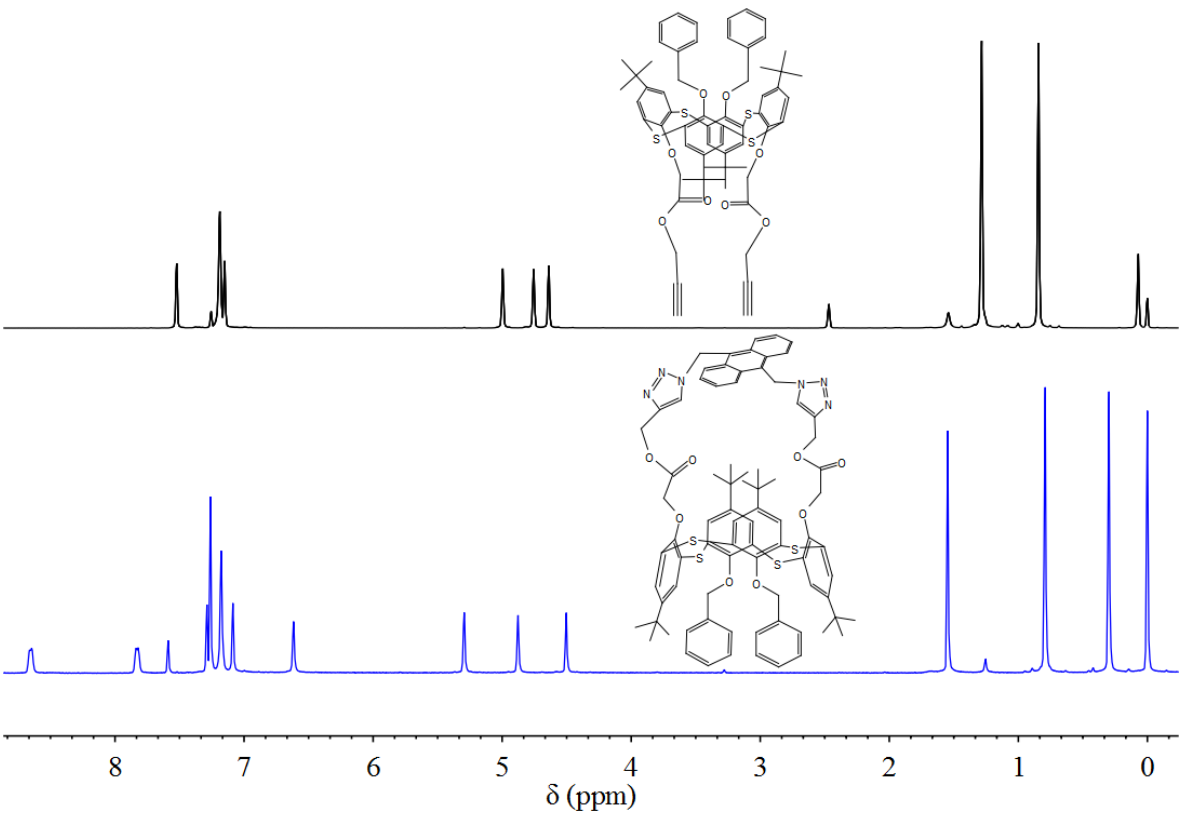

Figure 1. The ^{1}H NMR spectra of compounds **1d** and **T1**.

The degined thiacalix[4]arene derivative (**T1**), possessing a crown–shaped thiacalix[4]arene recognition motif functionalized with the anthracene moiety at the 9,10–positions, was employed as the photoactive unit. Use of **T1** had the advantage of limiting the possible number of photoproduct regioisomers to: (i) an intermolecular photodimerization isomer (**P1**) and (ii) an intramolecular endoperoxide isomer (**E1**), see Scheme 2.

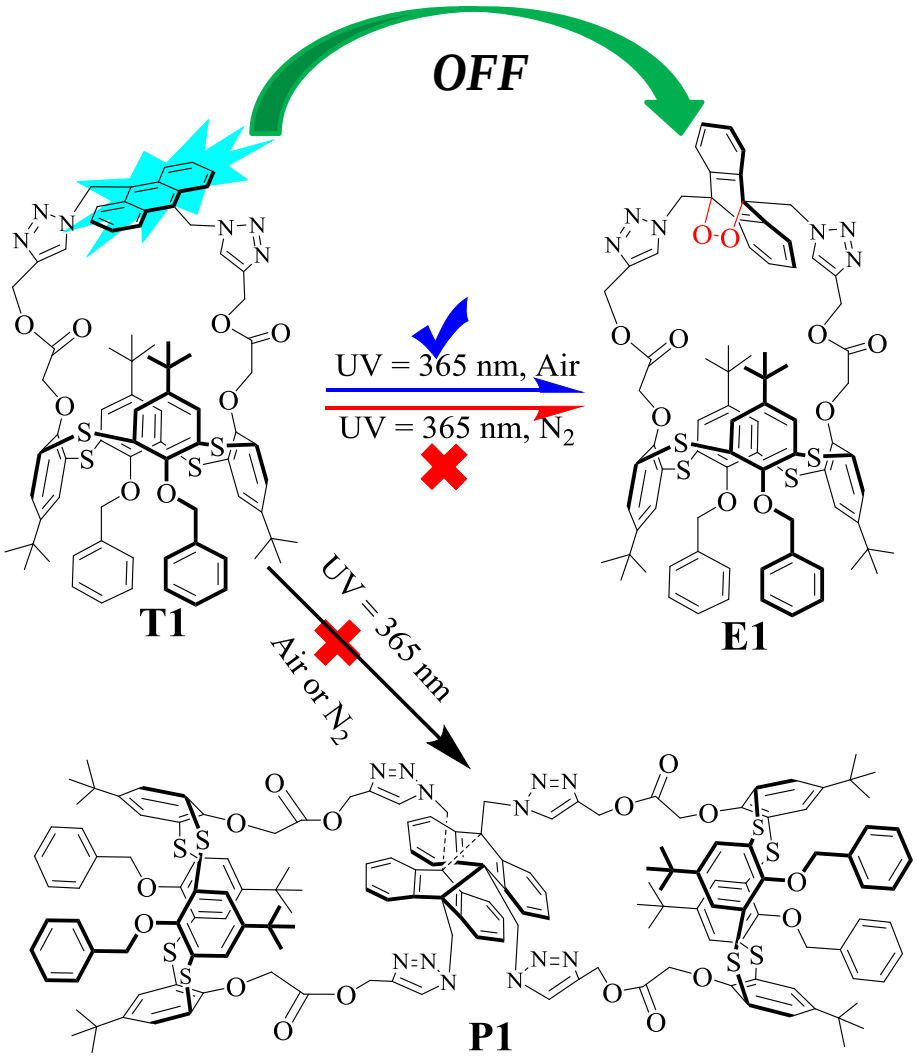

Scheme 2. Two possible photoproduct isomers **E1** and **P1**

4.2.2 Photochemical reaction study

The photochemical reaction processes of **T1** (Figure 2) was investigated by ^{1}H NMR spectroscopy. A 6 mM solution of **T1** in $CDCl_3$ was irradiated at 365 nm under air. Upon irradiation, a new group of proton signals (red colour peaks) immediately appeared with a concomitant decrease in the concentration of **T1** (blue colour peaks). An indication of the photochemical reaction process was the signals of the anthracene proton resonances (δ 7.83 and 8.65 ppm) which gradually decreased and finally disappeared. On gradually increasing the irradiation time, the conversion yield gradually increased as expected. After 90 min, the

quantitative conversion was indicated by the complete disappearance of all of the **T1** proton resonances, whilst a new unambiguous group of signals appeared. The photoactive anthracene motif resulted in xylene–like units for which proton signals appeared at δ 7.35 ppm and δ 7.58 ppm . The unusually up field *tert*-butyl protons (δ 0.30 ppm) dramatically shifted back to their 'normal' chemical shift position (δ 0.89 ppm) due to the deshielding effect after the loss of aromaticity of the central anthracene ring.

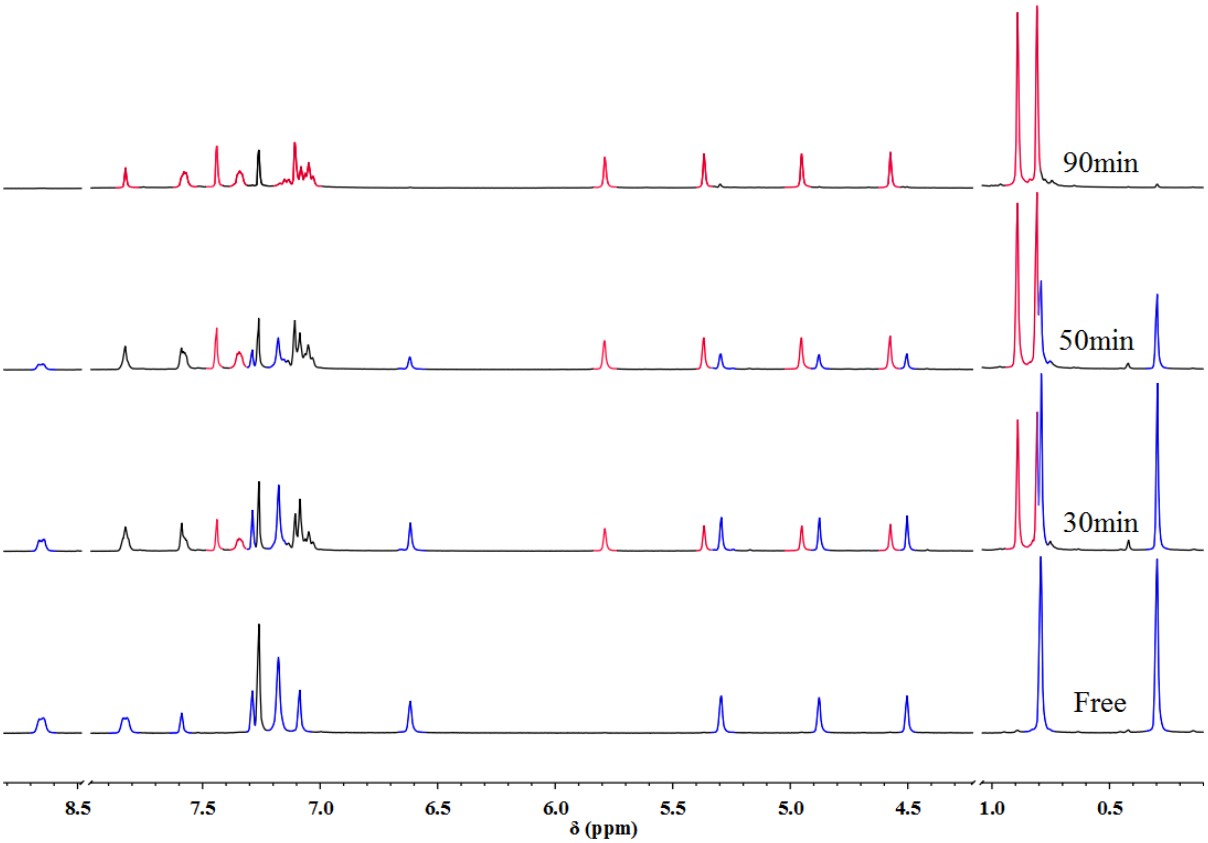

Figure 2. ^{1}H NMR ($CDCl_3$, 400 MHz, 25 ℃) spectra of a 6 mM solution of **T1**, after irradiation at 365 nm (0 min, 30 min, 50 min, 90 min).

Another indication of the photochemical process was the appearance of a new peak of the photoproduct at δ 79.7 ppm corresponding to the bridgehead $C_{9,10}$ carbons for the former central anthracene ring in the ^{13}C NMR spectra. The resulting UV absorption spectrum of **T1** after irradiation (Figure 3a) fully supported the formation of planar-symmetric photoproducts involving only the central anthracene ring and not the lateral anthracene aromatic rings, *i.e.* there was no absorption beyond 330 nm.[4a] A similar conclusion can be drawn from

fluorescence studies (Figure 3b). The characteristic anthracene moiety emission of **T1** in the 375–525 nm region was switched ‘‘off’’ after irradiation, which mirrored the non-fluorescence photoproduct formation. In contrast, a 6 mM solution of **T1** in degassed $CDCl_3$ was irradiated at 365 nm under an N_2 atmosphere. No detectable changes were observed in the ^1H NMR spectra, even after irradiating the compound for 6 h (Scheme 2).

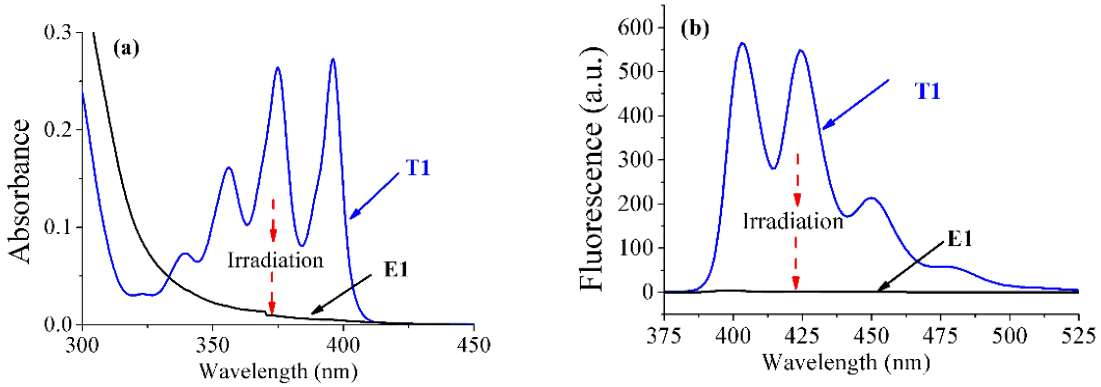

Figure 3. UV-visible spectra (a) and fluorescence spectra (b) of a 2.4×10^{-5} M solution of the **T1** in $CHCl_3$ under irradiation.

Normally the characterization of the photoproduct is the biggest challenge after the photochemical reaction, given the numerous possible photoproducts. Even in our simplest system, there are still two possible photoproduct isomers **E1** and **P1** as shown in scheme 2. Fortunately, the quantitative conversion provided a pure photoproduct which was easily confirmed by mass spectrometry. The observed mass results *m/z* = 1413.4907 $[M + H]^+$ (Figure 4b) for the photoproduct and *m/z* = 1380.4910 $[M]^+$ for unirradiated **T1** (Figure 4a) indicated that the photoproduct was the endoperoxide photoproduct **E1**.

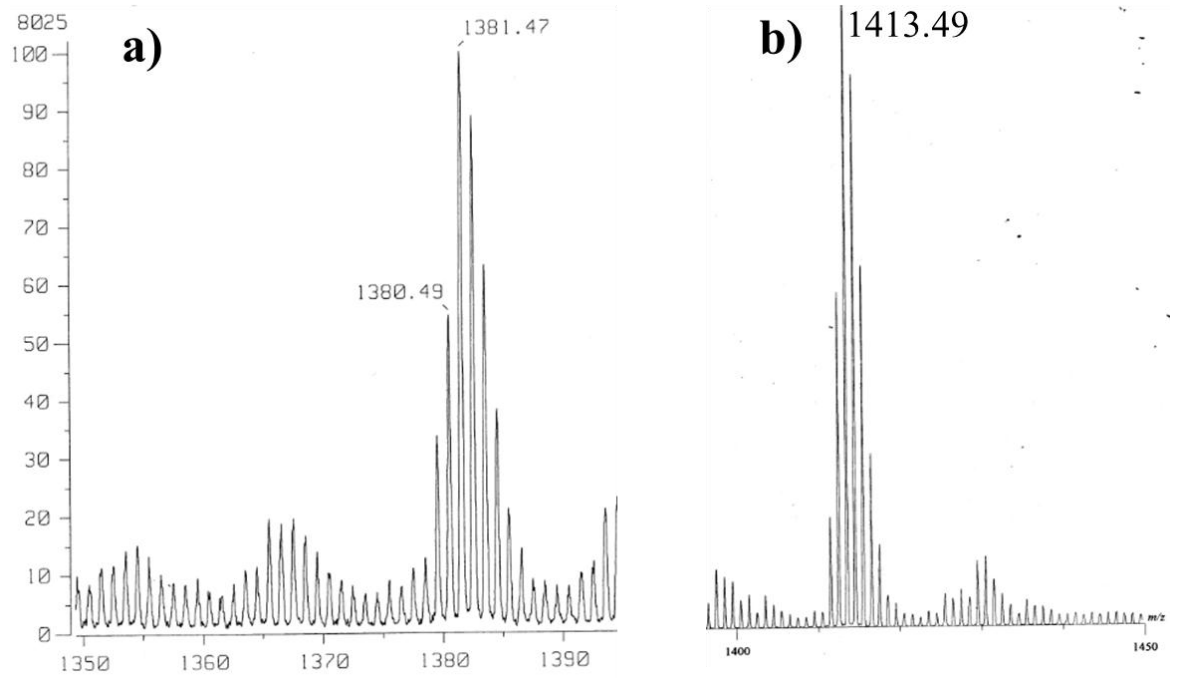

Figure 4. a) Mass spectrum of thiacalixarene derivertive **T1**; b) Mass spectrum of photoproduct **E1**.

Furthermore, X–ray crystallographic analysis[14] further confirmed the photoproduct molecular structure of **E1** as shown in Figure 5. The central anthracene ring moiety of the **T1** molecule has been oxidized rather than linking to another thiacalix[4]arene. These results for **E1** confirmed that the normally [4 + 4] photodimerization reaction had not occurred, but rather an unexpected [4 + 2] photosensitized oxygenation involving the cycloaddition of $^1O_2$ (singlet oxygen, an excited state of molecular oxygen which was generated from ambient air by directly irradiation with UV–light.)[8] on the electron-rich carbons of the central anthracene ring had occurred.[6,7]The most noteworthy feature was the position of the –O10–O9– bond which was oriented inward instead of the normally favorable outward direction, and this may be attributed to the inwardly crown–shaped structure required to trap the singlet oxygen.[9b] In the packing structure (Figure 6), there are two molecules of methanol which H-bond to each other, and one H-bonds to the calixarene at N(4). Calixarenes and methanol molecules are arranged in centrosymmetric pairs, but with no strong links between them. However, the possible underlying disorder among the methanol molecules may sometimes provide an H-bonded bis-methanol bridge between calixarenes. Overall there is a layer structure with hydrophilic(methanols, nitrogens, ester groups) and hydrophobic (Ph and tBu groups) layers.

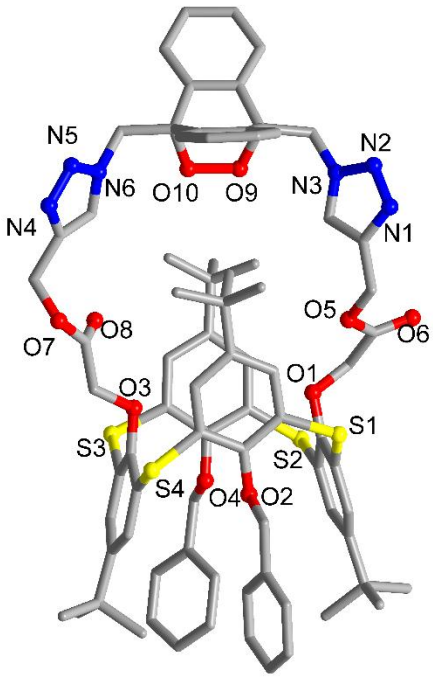

Figure 5. Single-crystal structure of **E1**. Hydrogen atoms and the two methanol molecules of crystallization have been omitted for clarity.

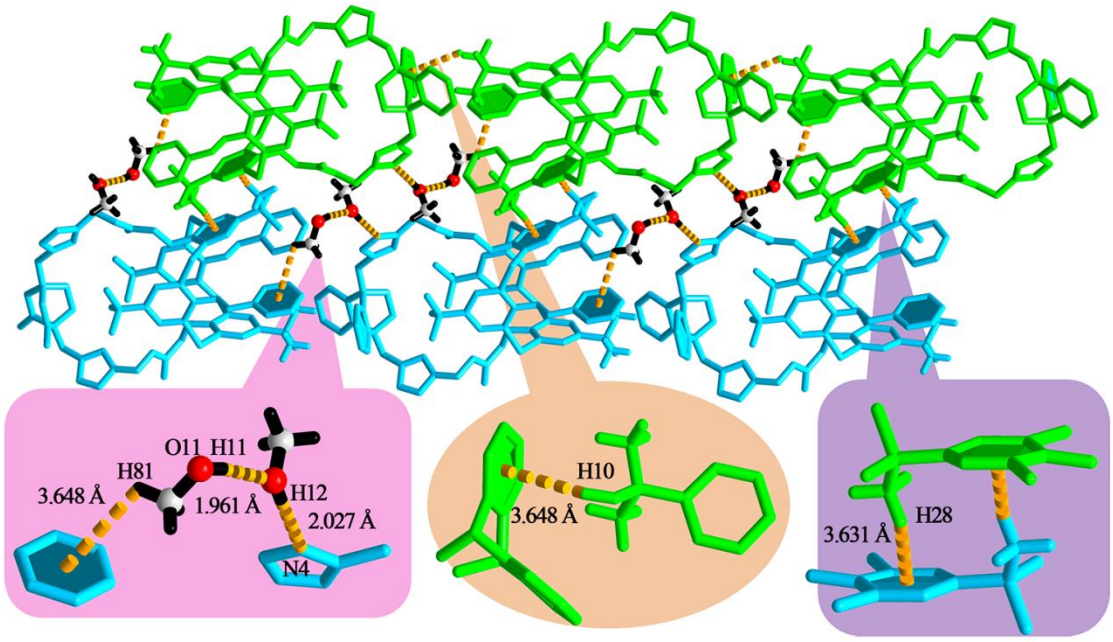

Figure 6. Packing structure of **E1**, in which methanol molecules reside between the layers and join them together.

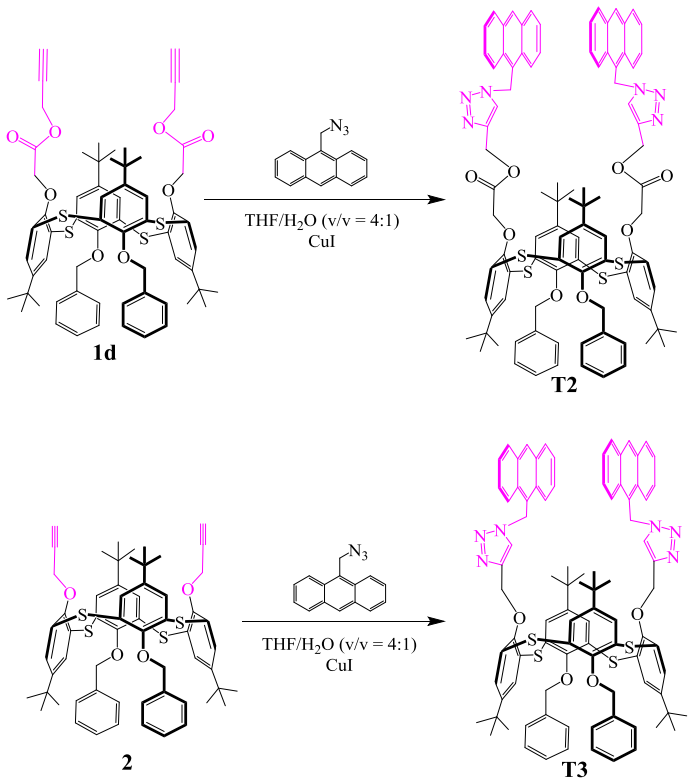

Scheme 3. The synthetic route of thiacalix[4]arene derivatives **T2** and **T3**.

In order to further investigate the formation of endoperoxide photochemical phenomenon, **T2** with 9–substituted anthracene moiety as the photoactive unit and **T3** with similar structure but short linkage have been introduced (Scheme 3). Interestingly, the changing for both of the UV absorption spectra and fluorescence spectra of compound **T2** and **T3** were almost the same with compound **T1** which were quenched after irradiation (Figure 7).

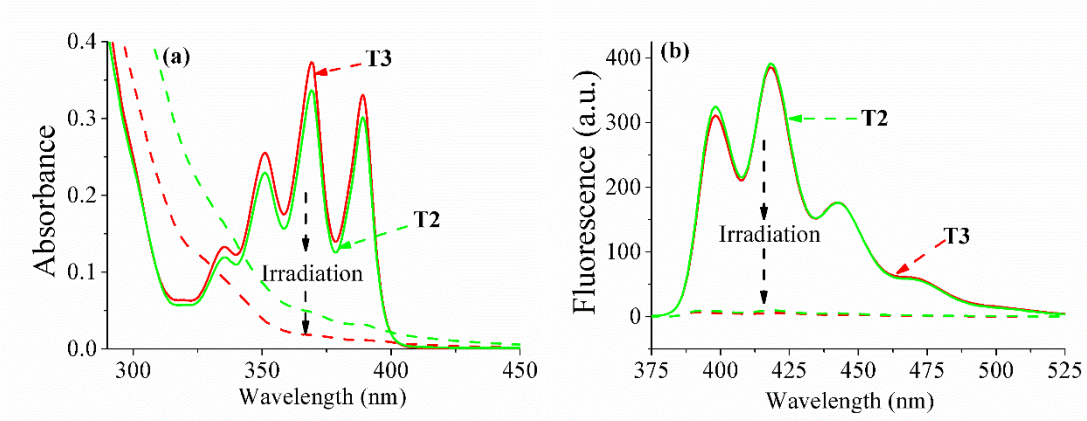

Figure 7. UV-visible spectra (a) and fluorescence spectra (b) of a 2.4×10^{-5} M solution of the **T2** and **T3** in $CHCl_3$ under irradiation.

However, the ^{1}H NMR spectroscopy were gradually changed to too complicate to identify any of the photoproducts when compound **T2** or **T3** was irradiated under the same condition with compound **T1** (Figure 8~9). The observed phenomenon in **T2** and **T3** after irradiation were similar with most reported results which was crudely defined to photodimerization.[2-8] This is very different with the ^{1}H NMR spectra with **T1**. The only difference between **T1** and **T2** is the photoactive units. It strongly suggested that 9,10–substituted anthracene crown–shaped moiety of compound **T1** played an important role in the formation of the rare endoperoxide photoproduct.

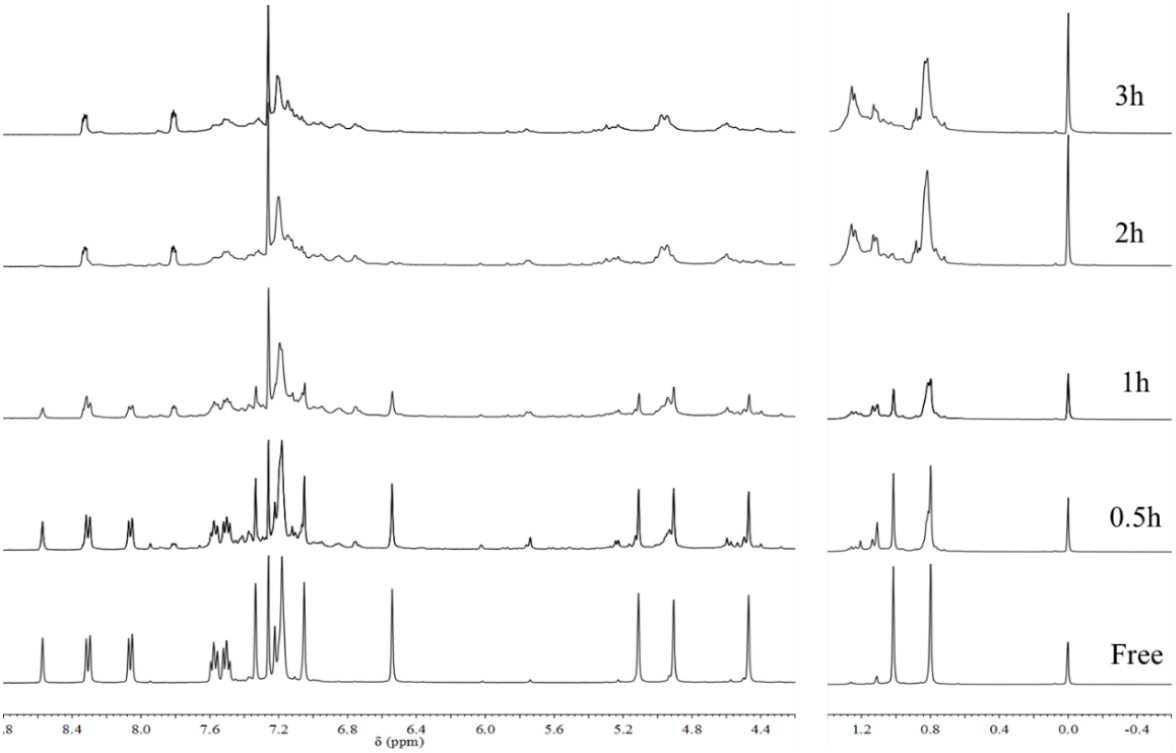

Figure 8. ^{1}H NMR ($CDCl_3$, 400 MHz, 25 ℃) spectra of a 6 mM solution of **T2**, after irradiation at 365 nm (0.5h, 1 h, 2h and 3h).

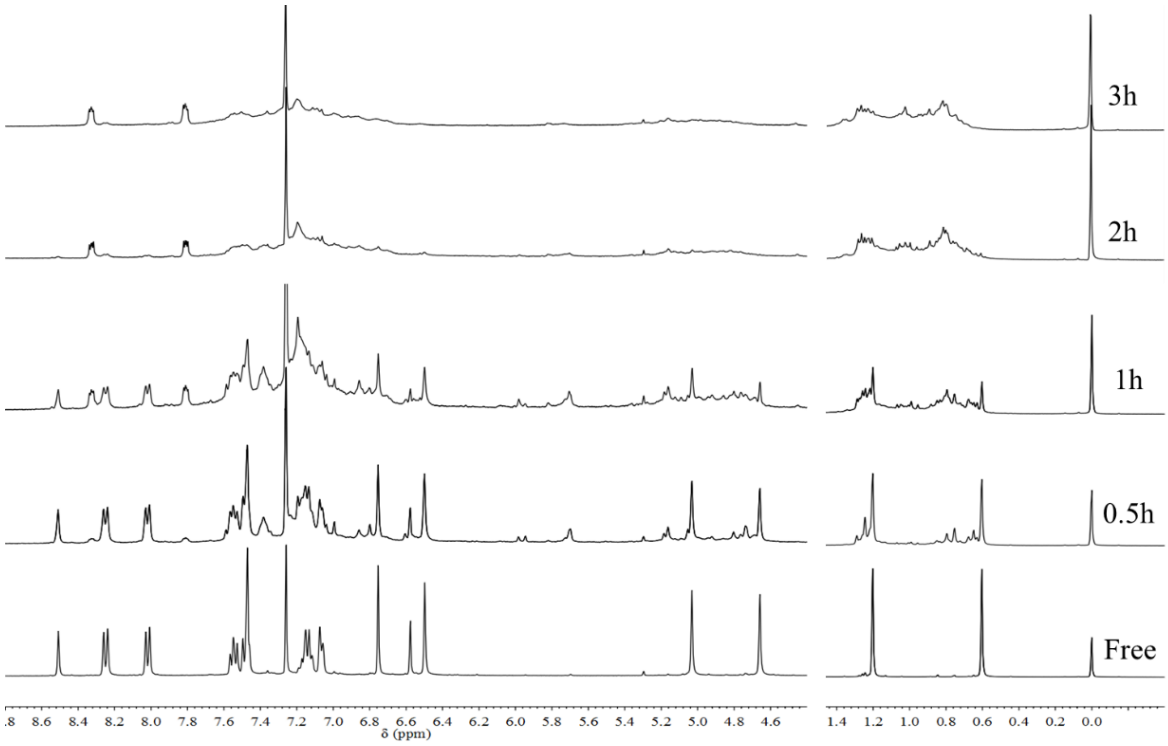

Figure 9. ^{1}H NMR ($CDCl_3$, 400 MHz, 25 ℃) spectra of a 6 mM solution of **T3**, after irradiation at 365 nm (0.5h, 1 h, 2h and 3h).

Furthermore, two reference compounds **R1** and **R2** possessing 9,10–substituted anthracene with different linkages have also been synthesized (Scheme 4). The photochemical reaction processes of **R1** and **R2** have also been investigated by UV absorption spectrum and ^{1}H NMR spectroscopy. Interestingly, all of the oberved results were exactly same with thiacalix[4]arene derivative **T1**. UV absorption spectrum of compound **R1** and **R2** were quenched after irradiation (Figure 10); a quantitative conversion was observed

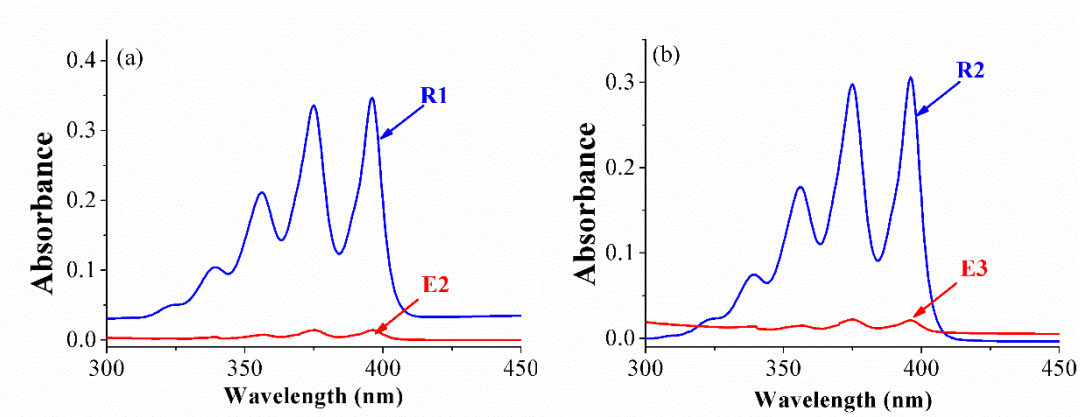

Figure 10. UV spectra of a 2.4×10^{-5} M solution of the (a) **R1** and (b) **R2** in $CHCl_3$ under irradiation.

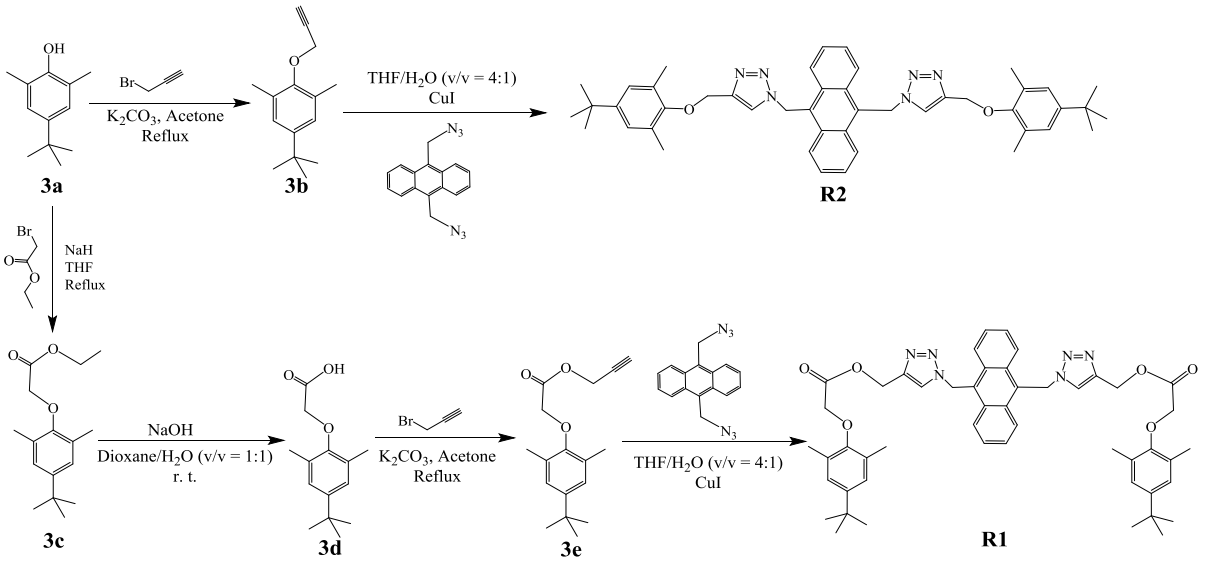

Scheme 4. The synthetic route of reference compounds **R1** and **R2**.

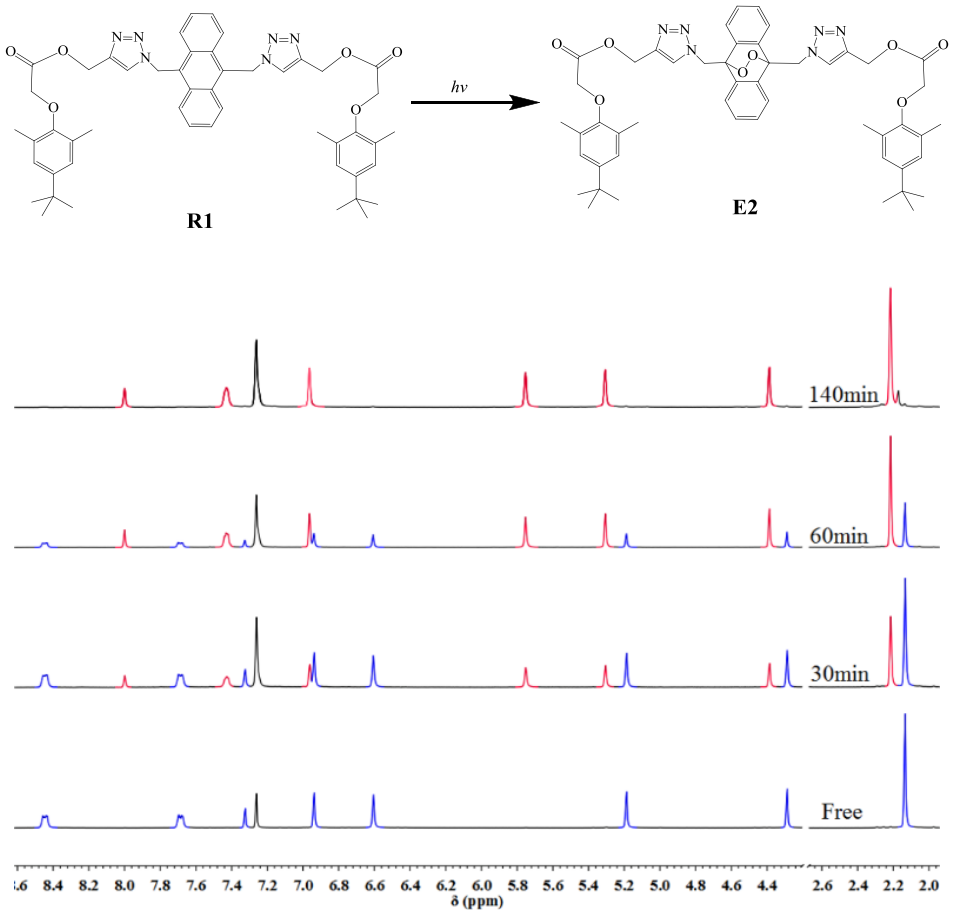

Figure 11. ^{1}H NMR ($CDCl_3$, 400 MHz, 25 ℃) spectra of a 6 mM solution of **R1**, after irradiation at 365 nm (0min, 30min, 60min, 140min).

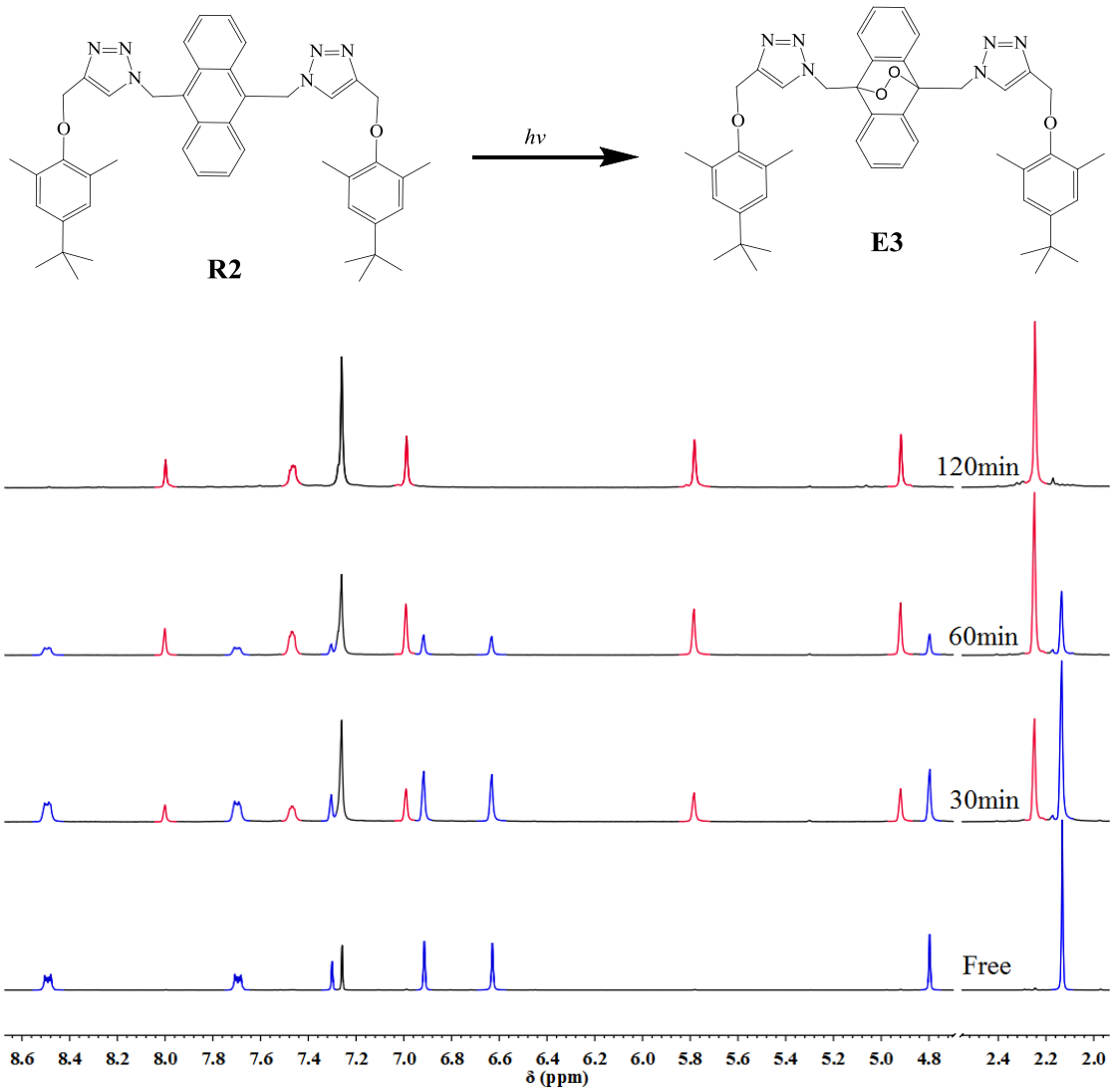

Figure 12. ^{1}H NMR ($CDCl_3$, 400 MHz, 25 ℃) spectra of a 6 mM solution of **R2**, after irradiation at 365 nm (0min, 30min, 60min, 120min).

by that all of the **R1** or **R2** proton resonances were replaced by a new unambiguous group of proton signals after irradiation (Figure 11~12). All of the observed results strongly suggested that **R1** and **R2** were also quantitatively converted to the corresponding endoperoxide photoproducts after irradiation. Thus, we drawn a conclusion that the compounds which were possessing 9,10–substituted anthracene in a symmetric structure (RCH_2-Anthracene-CH_2R) were favorable to form the endoperoxide photoproduct rather than dimerization photoproduct. More interestingly, we observed that the time it takes to complete the photochemical reactions process is very different. **T1**, **R1** and **R2** to corresponding **E1**, **E2**, and **E3** are 90,

140, and 120 min, respectively (Figure 13), which indicate a shorter time were need based on thiacalixarene platform than the other platform. It maybe attribute to the thiacalix[4]arene platform can be served as a host to capture oxygen which was conducive to form endperoxide photoproduct. It was consistent with the unique X-ray results, the position of the –O10–O9– bond which was oriented inward other than the normally favorable outward direction. Thus, the unique thiacalix[4]arene platform could greatly enhance the photochemical reaction rate.

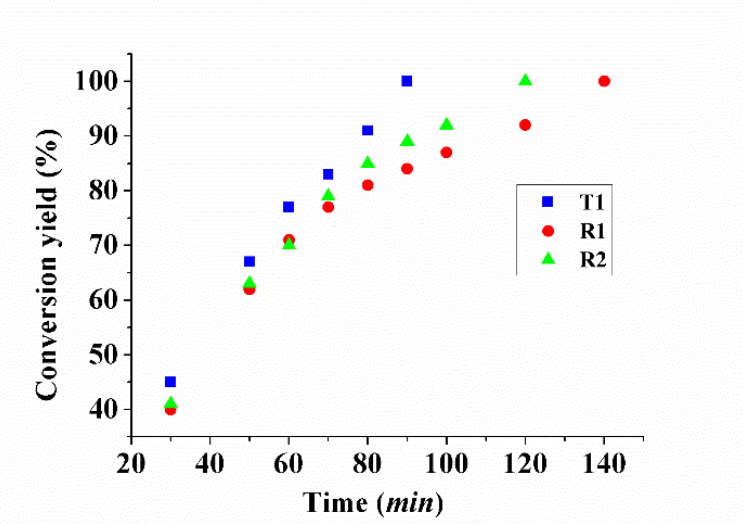

Figure 13. The conversion yield versus reaction time of a 6 mM $CDCl_3$ solution of **T1**, **R1** and **R2** under irradiation at 365 nm

Many researches have reported that the photoproducts would be decomposed either by thermally (~60 °C) or by irradiation with deep UV–light (<300 nm), or even occur naturally.[2b,11] However, we first tried the thermally method, there was no change in the ^{1}H NMR spectra and UV–vis spectra for the thermal decomposition of the endoperoxide photoproduct **E1**, even after heating the compound to 150 °C for 8 h. Another typical decompostion method was performed by irradiating the **E1** solution at deep UV–light (254 nm). However, there was also no change in the UV–vis and ^{1}H NMR spectra even after 4 h. These relative photon/thermal stabilities of the photoproduct suggested that the endoperoxide photoproduct **E1** has been shown to be very stable under these conditions.

4.3 Conclusions

In conclusion, a series anthracene containing derivatives have been synthesized and characterized, and the photochemical behaviours have been investigated by ^{1}H NMR, UV–vis and fluorescence spectroscopies. 9-10-anthracene containing derivatives **T1** converted it to the corresponding endoperoxide **E1** in quantitative yield upon irradiation at 365 nm. The structure of the rare endoperoxide photoproduct **E1** was unambiguously confirmed by ^{1}H NMR, ^{13}C NMR, Mass spectroscopy and X-ray crystallography. Further studies revealed that the compounds which were possessing 9,10–substituted anthracene in a symmetric structure (RCH_2-Anthracene-CH_2R) were favorable to form the endoperoxide photoproduct. Furthermore, the photochemical reaction rate could be greatly enhanced in the presence of thiacalix[4]arene platform which was attributed to the thiacalix[4]arene platform can be served as a host to capture oxygen.

4.4 Experimental Section

4.4.1 General methods: Melting points (Yanagimoto MP-S1) were uncorrected. Proton nuclear magnetic resonance (^{1}H NMR) spectra were recorded on a Nippon Denshi JEOL FT-300 spectrometer. Chemical shifts are reported as δ values (ppm) relative to internal Me_4Si. Mass spectra were obtained on a Nippon Denshi JMS-01SA-2 mass spectrometer at an ionization energy of 70 eV; *m/z* values reported include the parent ion peak. All the fluorescence spectra were recorded on JASCO FP-750 spectrometer. Elemental analyses were performed by Yanaco MT-5. Data of X-ray diffraction was collected on a Bruker Apex-2000 CCD diffractometer using graphite monochromated Mo Kα radiation (λ = 0.71073Å) with ω scan mode. Structural solution and full matrix least-squares refinement based on F^2 were performed with the SHELXS-97 and SHELXL-97 program package, respectively. All the non-hydrogen atoms were refined anisotropically. The hydrogen atoms were generated geometrically.

4.4.2 Materials

Unless otherwise stated, all reagents used were purchased from commercial sources and were used without further purification. Compound **1a**[17]**, 1b**[18]**, 1c**[18]**, 1d**[10], **2**[19], **3a**[20], **3c**[21], **3d**[21]

and 9–(azidomethyl)anthracene[22] and 9,10–bis(azidomethyl)anthracene[23] were prepared following the reported procedures. All solvents used were dried and distilled by the usual procedures prior to use.

4.4.2.1. Synthesis of thiacalix[4]arene derivative (T1) Copper iodide (20 mg) was added to a mixture of 9,10-bis(azidomethyl)anthracene (70 mg, 0.24 mmol) and **1d** (219 mg, 0.20 mmol) in 75 mL THF/H_2O (4:1) and refluxed for 15 h. The resulting solution was cooled and diluted with water and extracted with CH_2Cl_2. The organic layer was separated and dried ($MgSO_4$) and evaporated to give the solid crude product. The residue eluted from a column chromatography column of silica gel with CH_2Cl_2/EtOAc (20:1) gave the desired product **T1** (100 mg, 36%) as light yellow powder. M.p. 361–362 ℃. ^{1}H NMR (400 MHz, $CDCl_3$) δ = 0.30 (s, 18H, t*Bu*), 0.79 (s, 18H, t*Bu*), 4.50 (s, 4H, –O*CH*$_2$COO–), 4.88 (s, 4H, –O*CH*$_2$Benzyl), 5.29 (s, 4H, –O*CH*$_2$Triazole–), 6.62 (s, 4H, –Triazole*CH*$_2$An), 7.09 (s, 4H, Ar*H*), 7.18 (s, 10H, Ph*H*), 7.29 (s, 4H, Ar*H*), 7.59 (s, 2H, Triazole–*H*), 7.82 ~7.84 (m, 4H, An–*H*) and 8.65 ~ 8.66 (m, 4H, An–*H*) ppm. ^{13}C NMR (100 MHz) δ 29.8, 30.7, 33.2, 33.8, 47.3, 57.9, 67.0, 73.4, 123.5, 124.6, 127.1, 127.2, 127.4, 127.5, 128.0, 128.2, 128.5, 131.1, 131.2, 133.5, 137.9, 143.6, 145.4, 145.9, 156.9, 158.4 and 168.3 ppm. FABMS: *m/z*: $[M]^+$ Calcd for $C_{80}H_{80}N_6O_8S_4$ 1380.4921; Found 1380.4910.

A similar procedure using **1d**, **2**, **3b** and **3e** was followed for the synthesis of **T2**, **T3**, **R1** and **R2**.

4.4.2.2. Thiacalix[4]arene derivative (T2) was obtained as a light yellow solid (a column chromatography column of silica gel with hexane/CH_2Cl_2/EtOAc (10:10:1), 104 mg, 48%). M.p. 231–232 ℃. ^{1}H NMR (400 MHz, $CDCl_3$) δ = 0.80 (s, 18H, t*Bu*), 1.01 (s, 18H, t*Bu*), 4.47 (s, 4H, –O*CH*$_2$COO–), 4.91 (s, 4H, –O*CH*$_2$Benzyl), 5.11 (s, 4H, –O*CH*$_2$Triazole–), 6.54 (s, 4H, –Triazole*CH*$_2$An), 7.05 (s, 4H, Ar*H*), 7.18 (s, 10H, Ph*H*), 7.22 (s, 2H, Triazole–*H*), 7.34 (s, 4H, Ar*H*), 7.45– 7.54 (m, 4H, An-*H*), 7.54 – 7.63 (m, 4H, An-*H*), 8.05 ~ 8.07 (m, 4H, An-*H*), 8.29 ~ 8.31 (m, 4H, An-*H*) and 8.57 (s, 2H, An-*H*) ppm. ^{13}C NMR (100 MHz) δ 30.8, 30.9, 46.5, 57.6, 66.8, 73.1, 122.9, 123.1, 123.5, 125.4, 127.1, 127.4, 127.8, 128.2, 128.5,

129.5, 130.0, 130.80, 130.83, 131.5, 133.0, 138.0, 142.7, 145.9, 146.0, 156.0, 158.2 and 167.6 ppm. FABMS: *m/z*: $[M+H]^+$ Calcd for $C_{94}H_{91}N_6O_8S_4$ 1559.5781; Found 1559.5780.

4.4.2.3. Thiacalix[4]arene derivative (T3) was obtained as a light yellow solid (a column chromatography column of silica gel with hexane/CH_2Cl_2/EtOAc (20:10:1), 580 mg, 74%). M.p. 284–285 ℃. ^{1}H NMR (400 MHz, $CDCl_3$) δ = 0.60 (s, 18H, t*Bu*), 1.20 (s, 18H, t*Bu*), 4.66 (s, 4H, –O*CH*$_2$Benzyl), 5.03 (s, 4H, –O*CH*$_2$Triazole–), 6.50 (s, 4H, –Triazole*CH*$_2$An), 6.58 (s, 2H, Triazole–*H*), 6.75 (s, 4H, Ar*H*), 7.06 ~ 7.07 (m, 4H, Ph*H*), 7.12 ~ 7.17 (m, 6H, Ph*H*), 7.47 (s, 4H, Ar*H*), 7.46–7.49 (m, 4H, An-*H*), 7.53–7.56 (m, 4H, An-*H*), 8.01 ~8.03 (m, 4H, An-*H*), 8.24 ~ 8.26 (m, 4H, An-*H*) and 8.51 (s, 2H, An-*H*) ppm. ^{13}C NMR (100 MHz) δ 29.6, 30.3, 32.5, 33.2, 45.3, 61.9, 72.1, 121.9, 122.0, 122.6, 124.3, 125.8, 126.3, 126.6, 127.0, 128.3, 128.7, 128.9, 129.0, 129.8, 130.3, 133.0, 137.1, 142.5, 144.3, 144.9, 154.5 and 157.5 ppm. FABMS: *m/z*: $[M+H]^+$ Calcd for $C_{90}H_{87}N_6O_4S_4$ 1443.5672; Found 1443.5670.

4.4.2.4. Reference compound (R1) was obtained as a light yellow solid (a column chromatography column of silica gel with CH_2Cl_2/EtOAc (20:1), 260 mg, 57%). M.p. 256–257 ℃. ^{1}H NMR (400 MHz, $CDCl_3$) δ = 1.26 (s, 18H, t*Bu*), 2.13 (s, 12H, *CH*$_3$), 4.29 (s, 4H,–O*CH*$_2$COO), 5.19 (s, 4H, –O*CH*$_2$Triazole–), 6.60 (s, 4H, –Triazole*CH*$_2$An), 6.94 (s, 4H, Ar*H*), 7.32 (s, 2H, Triazole–*H*), 7.67–7.70 (m, 4H, An-*H*) and 8.43–8.46 (m, 4H, An-*H*) ppm. ^{13}C NMR (100 MHz) δ 16.4, 31.4, 34.1, 46.6, 57.9, 68.9, 123.5, 124.1, 125.8, 126.9, 127.8, 129.6, 130.7, 142.6, 147.1, 152.9 and 169.1 ppm. FABMS: *m/z*: $[M+H]^+$ Calcd for $C_{50}H_{57}N_6O_6$ 837.4340; Found 837.4376.

4.4.2.5 Reference compound (R2) was obtained as a yellow solid (recrystallized from 1:3 $CHCl_3$/hexane, 145 mg, 87%). M.p. 302–303 ℃. ^{1}H NMR (400 MHz, $CDCl_3$) δ = 1.23 (s, 18H, t*Bu*), 2.13 (s, 12H, *CH*$_3$), 4.80 (s, 4H,–O*CH*$_2$Triazole–), 6.63 (s, 4H, –Triazole*CH*$_2$An), 6.91 (s, 4H, Ar*H*), 7.30 (s, 2H, Triazole–*H*), 7.68–7.71 (m, 4H, An-*H*) and 8.48–8.50 (m, 4H, An-*H*) ppm. ^{13}C NMR (100 MHz) δ 16.6, 31.4, 34.1, 46.6, 65.6, 122.1, 124.2, 125.7, 127.1, 127.7, 129.9, 130.7, 145.2, 146.8 and 152.9 ppm. FABMS: *m/z*: $[M+H]^+$ Calcd for $C_{46}H_{53}N_6O_2$ 721.4230; Found 721.4244.

4.4.2.6 Photoproduct from T1 (**E1**) was obtained as a yellow solid (5 mg, 100%). M.p. 289–290 ℃. ^{1}H NMR (400 MHz, $CDCl_3$) δ = 0.81 (s, 18H, t*Bu*), 0.89 (s, 18H, t*Bu*), 4.57 (s, 4H, –O*CH*$_2$COO–), 4.95 (s, 4H, –O*CH*$_2$Benzyl), 5.37 (s, 4H, –O*CH*$_2$Triazole–), 5.79 (s, 4H, –Triazole*CH*$_2$C), 7.03–7.08 (m, 8 H, Ph*H*), 7.11 (s, 4H, Ar*H*), 7.14~7.17 (m, 2H, Ph*H*), 7.35 (br, 4H, Benzene–*H*), 7.44 (s, 4H, Ar*H*), 7.58 (br, 4H, Benzene–*H*) and 7.83 (s, 2H, Triazole–*H*) ppm. ^{13}C NMR (100 MHz) δ 30.5, 30.7, 33.8, 48.8, 58.5, 66.9, 72. 5, 79.7, 121.4, 126.2, 126.9, 127.0, 127.9, 128.12, 128.15, 128.4, 129.9, 132.5, 137.8, 138.2, 144.0, 145.98, 146.02, 155.8, 158.2 and 168.5 ppm. FABMS: *m/z*: $[M+H]^+$ Calcd for $C_{80}H_{81}N_6O_{10}S_4$ 1413.4897; Found 1413.4907.

4.4.2.7 Photoproduct from R1 (**E2**) was obtained as a light yellow solid (6 mg, 100%). M.p. 114–115 ℃. ^{1}H NMR (400 MHz, $CDCl_3$) δ = 1.27 (s, 18H, t*Bu*), 2.22 (s, 12H, *CH*$_3$), 4.39 (s, 4H,–O*CH*$_2$COO), 5.31 (s, 4H, –O*CH*$_2$Triazole–), 5.75 (4 H, s, –Triazole*CH*$_2$C), 6.96 (4 H, s, Ar*H*), , 7.26 (4 H, s, Ph-*H*), 7.43 (s, 4H, Ph-*H*) and 8.00 (s, 2H, Triazole–*H*). ^{13}C NMR (100 MHz) δ 16.5, 31.4, 34.1, 48.7, 57.9, 69.0, 80.0 121.2, 125.9, 126.7, 128.3, 129.7, 137.8, 143.2, 147.0, 153.0 and 169.0 ppm. FABMS: *m/z*: $[M+H]^+$ Calcd for $C_{50}H_{57}N_6O_8$ 869.4238; Found 869.4236.

4.4.2.8 Photoproduct from R2 (**E3**) was obtained as a light yellow solid (5 mg, 100%). M.p. 128–129 ℃. ^{1}H NMR (400 MHz, $CDCl_3$) δ = 1.27 (s, 18H, t*Bu*), 2.25 (s, 12H, *CH*$_3$), 4.92 (s, 4H,–O*CH*$_2$Triazole–), 5.78 (s, 4H, –Triazole*CH*$_2$C), 6.99 (s, 4H, Ar*H*), 7.26–7.27 (m, 4H, Ph-*H*), 7.46–7.48 (m, 4H, Ph-*H*) and 8.00 (s, 2H, Triazole–*H*). ^{13}C NMR (100 MHz) δ 16.7, 31.5, 34.1, 48.7, 65.5, 80.2, 121.3, 125.6, 125.8, 128.3, 130.0, 137.9, 145.7, 146.8 and 153.2 ppm. FABMS: *m/z*: $[M+H]^+$ Calcd for $C_{46}H_{53}N_6O_4$ 753.4128; Found 753.4128.

4.4.2.9 Synthesis of reference propargyl derivative (3e).

A suspension of **3d** (1.20 g, 5.08 mmol) and K_2CO_3 (2.80 g, 20.32 mmol) was heated at reflux for 1 h in dry acetone (70 mL), and a solution of propargyl bromide (1.20 g, 10.16 mmol) in dry acetone (10 mL) was added. The reaction mixture was refluxed for 17 h. The solvents were evaporated and the residue partitioned between 10% HCl and CH_2Cl_2. The organic layer was separated and dried ($MgSO_4$) and the solvents were evaporated. The

residue eluted from a column chromatography column of silica gel with CH_2Cl_2/Hexane (1:1) gave the desired product **3e** (1.30 g, 94%) as a colorless oil. ^{1}H NMR (400 MHz, $CDCl_3$) δ = 1.28 (9H, s, t*Bu*), 2.29 (s, 6H, *CH*$_3$) 2.51 (d, *J* = 2.3 Hz, 1H, *HC*C), 4.45 (s, 2H, HCC*CH*$_2$O–), 4.82 (d, *J* = 2.2 Hz, 4H, –O*CH*$_2$COO–) and 7.00 (s, 2H, Ar*H*) ppm. ^{13}C NMR (100 MHz) δ 16.6, 31.5, 34.1, 52.4, 69.0, 75.5, 77.1, 125.9, 129.7, 147.1, 153.0 and 168.5 ppm. HRMS (ESI/TOF-Q) *m/z*: $[M]^+$ Calcd for $C_{17}H_{22}O_3$ 274.1569; Found 274.1600.

A similar procedure using **3a** was followed for the synthesis of **3b**.

4.4.2.10 Reference propargyl derivative (3b) was obtained as a colorless oil (1.15 g, 95%). ^{1}H NMR (400 MHz, $CDCl_3$) δ = 1.28 (s, 9H, t*Bu*), 2.31 (s, 6H, *CH*$_3$) 2.49 (s, 1H, *HC*C), 4.47 (s, 2H, HCC*CH*$_2$O–) and 7.00 (s, 2H, Ar*H*) ppm. ^{13}C NMR (100 MHz) δ 16.7, 16.8, 31.4, 31.5, 34.1, 59.72, 59.76, 59.80, 74.6, 74.8, 79.58, 79.62, 125.7, 130.2, 146.9 and 153.0 ppm. HRMS (ESI/TOF-Q) *m/z*: $[M]^+$ Calcd for $C_{15}H_{20}O$ 216.1514; Found 216.1451.

4.5 References

1. (*a*) P. K. Kundu, G. L. Olsen, V. Kiss and R. Klajn, *Nat. Commun.*, 2014, **5**, 3588; (*b*) S. Chatani, C. J. Kloxin and C. N. Bowman, *Polym. Chem.*, 2014, **5**, 2187-2201; (*c*) S. Monti and I. Manet, *Chem. Soc. Rev.*, 2014, **43**, 4051-4067; (*d*) D. Habault, H. Zhang and Y. Zhao, *Chem. Soc. Rev.*, 2013, **42**, 7244-7256; (*e*) D. Gust, J. Andreasson, U. Pischel, T. A. Moore and A. L. Moore, *Chem. Commun.*, 2012, **48**, 1947-1957; (*f*) O. Yaroshchuk and Y. Reznikov, *J. Mater. Chem.*, 2012, **22**, 286-300; (*g*) J. M. Spruell and C. J. Hawker, *Chem. Sci.*, 2011, **2**, 18-26; (*h*) M. -M. Russew and S. Hecht, *Adv. Mater.*, 2010, **22**, 3348-3360; (*i*) T. F. Scott, B. A. Kow-alski, A. C. Sullivan, C. N. Bowman and R. R. McLeod, *Science* 2009, **324**, 913-917.
2. (*a*) S. V. Radl, M. Roth, M. Gassner, A. Wolfberger, A. Lang, B. Hirschmann, G. Trimmel, W. Kern and T. Griesser, *Eur. Polym. J.*, 2014, **52**, 98-104; (*b*) J. –F. Xu, Y.-Z. Chen, L.-Z. Wu, C.-H. Tung and Q.-Z. Yang, *Org. Lett.*, 2013, **15**, 6148-6151; (*c*) H. Bouas-Laurent, J. -P. Desvergne, A. Castellan and R. Lapouyade, *Chem. Soc. Rev.*, 2001, **30**, 248-263; (*d*) H. D. Becker, *Chem. Rev.*, 1993, **93**, 145-172.

3. V. Ramamurthy, Y. Inoue, Supramolecular Photochemistry: Con-trolling Photochemical Processes, John Wiley and Sons, Inc., Wein-heim, 2011.
4. (*a*) A. Tron, H. P. J. D. Rouville, A. Ducrot, J. H. Tucker, M. Baroncini, A. Credi and N. D. McClenaghan, *Chem. Commun.,* 2015, **51**, 2810-2813; (*b*) L. López-Vilanova, I. Martínez, T. Corrales and F. Catalina, *Eur. Polym. J.*, 2014, **56**, 69-76.
5. (*a*) Y. Kawanami, H. Umehara, J. Mizoguchi, M. Nishijima, G. Fukuhara, C. Yang, T. Mori and Y. Inoue, *J. Org. Chem.,* 2013, **78**, 3073-3085; (*b*) C. Yang, T. Mori, Y. Origane, Y. H. Ko, N. Selvapalam, K. Kim and Y. Inoue, *J. Am. Chem. Soc.*, 2008, **130**, 8574-8575.
6. (*a*) A. Lauer, A. L. Dobryakov, S. A. Kovalenko, H. Fidder and K. Heyne, *Phys. Chem. Chem. Phys.*, 2011, **13**, 8723-8732; (*b*) W. Fudickar and T. Linker, *Langmuir*, 2010, **26**, 4421-4428; (*c*) C. Bratschkov, *Eur. Polym. J.,* 2001, *37*, 1145-1149; (*d*) M. A. Fox and S. Olive, *Science,* 1979, **205**, 582-583.
7. (*a*) X. Li, G. Zhang, H. Ma, D. Zhang, J. Li and D. Zhu, *J. Am. Chem. Soc.*, 2004, **126**, 11543-11548; (*b*) J. M. Aubry, C. Pierlot, J. Rigaudy and R. Schmidt, *Acc. Chem. Res.*, 2003, **36**, 668-675.
8. (*a*) W. Fudickar and T. Linker, *Langmuir,* 2010, **26**, 4421-4428; (*b*) C. Bratschkov, *Eur. Polym. J.*, 2001, **37**, 1145-1149.
9. (*a*) R. Kumar, Y. O. Lee, V. Bhalla, M. Kumar and J. S. Kim, *Chem. Soc. Rev.*, 2014, **43**, 4824-4870; (*b*)J. J. Gassensmith, J. M. Baumes, J. Eberhard and B. D. Smith, *Chem. Commun.,* 2009, 2517-2519.
10. J. L. Zhao, H. Tomiyasu, C. Wu, H. Cong, X. Zeng, S. Rahman, P. E. Georghiou, D. L. Hughes, C. Redshaw and T. Yamato, *Tetrahedron* 2015, **71**, 8521-8527.
11. (*a*) C. Schäfer, R. Eckel, R. Ros, J. Mattay and D. Anselmetti, *J. Am. Chem. Soc.,* 2007, **129**, 1488-1489; (*b*) C. Schäfer, B. Decker, M. Letzel, F. Novara, R. Eckel, R. Ros, D. Anselmetti and J. Mattay, *Pure Appl. Chem.*, 2006, **78**, 2247-2259; (*c*) C. Schäfer and J. Mattay, *Photochem. Photobiol. Sci.*, 2004, **3**, 331-333; (*d*) S. i. Nakatsuji, T. Ojima, H. Akutsu and J.-i.Yamada, *J. Org. Chem.,* 2002, **67**, 916-921; (*e*) T. Tsudera, A. Ikeda and S. Shinkai, *Tetrahedron,* 1997, **53**, 13609-13620; (*f*) G. Deng, T. Sakaki, Y. Kawahara and S. Shinkai, *Supramol. Chem.,* 1993, **2**, 71-76; (*g*) G. Deng, T. Sakaki, K. Nakashima

and S. Shinkai, *Chem. Lett.*, 1992, 1287-1290; (*h*) G. Deng, T. Sakaki, Y. Kawahara and S. Shinkai, *Tetrahedron Lett.*, 1992, **33**, 2163-2166.

12. (*a*) G. Terentyuk, E. Panfilova, V. Khanadeev, D. Chumakov, E. Genina, A. Bashkatov, V. Tuchin, A. Bucharskaya, G. Maslyakova, N. Khlebtsov and B. Khlebtsov, *Nano Res.*, 2014, **7**, 325-337; (*b*) P. Kang and C. S. Foote, *J. Am. Chem. Soc.*, 2002, **124**, 4865-4873; (*c*) J. Cadet, T. Douki, J. P. Pouget and J. L. Ravanat, *Methods Enzymol.*, 2000, **319**, 143-153; (*d*) L. O. Klotz, K. Briviba and H. Sies, *Methods Enzymol.*, 2000, **319**, 130-143; (*e*) S. W. Ryter and R. M.Tyrrell, *Free Radical Biol. Med.*, 1998, **24**, 1520-1534; (*f*) H. H. Wasserman and R. W. Murray, Singlet Oxygen, Academic Press, New York, 1979.
13. (*a*) C. Laloi and M. Havaux, *Front. Plant Sci.*, 2015, **6**, 39; (*b*) D. Maggioni, M. Galli, L. D'Alfonso, D. Inverso, M. V. Dozzi, L. Sironi, M. Iannacone, M. Collini, P. Ferruti, E. Ranucci and G. D'Alfonso, *Inorg. Chem.*, 2015, **54**, 544-553; (*c*) C. Schweitzer and R. Schmidt, *Chem. Rev.*, 2003, **103**, 1685-1758.
14. Crystal data for TD: $C_{80}H_{80}N_6O_{10}S_4$ 2(CH_4O), M = 1477.82, monoclinic, P21/n, a = 18.515(4), b = 20.431(4), c = 21.572(4) Å, β = 115.272(3)°, V = 7379(3) $Å^3$, Z = 4, μ(Mo-Kα) = 0.251 mm–1, 57265 reflections measured, 12990 unique, Rint = 0.091, R1[F2>2σ(F2)] = 0.091, wR2 (all data) = 0.288. Crystallographic data for this structure have been deposited with the Cambridge Crystallo-graphic Data Centre with code number CCDC 1432129. Copies of the data can be obtained, free of charge, on application to CCDC, 12 Union Road, Cambridge CB2 1EZ, UK [fax: 144 1223 336033 or e-mail: depost@ccdc.cam.ac.uk].
15. (*a*) Z. Xu, J. Yoon and D. R. Spring, *Chem. Soc. Rev.*, 2010, **39**, 1996-2006; (*b*) J. S. Kim, and D. T. Quang, *Chem. Rev.*, 2007, **107**, 3780-3799.
16. (*a*) H. Yu, X. Liu, Q. f. Wu, Q. Li, S. Wang and Y. Guo, *Chem. Lett.*, 2015, **44**, 244-246; (*b*) S. Kim, T. Tachikawa, M. Fujitsuka and T. Majima, *J. Am. Chem. Soc.*, 2014, **136**, 11707-11715; (*c*) S. K. Pedersen, J. Holmehave, F. H. Blaikie, A. Gollmer, T. Breitenbach, H. H. Jensen and P. R. Ogilby, *J. Org. Chem.*, 2014, **79**, 3079-3087; (*d*) R. Ruiz-Gonzalez, R. Zanocco, Y. Gidi, A. L. Zanocco, S. Nonell and E. Lemp, *Photochem. Photobiol.*, 2013, **89**, 1427-1432; (*e*) X. Li, G. Zhang, H. Ma, D. Zhang, J. Li, D. Zhu, *J.*

Am. Chem. Soc., 2004, **126**, 11543-11548; (*f*) K. Tanaka, T. Miura, N. Umezawa, Y. Urano, K. Kikuchi, T. Higuchi and T. Nagano, *J. Am. Chem. Soc.*, 2001, **123**, 2530-2536.

17. T. Yamato, C. Pérez-Casas, H. Yamamoto, R. J. M. Elsegood, S. H. Dale and C. Redshaw, *J. Incl. Phenom. Macrocycl. Chem.*, 2006, **54**, 261-269.
18. C. Pérez-Casas, S. Rahman, N. Begum, Z. Xi and T. Yamato, *J. Incl. Phenom. Macrocycl. Chem.*, 2008, **60**, 173-185.
19. X.-L. Ni, X. Zeng, D. L. Hughes, C. Redshaw and T. Yamato, *Supramol. Chem.*, 2011, **23**, 689-695.
20. U. Svanholm and V. D. Parker, *J. Chem. Soc., Perkin Trans. 1*, 1973, **1**, 562-566.
21. T. Yamato and F. Zhang, *J. Incl. Phenom. Macrocycl. Chem.*, 2001, **39**, 55-64.
22. O. Tosic and J. Mattay, *Eur. J. Org. Chem.*, 2011, **2**, 371-376.
23. R. Reuter and H. A. Wegner, *Chem. Commun.*, 2013, **49**, 146-148.

Summary

Thiacalixarene is the second subclass in calix[*n*]arene family, which is an important class of calixarene and is an ideal platform for the development of cation, anion, and neutral molecule recognition. In comparison to the conventional calixarene platform, thiacalixarene had the advantage of: 1) the bridging sulfur atom could be facilely oxidized to sulfoxide and sulfone which could change the properties of the cavity formed by the calix benzene rings; 2) the ring linkages containing hetero atom sulfur atoms which may act as extra binding sites.

According to the reported literature, the thiacalix[4]arene scaffold possessing almost unlimited possibilities for functionalization on the up rim, low rim, bridging sulfur atoms. It has been attracted great attention to construct different types of host molecules in many ways. During the past two decade, there are numerous thiacalix[4]arene host molecules have been developed as ion recognition reagents (non-fluorescent receptors), florescent chemosensors (florescent receptors), allosteric effect reagents, molecular switches, logic gates and devices, self-assembled coordination networks, magnetic materials, luminescent materials and so on.

Thus, against this background, a series of receptors for heavy metal ions and anions were designed and synthesized based on thiacalix[4]arene in this dissertation. The photochemical properties, sensitivity and selectivity properties of these receptors were fully evaluated.

In chapter 1, a shortly review of the the application of thiacalix[4]arene derivatives in various fields. Such as, as anti-cancer agent, adsorption for organic dyes, solvent extraction, chiral anion recognition, fluorescent probe, molecular logic gate, phase transfer catalyst, supramolecular polymeric material, and so on. Although many efforts have already been devoted in thiacalixarene chemistry. However, compare to the conventional calixarene chemistry, there is still a large space worthy us to explore the thiacalixarene chemistry in the future. Thus, we further explored the synthesis and application of thiacalix[4]arenes in this thesis.

With this in mind, in chapter 2, a new thiacalix[4]arene based fluorescent chemosensor **L** bearing two pyrenyl groups in a 1,3-*alternate* conformation has been synthesized, and its metal ion-binding and fluorescence-sensing properties were investigated in ethanol. The designed chemosensor **L** exhibited high selectivity toward Cu^{2+} ions *versus* other tested metal ions with a detection limit of up to 1.44×10^{-7} M. The chemosensor **L** was capable

of acting as an efficient ratiometric fluorescent chemosensor at low ion concentration or as a fluorescence quenching type chemosensor due to the PET and heavy atom effects operating in high ionic strength solution. Further studies revealed that chemosensor **L** acted as a reversible sensor in the presence of Cu^{2+} and ethylenediamine.

Following the same interest, in chapter 3, two novel receptors **L1** and **L2** possessing imidazole moieties based on thiacalix[4]arene in the 1,3-*alternate* conformation have been synthesized and characterized. The crystal structures of **L1** and **L2** have been determined. The binding behaviour towards Li^+, Na^+, K^+ and Ag^+ ions has been examined by ^1H NMR titration experiments in ($CDCl_3/CD_3CN$; 10:1, v/v) solution. The exclusive formation of mononuclear complexes of **L1** with metal cations is of particular interest revealing a negative allosteric effect in the thiacalix[4]arene family. Liquid-liquid extraction experiments indicate that synthesized **L2** can be utilized as an efficient reusable extractant for dichromate anion by controlling the pH of the aqueous solution.

In chapter 4, a rare photochemical reaction has been observed. The exclusive endoperoxide photoproduct was quantitatively obtained from a thiacalix[4]arene crown-shaped derivative upon irradiation at 365 nm; the structure was unambiguously confirmed by $^1H/^{13}C$ NMR spectroscopy and X-ray crystallography. The prerequisites for the formation of endoperoxide photoproduct have also been discussed. Furthermore, the photochemical reaction rate could be greatly enhanced in the presence of thiacalix[4]arene platform because it served as a host to capture oxygen.

In summary, several kinds of receptors for ions and anions were designed and synthesized based on the unique topology of thiacalix[4]arene. We expect that the present design strategy and the remarkable photophysical properties of these receptors will help us to extend the potential applications of thiacalixarenes.

Publications

1. Synthesis and evaluation of a novel ionophore based on a thiacalix[4]arene derivative bearing imidazole units
   J.-L. Zhao, H. Tomiyasu, X.-L. Ni, X. Zeng, M. R. J. Elsegood, C. Redshaw, S. Rahman, P. E. Georghiou and T. Yamato
   New J. Chem. **2014**, 38, 6041–6049.

2. The first study about the relationship between the extractability of thiacalix[4]arene derivatives and the position of the coordination binding sites
   J.-L. Zhao, H. Tomiyasu, X.-L. Ni, X. Zeng, M. R. J. Elsegood, C. Redshaw, S. Rahman, P. E. Georghiou, S. J. Teat and T. Yamato
   Org. Biomol. Chem. **2015**, 13, 3476–3483.

3. Synthesis, crystal structure and complexation behaviour study of an efficient Cu^{2+} ratiometric fluorescent chemosensor based on thiacalix[4]arene
   J.-L. Zhao, H. Tomiyasu, C. Wu, H. Cong, X. Zeng, S. Rahman, P. E. Georghiou, D. L. Hughes, C. Redshaw and T. Yamato
   Tetrahedron **2015**, 71, 8521–8527.

4. A rare and exclusive endoperoxide photoproduct derived from thiacalix[4]arene rown-shaped derivative bearing 9,10–substituted anthracene moiety
   J.-L. Zhao, C. Wu, H. Tomiyasu, X. Zeng, M. R. J. Elsegood, C. Redshaw and T. Yamato
   Chem. Asian J. **2016**, 11, 1606–1612.

5. Thiacalix[4]arene derivatives bearing imidazole units: a ditopic hard/soft receptor for Na^+ and K^+/Ag^+ with allosteric effect and a reusable extractant for dichromate anions
   J.-L. Zhao, C. Wu, X. Zeng, S. Rahman, P. E. Georghiou, M. R. J. Elsegood, T. G. Warwick, C. Redshaw, S. J. Teat and T. Yamato
   ChemistrySelect **2016**, 1, 1541–1547.

6. An Unprecedented Photochemical Reaction for Anthracene-Containing Derivatives
   J.-L Zhao, X.-K. Jiang, C. Wu, C.-Z. Wang, X. Zeng, C. Redshaw, T. Yamato
   ChemPhysChem **2016**, DOI:10.1002/cphc.201600783